AD-783 913

# ON THE AVOIDANCE OF LIMB FLAIL INJURY BY EJECTION SEAT STABILIZATION

Peter R. Payne

Payne, Incorporated

Prepared for:

Aerospace Medical Research Laboratory

May 1974

# DISCLAIMER NOTICE

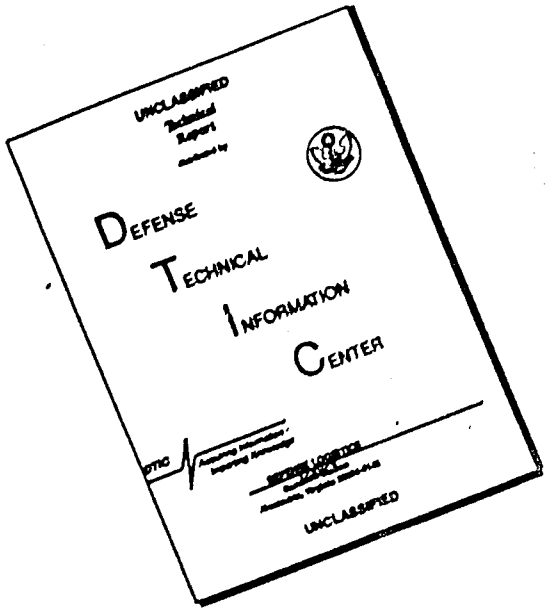


THIS DOCUMENT IS BEST QUALITY AVAILABLE. THE COPY FURNISHED TO DTIC CONTAINED A SIGNIFICANT NUMBER OF PAGES WHICH DO NOT REPRODUCE LEGIBLY.

UNCLASSIFIED

SECURITY CLASSIFICATION OF THIS PAGE (When Data Entered)

| REPORT DOCUMENTATION PAGE | READ DISTRUCTIONS BEFORE COMPLETING FORM |
|---|---|
| 1. REPORT NUMBER: AMRL-TR-74-9 | 2. GOVT ACCESSION NO. / 3. RECIPIENT'S CATALOG NUMBER |
| 4. TITLE (and Subtitle): ON THE AVOIDANCE OF LIMB FLAIL INJURY BY EJECTION SEAT STABILIZATION | 5. TYPE OF REPORT & PERIOD COVERED: Final Report 1 Oct. 1972 - 31 March 1974 |
| | 6. PERFORMING ORG. REPORT NUMBER: 106-5 |
| 7. AUTHOR(s): Peter R. Payne | 8. CONTRACT OR GRANT NUMBER(s): F33615-73-C-4006 |
| 9. PERFORMING ORGANIZATION NAME AND ADDRESS: Payne, Incorporated 2200 Somerville Road Annapolis, Maryland 21401 | 10. PROGRAM ELEMENT, PROJECT, TASK AREA & WORK UNIT NUMBERS: Program Element 62202F Project 7231 Task 723106 Work Unit No. 36 |
| 11. CONTROLLING OFFICE NAME AND ADDRESS: Aerospace Medical Research Laboratory, Aerospace Medical Div., Air Force Systems Command, Wright-Patterson AFB, Ohio | 12. REPORT DATE: May 1974 |
| | 13. NUMBER OF PAGES: 87 |
| 14. MONITORING AGENCY NAME & ADDRESS(if different from Controlling Office) | 15. SECURITY CLASS. (of this report): UNCLASSIFIED |
| | 15a. DECLASSIFICATION/DOWNGRADING SCHEDULE |

16. DISTRIBUTION STATEMENT (of this Report)

Approved for public release; distribution unlimited

17. DISTRIBUTION STATEMENT (of the abstract entered in Block 20, if different from Report)

18. SUPPLEMENTARY NOTES

19. KEY WORDS (Continue on reverse side if necessary and identify by block number)

Aircraft Ejection Seats
Flail Injury
Aircraft Safety
Limb Flailing
Ejection Seat Stability

20. ABSTRACT (Continue on reverse side if necessary and identify by block number)

After a review of the various causes of limb flail injury during high speed escape from an aircraft in an open ejection seat, the problem of flailing due to seat aerodynamic instability is addressed. We concluded that there is no practical way of avoiding injury in an unstable seat. The causes of ejection seat instability are then examined, and a number of conventional and unconventional stabilization systems discussed. We concluded that a new approach - the in-plane stabilizer - is probably the optimum solution to the problem.

(continued)

DD FORM 1 JAN 73 1473 EDITION OF 1 NOV 65 IS OBSOLETE

UNCLASSIFIED

SECURITY CLASSIFICATION OF THIS PAGE (When Data Entered)

20.

The theory of the in-plane stabilizer is developed and its effectiveness confirmed by full scale wind tunnel tests with an F-105 seat containing live human subjects.

# PREFACE

The research reported herein was accomplished by Payne, Inc., 2200 Somerville Road, Annapolis, Maryland, for the Aerospace Medical Research Laboratory, Wright-Patterson Air Force Base, Ohio under Contract F33615-73-C-4006, and in support of Project 7231, "Biomechanics of Aerospace Operation," Task 723106, "Impact Exposure Limits and Personnel Protection Criteria." Mr. Peter R. Payne was the principal investigator for Payne, Inc. Mr. James W. Brinkley of the Impact Branch, Biodynamics and Bionics Division, was the contract monitor for the Aerospace Medical Research Laboratory.

This report is one of a series of reports prepared under Contract F33615-73-C-4006 to provide a better understanding of the factors contributing to limb flailing injuries resulting from ejection from high speed aircraft. The ultimate objective of this research is to provide design criteria for emergency escape systems and personnel protection equipment. The work was performed during the period of October 1972 to October 1973.

TABLE OF CONTENTS

## LIST OF FIGURES

LIST OF FIGURES (continued)

## LIST OF FIGURES (continued)

## INTRODUCTION -- THE FLAIL INJURY PROBLEM

Flail injury results when one or more limbs of an ejection seat occupant are dislodged from their stowed position. The windblast usually carries the limbs outward and backward, and by the time they are arrested, either by the seat structure or the natural limit of travel of the joints, they have acquired a considerable relative velocity to the torso and seat. The energy required to bring the limbs back to seat/torso velocity is the basic cause of injury, and this energy varies with the square of the airspeed at which dislodgement took place.[2] Thus, at low airspeeds, there may be no significant injury, while at high speeds, severe fractures and even death may result.

The probability of serious flail injury, as a function of airspeed at ejection, is given in figure 1, based on USAF non-combat experience in the period 1964-1970[1]; together with earlier RAF experience[1] with flail injury, and quite recent U.S. Navy experience. Some theoretical background to flail injury is given in reference 2.

Although not strictly flail, the problem of helmet loss in high speed ejections is clearly related. Helmet loss is caused by a predominently vertically acting (upwards) force on the helmet, due principally to suction forces acting on the outside, over the top.[6] It is obviously desirable to find a way of preventing helmet loss.

There are two basic causes of limb dislodgement; aerodynamic loads on the limbs and inertial loads due to local accelerations. The force tending to dislodge a limb may be due to either of these, or to a combination of both. For simplicity, they will be considered separately in the discussion which follows.

### Acceleration Loads

Since force = mass times acceleration, the limb segments will experience forces of magnitude and direction appropriate to their local acceleration. After the simple linear acceleration of the catapult stroke, the acceleration environment becomes quite complex. The rocket contributes linear and angular acceleration. The aerodynamic forces cause linear acceleration (a rapid loss of airspeed) and generally, angular acceleration as well because the pitching and yawing moments are not zero.

Consider a seat that is pitching only, as shown in figure 2. The accelerations on an element of mass $\delta m$, situated a distance $\ell$ from the CG are

$$\frac{du}{dt} \quad \text{and} \quad \ell \frac{d^2\theta}{dt^2} \tag{1}$$

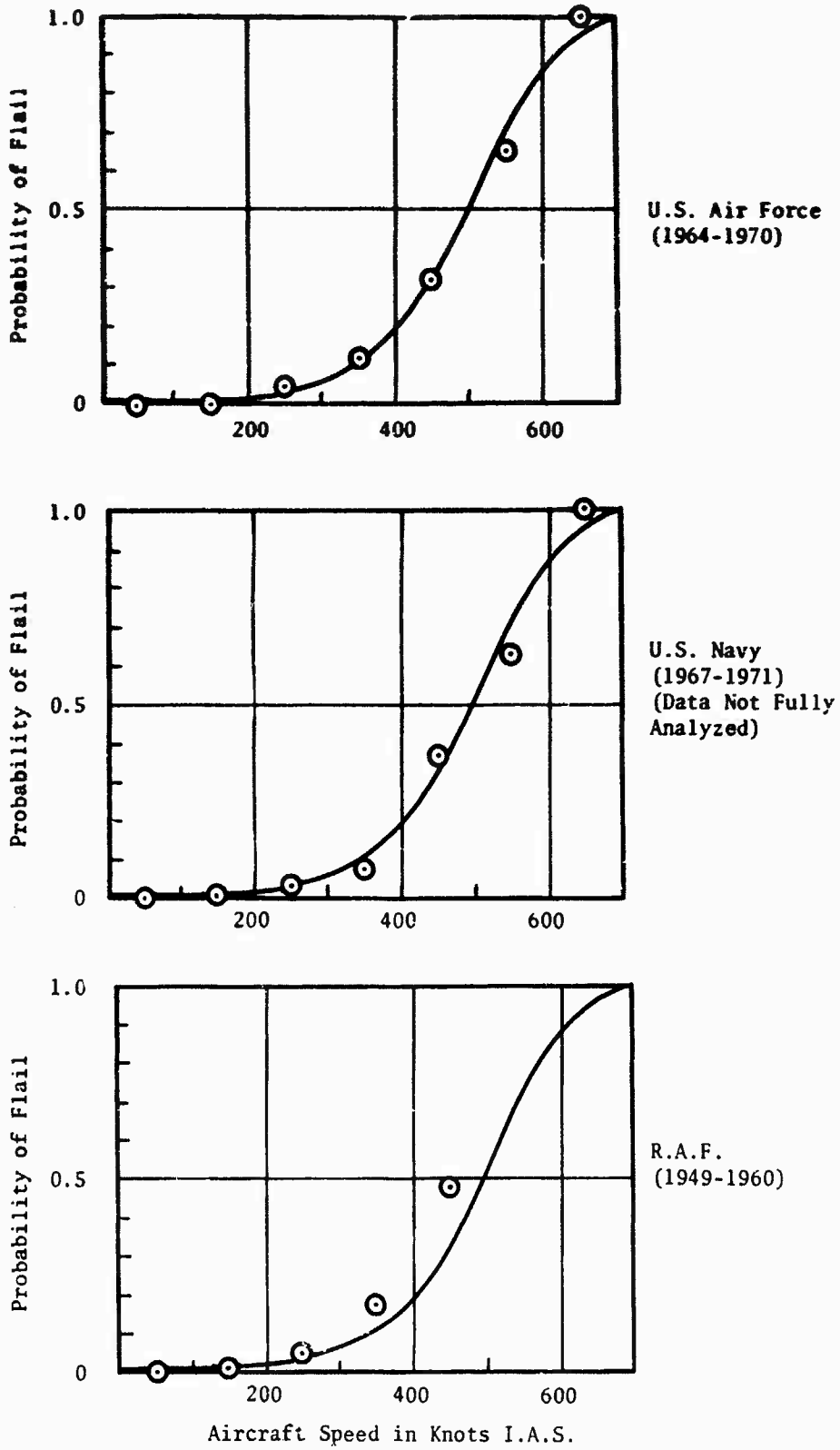


Figure 1. Comparative Flail Injury Probability for Three Services, as a Function of Aircraft Speed at Ejection. The solid line is the best fit to the USAF data, taken from reference 1.

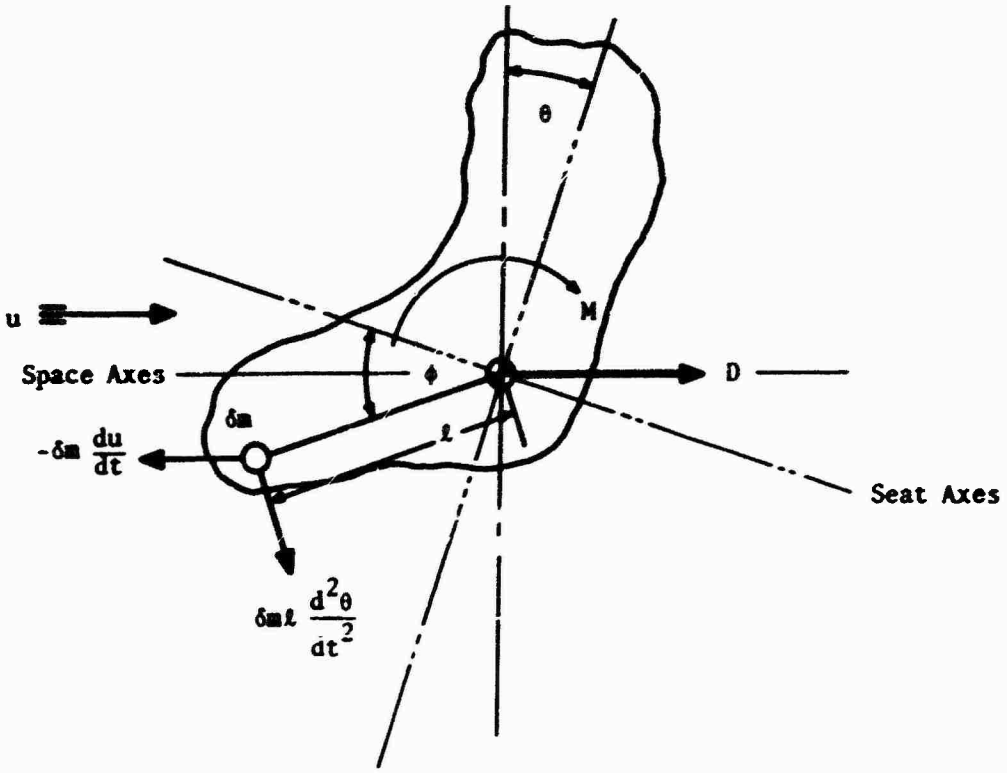


Figure 2. Basic Geometry.

If $m_s$ is the total mass of the seat plus occupant, and $r_G$ its radius of gyration, the equations of motion can be written approximately as

$$\left.\begin{aligned} m_s \frac{du}{dt} &= -A_D q \\ m_s r_G^2 \frac{d^2\theta}{dt^2} &= V_m q \end{aligned}\right\} \qquad (2)$$

where $A_D$ = seat drag area = drag/q

$V_m$ = seat moment volume = moment/q

q = dynamic pressure $\frac{1}{2} \rho u^2$

Then from equations 1 and 2, the acceleration force components on an elemental particle $\delta m$ are initially

$$-\frac{\delta m}{m_s} A_D q \quad \text{and} \quad \frac{\delta m}{m_s} \frac{V_m}{r_G^2} q \tag{3}$$

Additionally, due to the seat's spin rate $\dot{\theta}$, a centripetal acceleration $\ell(\dot{\theta})^2$ acts on each particle, giving an elemental radial force of

$$\frac{\delta m \ell}{(m_s r_G^2)^2}\left[\int V_m q \, dt\right]^2 = \delta m \ell \left(\frac{V_m}{r_s r_G^2}\right)^2 q^2 t^2 \tag{4}$$

if $V_m$ and q are constant.

Unlike the other acceleration terms then, centripetal acceleration initially increases with time, if the seat spins, and with the square of the dynamic pressure at a given time.

Total force will clearly depend on the mass $\int \delta m$ of the appropriate limb segment, and the mass moment $\int \ell \, \delta m$ as well as the linear and angular acceleration. Specific values can be worked out for a particular seat when $A_D$ and $V_m$ are known.

From equation 3, the initial inertial forces vary with the dynamic pressure, q, just like the direct aerodynamic forces to be discussed later. Indeed, we might refer to inertial forces as "indirect aerodynamic forces," to contrast them with the direct aerodynamic forces due to airflow over the limbs and the general pressure field of the seat.

Some typical accelerations are given in figure 3, for an F-101 ejection seat, using the pitching moment data of Galigher,[3] which shows $V_m = 3.1$ ft$^3$ at the normal ejection attitude, $A_D = 7.0$ ft$^2$. The initial tangential acceleration is seen to be almost an order of magnitude less than the longitudinal acceleration. The centripetal acceleration is calculated by assuming angular acceleration to remain constant at the initial value, and so can only be regarded as a rough indicator of the size of this term. But it is clearly comparable in magnitude with linear acceleration at the higher speeds, and may be substantially greater. If a seat spins after ejection at a high airspeed, it cannot be expected that the limbs will remain in their stowed position, and for practical purposes, flail injury is a sine qua non.

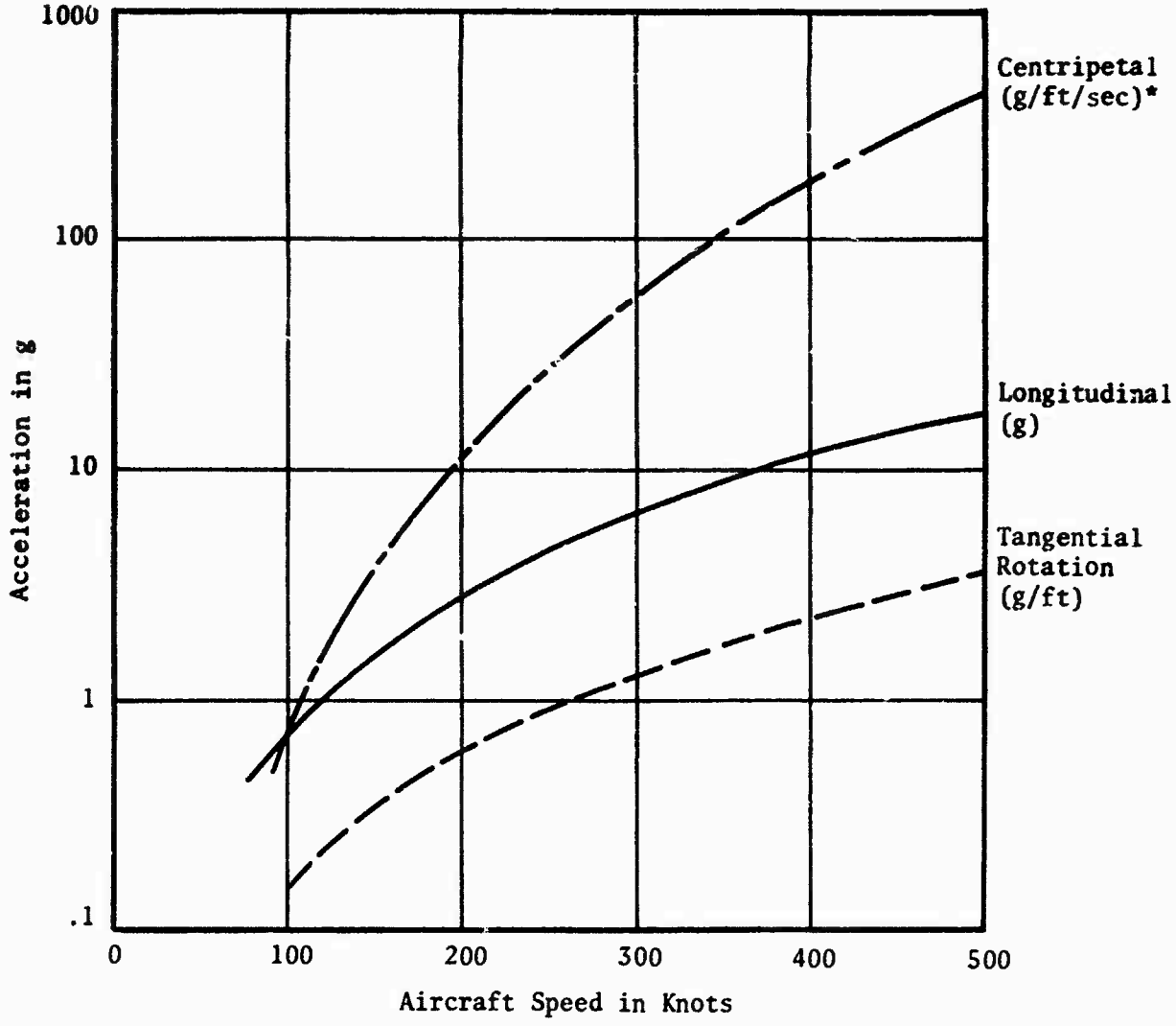


Figure 3. Typical Seat Acceleration, Assuming $V_m$ = 3.1 $ft^3$, $A_D$ = 7.0 $ft^2$, a Seat Mass of 10 slugs, and $r_G$ = 1.5 ft.

[*Note that centripetal acceleration varies as $(time)^2$. Thus 0.1 seconds after ejection, it will be 0.01 times the value shown.]

## Aerodynamic Loads

Aerodynamic loads on the limbs may be divided into five main categories:

- Gross aerodynamic drag.
- Gross lateral suction.
- Deflected flow forces - man alone.
- Deflected flow forces - due to the seat.
- Proximity effects.

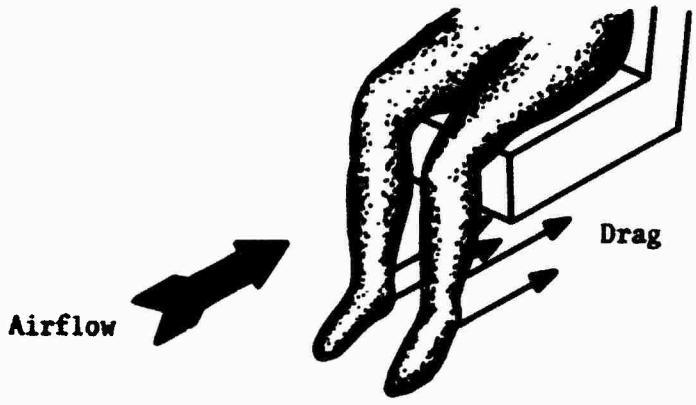


Figure 4. Gross Aerodynamic Drag on the Lower Legs.

The first type of load, illustrated in Figure 4, is easy to understand and does not require elaboration.

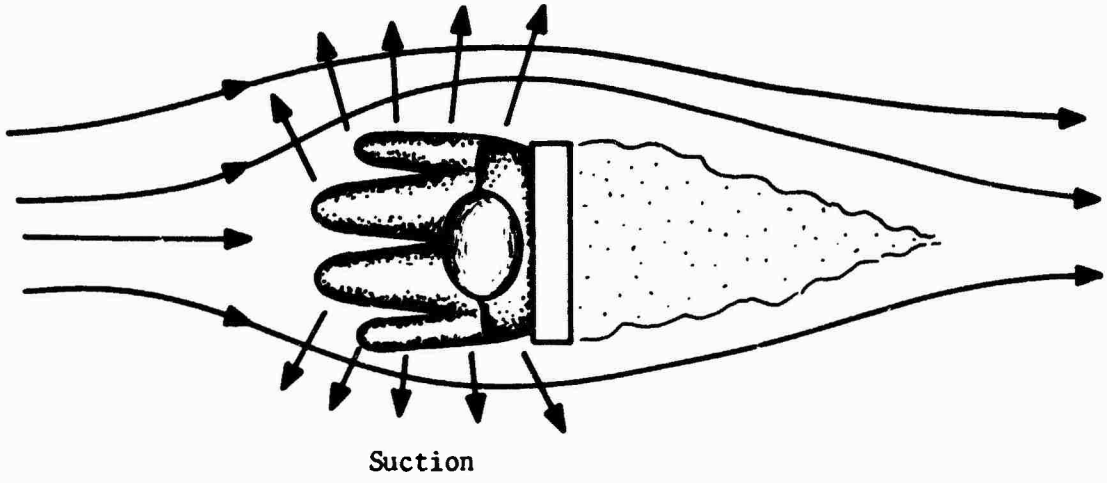


Figure 5. Gross Lateral Suction.

Although not often discussed, the lateral surfaces of any body moving through a fluid are at lower than ambient pressure, while the forward face is at higher than ambient. The effect is discussed theoretically by Band and Payne[4] who show that this effect by itself can account for the outward acting forces on the arms and legs of an ejection seat occupant. It also partly accounts for the upward force on his helmet. It might be said that windblast tends to pull a body apart in the plane normal to the flow, and when parts of the body are movable, like arms and legs, they are thus pulled into the main airflow. Once this has happened, their aerodynamic drag pulls them backwards, relative to seat axes, and flail injury occurs when they reach a limit of travel.

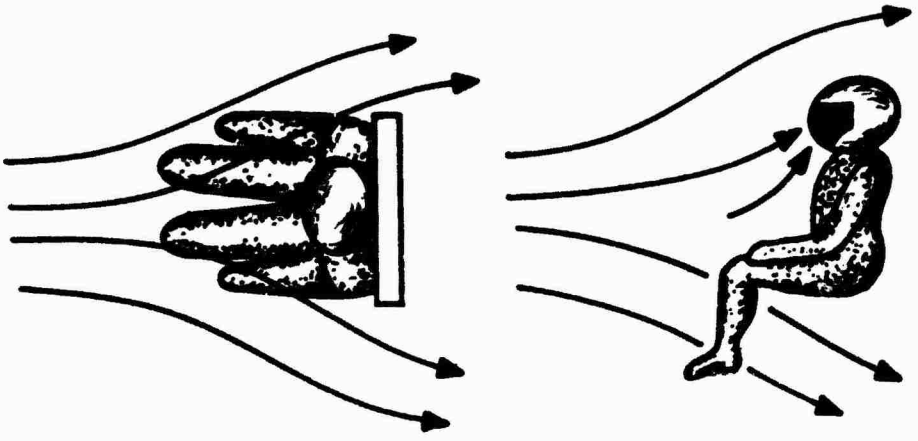

Figure 6. Flow Deflection.

There is a subtle difference between the local flow deflection, illustrated in figure 6 and gross lateral suction, so that it is worth separating the two. But the effect is the same; a tendency to pull the body apart laterally.

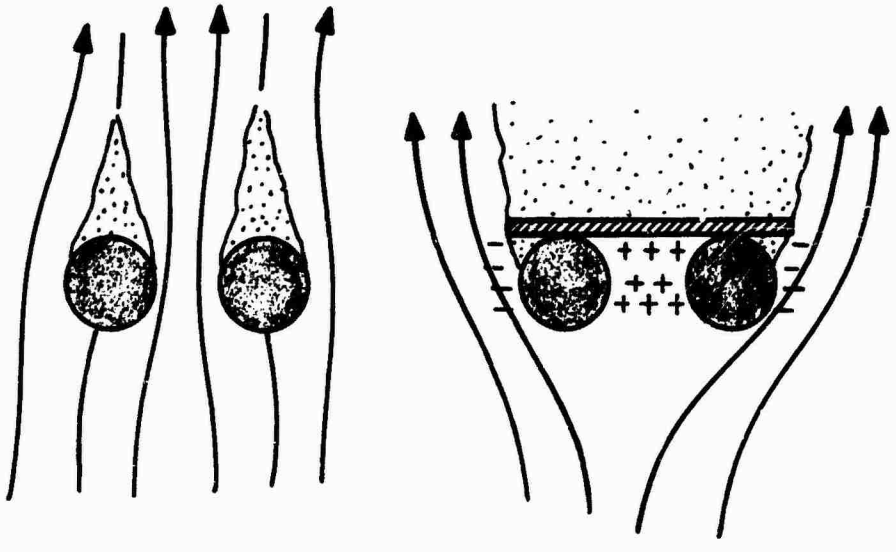

Figure 7. Seat Proximity Effects.

Two cylinders by themselves (representing legs, say), shown to the left of figure 7, would actually be drawn together in the airflow, because suction forces on their insides are greater than on their outer surfaces. This is an illustration of "proximity effect," which is well known as a troublesome problem in ship maneuvering. When some obstacle, like the forward face of a seat pan, is placed behind them, they are repelled from each other. The air between them, essentially dead air, is all at ram pressure, while there is suction on the outer surfaces. This effect can be very powerful indeed, and the importance of minimizing seat blockage behind the lower legs cannot be too much emphasized. Measurements of this effect are reported in reference 2.

Seat proximity effects can be very subtle and unpredictable. In the side trigger configuration, experimental observation[2] with two seats gave an expected result; there was a substantial outwards and backwards force on the arms and hands. Yet when an F-105 seat was evaluated in the wind tunnel[6], the outward acting force reacted by the subject's hands was so small as to be unmeasurable with the instrumentation then in use. The reasons for this anamoly are not yet understood.

In the discussion so far, we have considered the seat to be pointing stably into the airflow. When the seat is pitching and/or yawing (as it generally is) the picture becomes enormously more complicated. The rotation induces additional velocity components, and the direction of resultant velocity, relative to seat axes, changes continuously. Although we have gained some insight into the magnitude and direction of the limb forces by wind tunnel tests at different yaw and pitch angles, a complete understanding of the flow field and development of a predictive capability is probably quite impractical without an order of magnitude increase in research effort. Fortunately, it is probably not necessary to know the force magnitude and direction, except in very general terms.

## SOME SOLUTIONS TO THE PROBLEM WHEN THE SEAT IS STABILIZED

We have three main problems to solve

- Helmet loss, which is due to aerodynamic forces only
- Arm Dislodgement } Combined aerodynamic and inertial loads
- Leg Dislodgement }

If a system of clamps were automatically deployed to hold the extremities just prior to firing the catapult, the flail injury problem would be solved once and for all.* Aircrew have traditionally rejected such an approach, principally because of worries as to whether the clamps would unclamp at the time of man/seat separation. We are left with the alternatives of either

- Reducing dislodgement forces to a tolerable level, or
- Arranging for aerodynamic forces to trap the limbs in a safe position.

If either of these approaches is to be successful, it is clearly imperative that the seat fly stably.

Present day ejection seats are either unstabilized, or stabilized by a drogue parachute. All of the seat configurations which have been wind tunnel tested are aerodynamically unstable, and there is no reason to suppose that this observation cannot be generalized; to the statement that most steat are unstable before the drogue chute is deployed.

Generally speaking, some time elapses between the seat leaving its rails, and drogue chute deployment. At high speeds, the unstable seat can reach a large pitch and/or yaw angle before the deployed drogue chute can start to correct its attitude. At higher speeds still, it will spin, with the drogue chute ineffectually wrapped around it. At high speed, a spinning seat almost certainly equates to a dead or maimed occupant.

There are several reasons for this unfortunate state of affairs, but two key ones are of particular interest. As equation 4 shows, an unstable seat initially builds up rotational energy as the fourth power of the speed, in unit time. If there is a constant time delay in drogue deployment time, the drogue's ability to stop the rotation (which varies as the square of the speed) will clearly reduce with increasing speed.

Secondly, for a seat to be equally well stabilized at all speeds, the drogue opening time must vary inversely with speed. And very elementary theory, assuming rigid risers and shrouds does give

---

* But not the problem of death due to intolerably high spin rates.

$$\tau_o = \frac{t_o u_o}{R_o} = \text{constant}$$

where

$t_o$ = the opening time

$u_o$ = the initial free-stream velocity

$R_o$ = the flat radius of the canopy

Payne[5] has shown that riser, shroud and canopy stiffness have a dominant influence on opening time, however, so that in the real world of finite stiffnesses, $\gamma_o$ will reduce with increasing speed. Indeed, above a certain speed, it may not open at all.*

For these and other reasons, the writer believes that drogue stabilization is unsatisfactory and that seats should be stabilized by suitable changes in their shape. An analysis of the seat stabilization problem is given later in this report.

In the rest of this section, we shall assume that the seat is stabilized, and that pitch and yaw perturbations will not exceed about 20°. The technology needed to achieve this is felt to be available, and if it is not in fact employed, then we might as well accept high speed flail injury as an unfortunate political fact of life, and turn our attention elsewhere. We will never find a non clamping means of preventing flail in a randomly spinning seat.

## Seat Configuration

Apart from stability considerations, the seat itself contributes to dislodgement forces. A deep front to the pan, or a backboard, forces the lower legs outwards, as mentioned in the discussion of figure 7.

Ideally, the seat pan should be as thin as possible, and the survival kit stowed elsewhere.

The upper legs will still be pushed apart by the ram pressure air "trapped" between them and the seat pan. This can be accepted, if robust sides to the seat support the thighs. Alternatively, the front center of the seat pan can be either eliminated altogether, or "left behind" when the seat is ejected. This will allow airflow between the thighs, and reduce (perhaps eliminate) the outward pressure.

---

* Unsatisfactory opening of parachutes at supersonic speeds has been attributed to shocks from the risers and boundary layer growth. But it might also be due to riser and shroud stiffnesses which are too low for the dynamic pressures involved.

Seat weight and drag are also important. We should strive for minimum ejected weight, for the reasons explained in reference 2, while high drag is usually beneficial.

## Local Flow Deflection

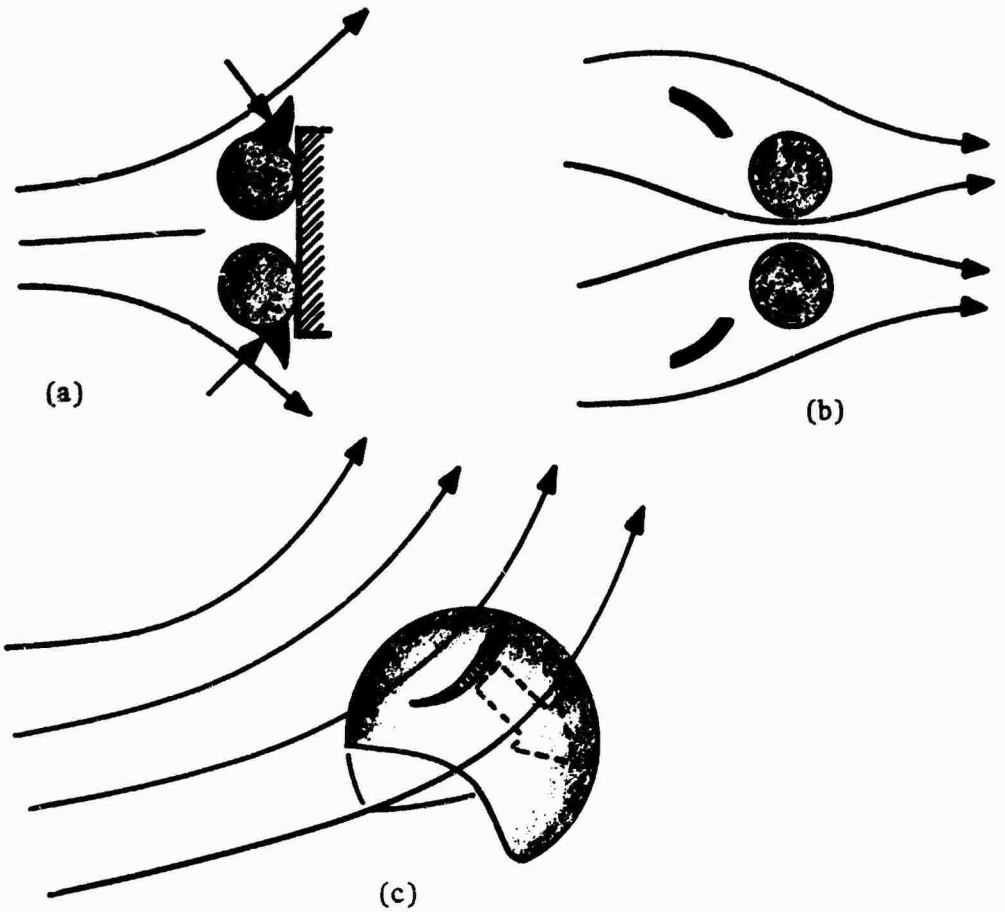


Figure 8. Three Local Flow Deflectors.

By locally deflecting the flow, we can achieve a measure of control over the magnitude and direction of the local forces on the body. Figures 8(a) and 9 show how spoilers or deflectors can be attached to the lower legs of a flight suit. As reported in references 2 and 6, they eliminated the outward force on the lower legs at zero pitch and yaw. The configurations tried so far have not been effective in reducing knee-out forces, or in controlling foot forces when the seat is yawed, however.

The same effect can possibly be obtained with flow deflectors attached to the seat structure, as shown in figure 8(b). Such a configuration has the disadvantage of degrading seat stability.

Figure 9. Flight Suit Mounted Flow Deflectors Tested and Reported in Reference 2.

The helmet flow deflector shown in figure 8(c) is thought to be an acceptable solution to the helmet loss problem (based on the tests reported in reference 6), provided it can be accommodated within existing canopy clearance limitations. But further modification and evaluation over a range of yaw and pitch angles is needed before a hardware commitment can be made.

Entrapment Devices

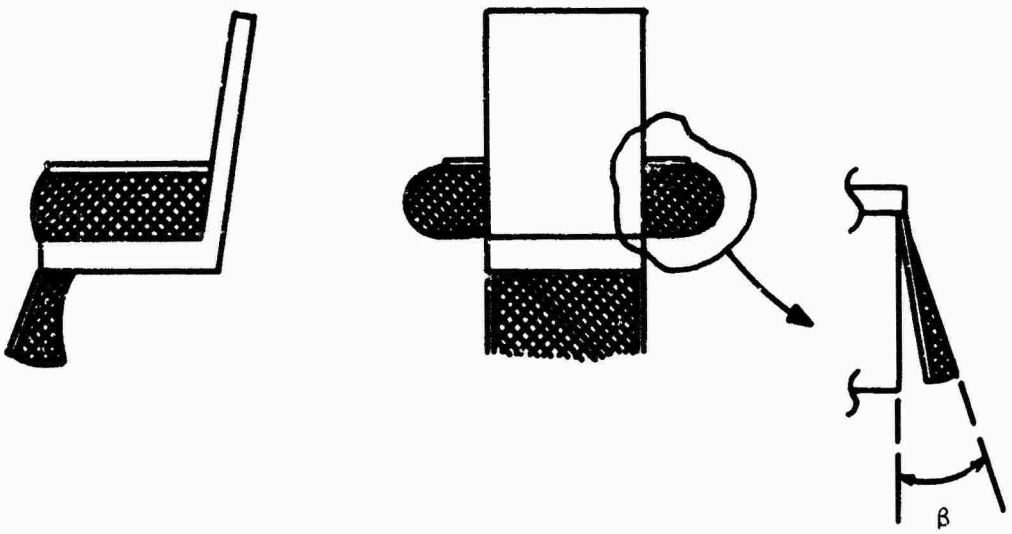


Figure 10. Net Entrapment Devices.

Suggested by James W. Brinkley of the Aerospace Medical Research Laboratory, Wright-Patterson Air Force Base, the entrapment nets shown in figure 10 offer hope of complete flail protection up to yaw angles defined by the net angle β. These devices have been evaluated (reference 6) up to 30° yaw, with ±15° pitch excursions, in mock-up form, and appear to be completely satisfactory.

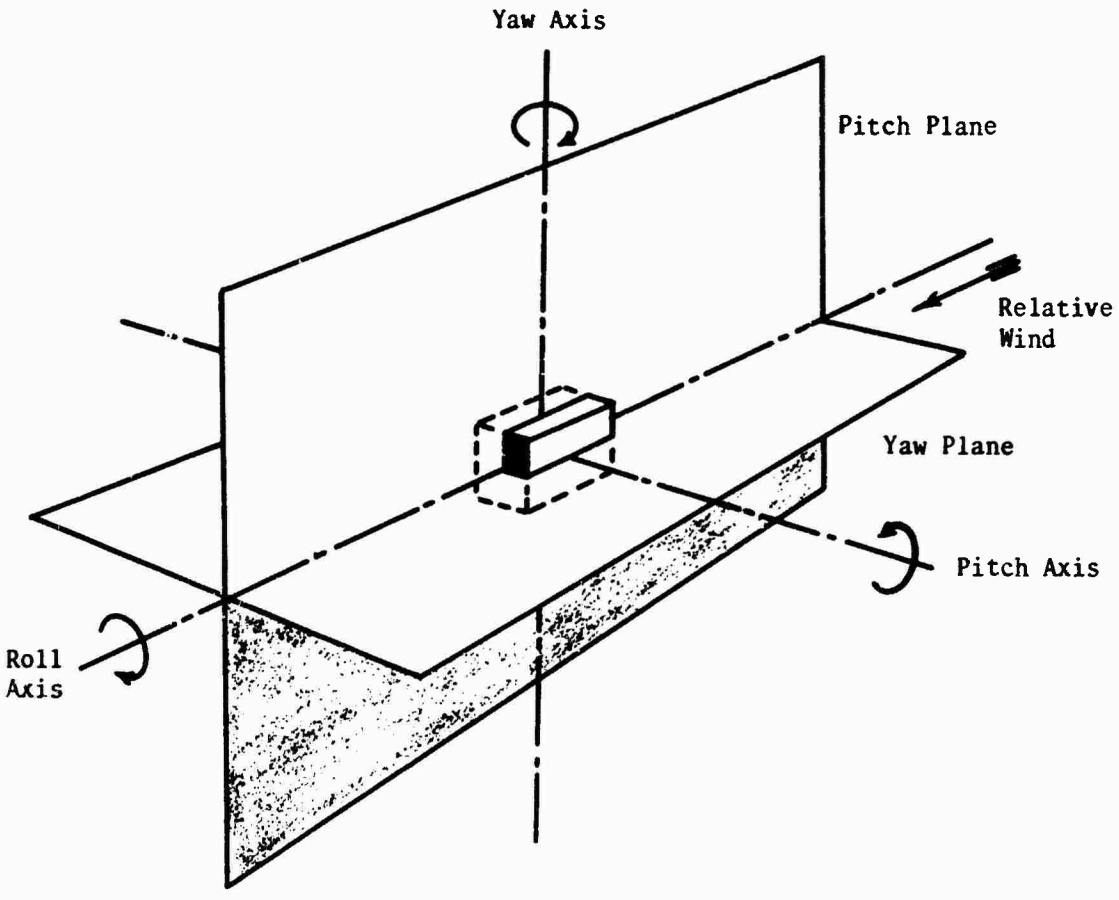


Figure 11. Definition of Axes.

Consider a body at rest, or moving steadily through a fluid, and suppose that its angle to the flow is changed to a new angle by some disturbance. We may say that the body is statically stable if the fluid dynamic forces acting on it tend to return it to the original angle. In a more general sense, a body is statically stable, if, after being disturbed from equilibrium, it tends to return to equilibrium. Conversely, it is statically unstable if, after disturbance, the forces tend to drive it even further away from equilibrium.

This is not, by itself, a sufficient criteria for total stability. A statically stable body may be dynamically unstable. In this case, the statically stable body returns to equilibrium after a disturbance, but overshoots on the other side to a value greater than the original disturbance. Dynamic instability is thus characterized by an oscillatory motion, the amplitude of which increases with time.

Assuming positive static stability and damping, true dynamic instability can only occur when two or more modes (degrees of freedom) are coupled together; each mode is statically stable and may be positively damped by itself, but the coupling between them results in an oscillatory divergence. Familiar examples are wing flutter (binary flutter resulting from the coupling of torsion and flap, for example), Lanchester's phugoid for an airplane with drag and lift degrees of freedom, and the porpoising of planing boats free to heave and pitch. The divergent oscillation in a single degree of freedom can only be due to negative damping, the rate analog of static instability. In the ejection seat problem, modal couplings are weak, so that there is little danger of dynamic instability. Should it occur with some unusual seat configuration, the corrective action would be to increase pitch and/or yaw static stability and damping.

In this report, we are concerned with stabilizing bodies which are, by themselves, statically unstable. We shall consider only static stability, in view of the remarks above.

From figure 11, the difference between pitch and yaw stability is merely one of axis definition, so far as theory is concerned. Thus, the following discussion is applicable to either axis. Static instability in the sense of divergence about the roll axis cannot occur, so long as the seat is flying stably in pitch and yaw. Any rolling moment which then exists must be due to the airflow past the body acquiring an equal and opposite angular momentum - a canted plate near a seat extremity could cause this - but such moments will not vary with roll angle. There is no need for an otherwise stable ejection seat to experience a rolling moment at all. If it does, it will start to rotate about the roll axis, speeding up until it reaches a steady rotation rate. The steady "auto-rotation" speed will vary directly with airspeed, and otherwise depend on the nature of the asymmetry causing roll. There is no correlation between auto-rotation rate and the magnitude of the static rolling moment.

If a seat is yawed, a rolling moment will generally develop, and the seat may even spin about the roll axis. But the cure is clearly to stabilize the seat in yaw; not to alter the roll characteristics.

## The Presentation of Aerodynamic Data for Ejection Seats

The familiar aerodynamic force and moment coefficients are founded upon the basic premise of geometric similarity. The model in the wind tunnel is a model of the full scale article, so far as the airflow over it is concerned. The model data can be applied, at least conceptually, to a geometrically similar body of any size. In this context, non dimensionalizing by area and characteristic length makes good sense. One can readily make comparisons between similar, but not necessarily identical body shapes.

The case of the aerodynamic forces acting on the human body is different. It is difficult to define frontal area precisely, and characteristic length has less meaning. Since the density of the human body does not vary greatly, and both weight (W) and height (L) are readily determined, it is better (Payne[2]) to divide by $\sqrt{WL}$ for forces, and $L\sqrt{WL}$ for moments. The resulting coefficients are not non dimensional, it is true; it is also irrelevant.

The ejection seat presents a different problem again. All ejection seats must accommodate human crew members, so that the functional size will not vary greatly. This is not true of actual frontal area or characteristic length, which to a certain extent depend upon the whim of the designer. Whatever they are, they are unimportant, and their use to obtain a coefficient is a waste of time. No one is ever going to want to know the forces on, say, an F-105 seat ten times the size of the present one.

It seems very clear to the writer that for ejection seats, all forces should be expressed in the simplest possible way, as "force areas"; i.e.

$$\text{Force Area } (A_F) = C_D S = \frac{\text{Force}}{\frac{1}{2}\rho u_o^2} \qquad (ft^2)$$

Similarly, moments should be expressed as "moment volumes"; i.e.

$$\text{Moment Volume } (V_m) = C_M SL = \frac{\text{Moment}}{\frac{1}{2}\rho u_o^2} \qquad (ft^3)$$

Typical seat drag and moment data in this form is presented in figure 12. Elsewhere in this report, the conventional coefficient form has sometimes been retained when it is more convenient for comparison with existing data.

## The Cause of Pitching Moments

For the sake of clarity in what follows, we shall refer to motion about the pitch axis, bearing in mind that the remarks are all equally applicable to motion in yaw instead or as well.

As indicated in figure 13 an elongated or streamline body is naturally unstable because of the additional suction forces which act upon it when it is inclined to the flow.

The same effect is undoubtedly present for bluff bodies like an ejection seat and its occupant, but the magnitude of the resulting moment is likely to be much smaller, partly because of the reduced moment arm, and partly because the suction forces themselves are reduced. It seems likely that the main causes of bluff body pitching moment are the imbalance of the fore and aft (drag) pressure distributions, and flow deflection. Both mechanisms are illustrated in figure 14. Another aspect of the flow deflection mechanism is illustrated in the idealization of figure 15.

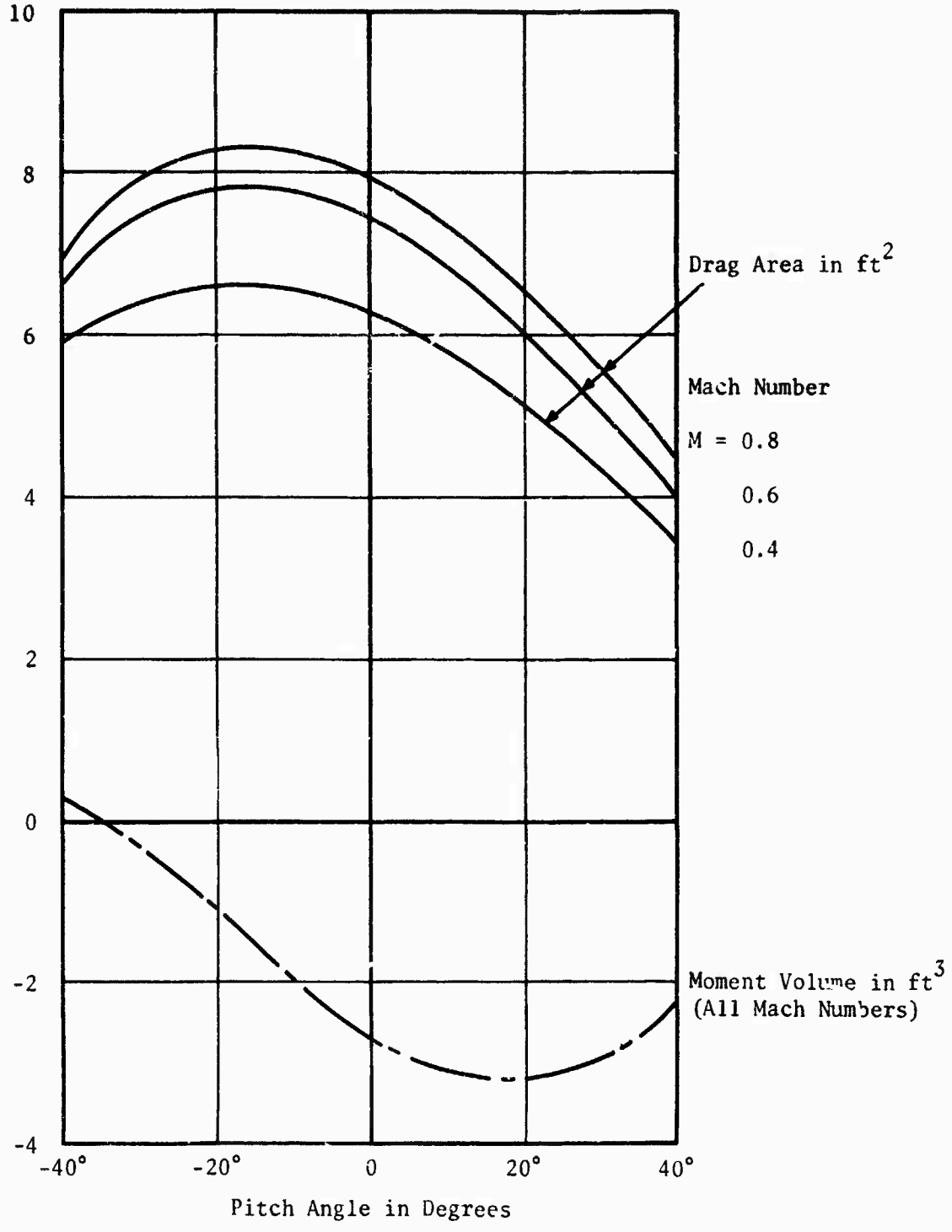


Figure 12. Drag Area and Moment Volume for an F-101 Ejection Seat. (Galigher[3])

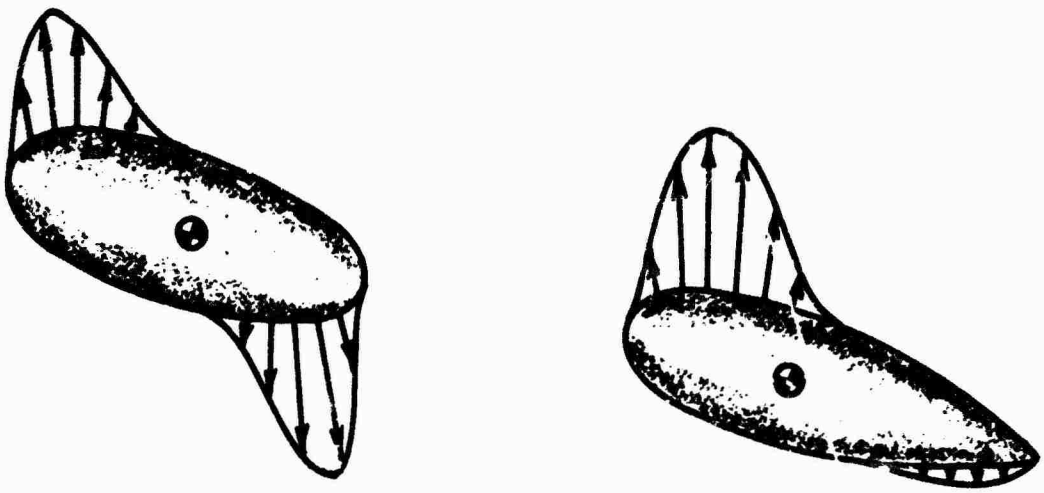

(a) Inviscid Flow

(b) Real Viscous Flow

Figure 13. Pressure Distribution Change Over a Streamline Body Due to Pitch Angle.

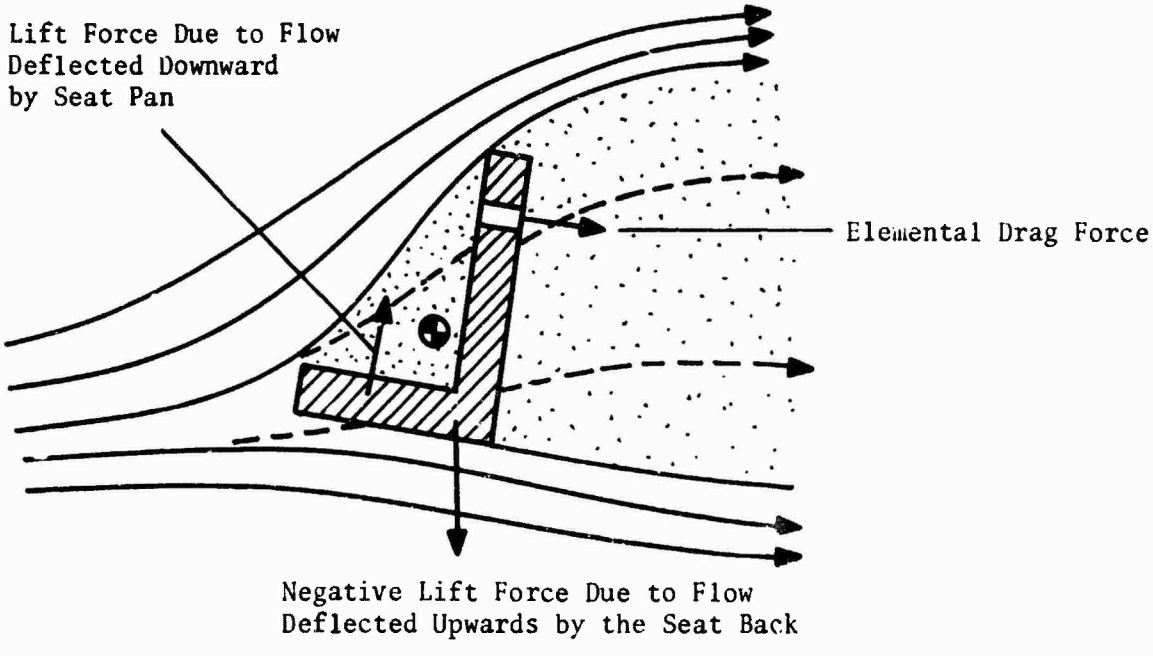


Figure 14. Two Mechanisms for the Pitching Moment on a Bluff Body.

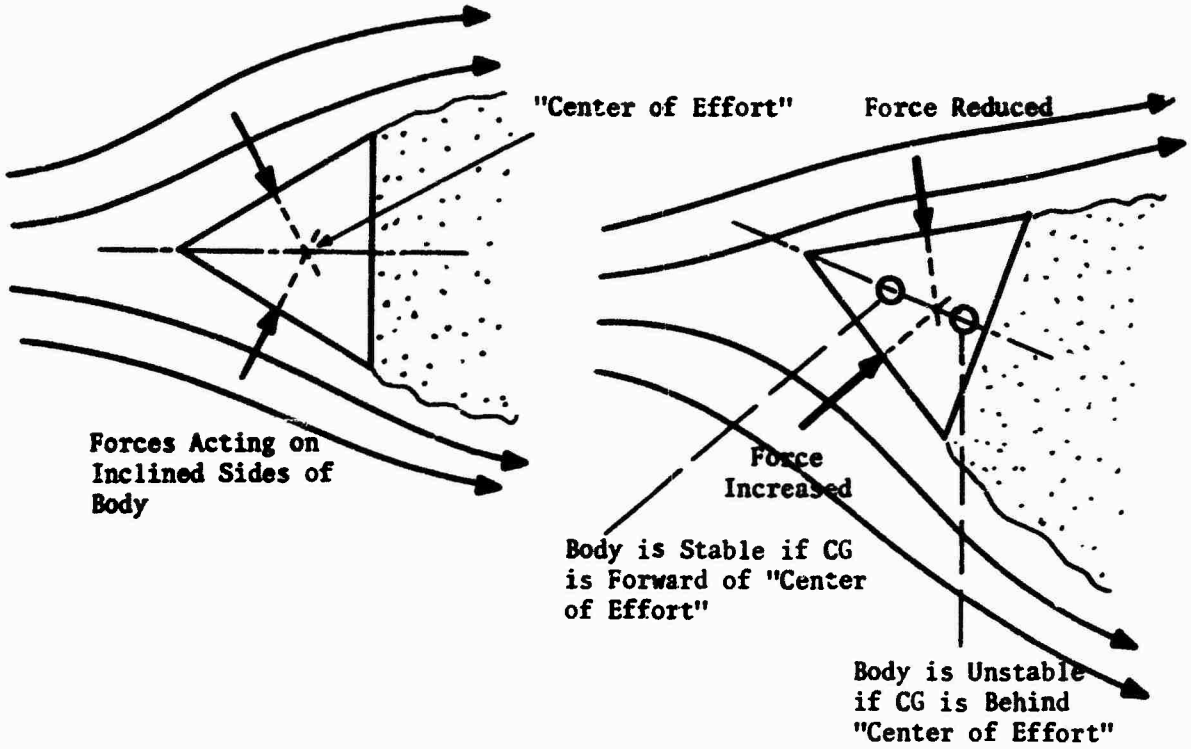


Figure 15. An Idealization of Pitching Moment Due to Flow Deflection, and the Effect of CG Position on Stability.

In visualizing the various contributions to the total pitching moment, it is important to differentiate between forces and couples. The pressure distribution in figure 13(a) results in a couple with no net resultant normal force. The body will therefore be unstable no matter how far forward we arrange for the CG to be. But, when a side force is developed, then as shown below, stability can always be achieved by putting the CG far enough forward.

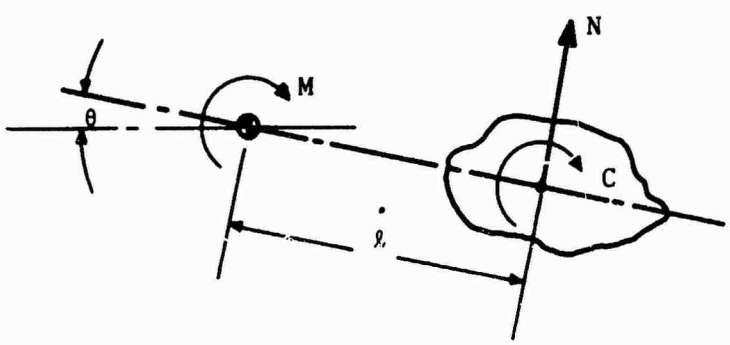


Figure 16. Stability as a Function of CG Position.

In figure 16, assume that a normal force (N) acts at the aerodynamic center, that C is the couple on the body, and $\ell$ is the distance between the CG and the aerodynamic center. Then the moment (M) about the CG is

$$M = C - N\ell$$

Hence

$$\frac{\partial M}{\partial \theta} = \frac{\partial C}{\partial \theta} - \ell \frac{\partial N}{\partial \theta}$$

The body is stable if $\ell > \frac{\partial C}{\partial \theta} \Big/ \frac{\partial N}{\partial \theta}$

Since $\partial N/\partial \theta$ is generally positive, we move the CG forward to increase stability. This is rarely practicable for an ejection seat, although it was accomplished on the Lockheed F-104 Model B downward ejection seat by projecting a heavy skip flow generator forward on the end of a boom. The resulting combination of forward CG and a wake stabilization effect (to be discussed later) resulted in a seat which was stable for small angles of perturbation, in linear, uniform flow.

## Criteria for Spinning

We have shown that the formal requirement for static stability is $\partial M/\partial \theta < 0$. But it is also necessary for the magnitude of the moment M to be small at the angle at which the seat leaves the aircraft. If $\partial M/\partial \theta < 0$, but $M \neq 0$, the seat will start to rotate towards the trim angle (the angle at which $M = 0$), but will often have acquired so much rotational energy by the time it reaches the trim angle that it will overshoot into a region of instability and commence to spin.

It is very misleading to say, as Galigher[3] says of the data for the F-101 seat in figure 12 "the model was longitudinally stable . . .", because $\partial M/\partial \theta < 0$. The relatively large value of $V_m = -3.0$ ft$^3$ at the initial angle of ejection means that the seat will reach the trim angle of -35° with a large angular velocity. Whether it will spin or not depends upon the unknown (because unmeasured) variation of $V_m$ with $\theta$ for angles below -40°, but experience indicates that it probably would spin. Hence, in any reasonable vocabulary, the F-101 seat is unstable in pitch.

A complete criterion for defining static stability must be more rigorous than $\partial M/\partial \theta < 0$.

On the other hand

$$\partial M/\partial \theta < 0, \quad M = 0$$

although correct, is too restrictive. Seat motion can still be satisfactory if $|M| > 0$, so long as its initial angle is not too far from the trim angle, where $M = 0$. This is admittedly a very imprecise statement, and it is difficult to quantize mathematically because the problem, in mathematical form, involves

two degrees of freedom, and the equations are non linear. We have already seen that for pitch, the equation is

$$I\ddot{\vartheta} = V_m q \quad , \text{ and} \tag{5}$$

for velocity (u) the equation is

$$m \frac{du}{dt} = - A_F q \tag{6}$$

where $q = \frac{1}{2} \rho u^2$

$I$ = Seat Moment of Inertia

$m$ = Seat Mass

and the force area ($A_F$) and moment volume ($V_m$) both vary with seat angle $\theta$ in some arbitrary way. It is of some interest to note that if $V_m(\theta)$ and $A_F(\theta)$ are analytical functions, a solution is possible (in principle) if the equations are transformed to a non-dimensional time parameter

$$\tau = \frac{ut}{L} \tag{7}$$

where L is a reference length.

It follows that

$$\frac{d\tau}{dt} = \frac{u}{L}, \quad \frac{d^2\tau}{dt^2} = \frac{1}{L} \frac{du}{dt}$$

Since $q = \frac{1}{2} \rho u^2$, $\quad u = \frac{1}{\sqrt{\frac{1}{2} \rho}} q^{1/2}$

$$\frac{du}{dt} = \frac{du}{dq} \frac{dq}{dt} = \frac{\frac{1}{2}}{\sqrt{\frac{1}{2} \rho}} q^{-1/2} \frac{dq}{dt} = \frac{1}{\rho u} \frac{dq}{dt} = \frac{1}{\rho L} \frac{dq}{d\tau}$$

$$\frac{d\theta}{dt} = \frac{d\vartheta}{d\tau} \frac{d\tau}{dt}$$

$$\frac{d^2\theta}{dt^2} = \frac{d}{d\tau}\left[\frac{d\theta}{d\tau} \frac{d\tau}{dt}\right] = \frac{d\theta}{d\tau} \frac{d^2\tau}{dt^2} + \frac{d\tau}{dt} \frac{d}{d\tau}\left(\frac{d\theta}{d\tau}\right) \frac{d\tau}{dt}$$

$$= \frac{1}{\rho L^2} \frac{dq}{d\tau} \frac{d\theta}{d\tau} + \frac{u^2}{L^2} \frac{d^2\theta}{d\tau^2}$$

$$= \frac{1}{\rho L^2} \frac{dq}{d\tau} \frac{d\theta}{d\tau} + \frac{2q}{\rho L^2} \frac{d^2\theta}{d\tau^2}$$

Making these substitutions in the equations of motion, the velocity equation becomes

$$\frac{dq}{d\tau} = -\left(\frac{\rho L A_F}{m}\right) q \tag{8}$$

The pitch equation is

$$\frac{I}{\rho L^2}\left[\frac{dq}{d\tau}\frac{d\theta}{d\tau} + 2q\frac{d^2\theta}{d\tau^2}\right] = V_m q \tag{9}$$

Dividing throughout by $\frac{2qI}{\rho L^2}$ gives

$$\frac{d^2\theta}{d\tau^2} = \left(\frac{\rho L^2 V_m}{2I}\right) - \frac{1}{2q}\frac{dq}{d\tau}\frac{d\theta}{d\tau}$$

But from equation 8 $\quad \frac{1}{2q}\frac{dq}{d\tau} = -\frac{\rho L A_F}{2m}$

Thus, the pitch equation finally becomes

$$\frac{d^2\theta}{d\tau} - F_A \frac{d\theta}{d\tau} - F_V = 0 \tag{10}$$

where

$$F_A = \frac{\rho L A_F}{2m} \quad [A_F = f(\theta)]$$

$$F_V = \frac{\rho L^2 V_m}{2I} \quad [V_m = f(\theta)]$$

A solution to equation 10 may be obtained if $A_F$ can be expressed as

$$A_F = A_o + \Delta A(\theta) \quad \text{and} \quad \Delta A << A_o$$

Written in the form

$$\frac{d^2\theta}{d\tau^2} = F_V + F_A \frac{d\theta}{d\tau} \qquad (10a)$$

it is clear that the second term on the right-hand side - which is due to deceleration - is tending to increase the angular acceleration. Apart from this, not much additional information about the stability of the system can be gleaned from equation 10, unless one resorts to numerical analysis.

In the real world of engineering problems, if numerical analysis is to be employed, one might just as well solve equations 5 and 6 in real time, for a specific seat-man combination.

The only data on seat drag and pitching moment throughout the entire 360° range of pitch angles is that due to Reichenau, so far as is known. A segmented straight line best fit to his data was constructed, as shown in figures 17 and 18, and equations 5 and 6 programmed in conjunction with it. Seat mass was arbitrarily taken as 10 slugs, and the rather unrealistically high figure of 3.0 ft was used for the radius of gyration. Taking an initial ejection speed of 670 ft/sec at sea level, the program was run with different initial seat angles. As can be seen from figure 19, the seat spun for all ejection angles tried, except for the $\theta_o = -30°$ case.

The reason for the stable behavior when $\theta_o = -30°$ is made clear by figure 21. The seat was evidentally close enough to the -43° trim angle not to overshoot past $\theta = -87°$, where it would have started to spin. The same behavior would be expected if the initial angle were close to the other stable trim point of $\theta = +171°$. But when started at $\theta = 0°$ (or 360°) because area A in figure 21 is so much larger than area B, the seat spins rapidly in a negative direction. It is of interest to note in passing, that even if area B > A, the seat might still spin, since dynamic pressure will be falling continuously as it passes from zone A to zone B.

The variation of angular rate with time during a typical spin is illustrated in figure 20. The maximum rate of rotation is evidently achieved during the first revolution. Thereafter the mean rotation rate is constant (because damping terms have not been included) and the fluctuations about the mean decrease as the airspeed falls off.

Comparing figures 20 and 21, the initial angular acceleration is provided by the negative $V_m$ between the starting point of $\theta = +30°$ and -43°. Area B in figure 21 is then responsible for the small reduction in spin rate. Once past -87°, the spin rate increases rapidly again, reaching an absolute maximum at -188°.

As can be seen from figure 22, the variation of maximum spin rate with initial (ejection) airspeed is linear, so that the foregoing results can be extrapolated to any airspeed. Despite the large radius of gyration assumed, the spin rates are very high, and at a speed corresponding to Mach = 1.0, result in a centri-

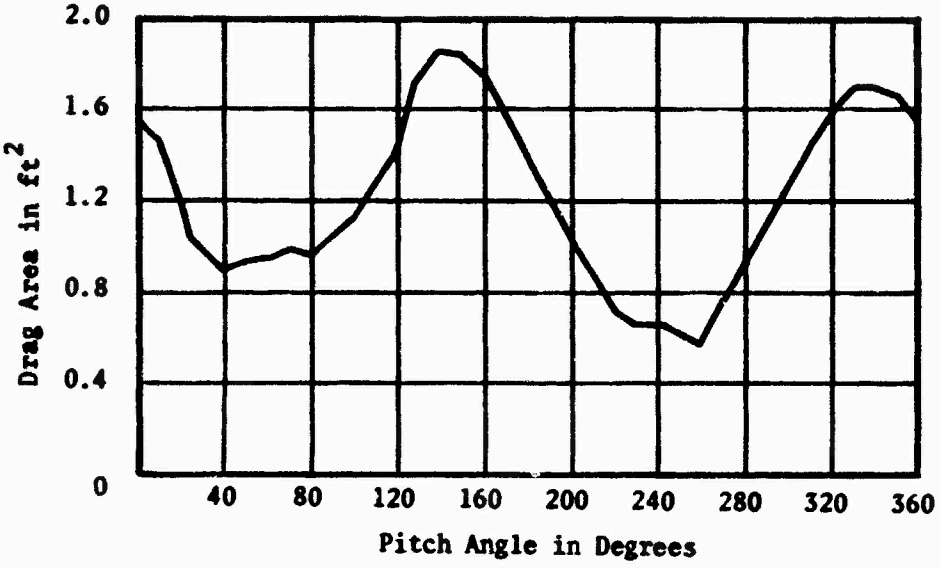


Figure 17. Digitized Fit to the Model Seat Drag Area of Reichenau.[9] M = 0.6 (Half Scale Model; Full Scale Drag Areas are Four Times the Values Shown).

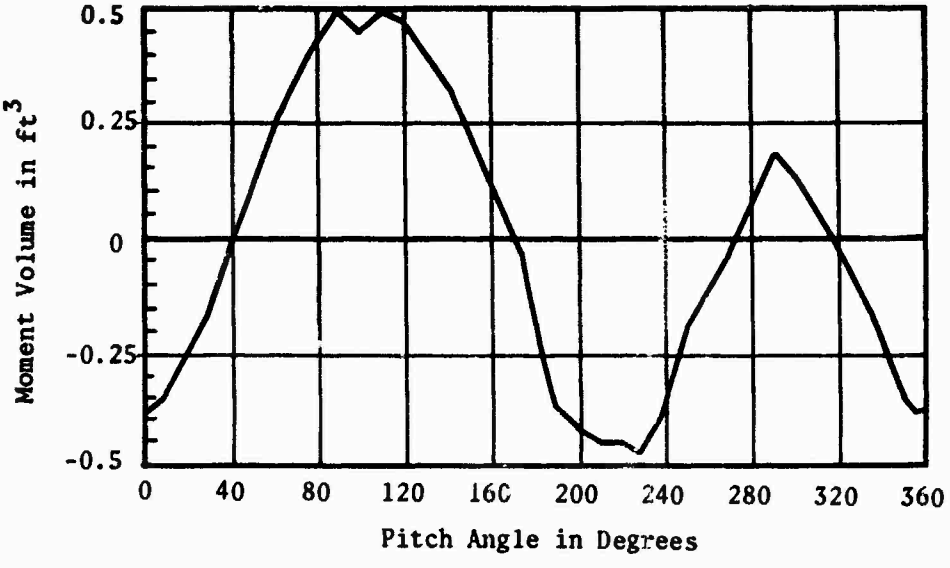


Figure 18. Digitized Fit to the Model Seat Moment Data of Reichenau.[9] M = 0.6 (Half Scale Model; Full Scale Moment Volumes are Eight Times the Values Shown).

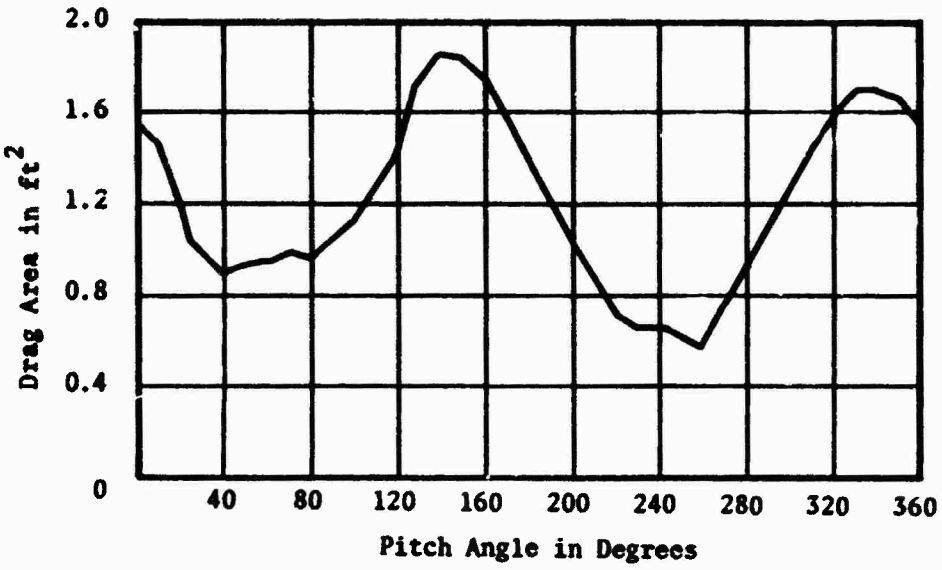


Figure 17. Digitized Fit to the Model Seat Drag Area of Reichenau.[9] M = 0.6 (Half Scale Model; Full Scale Drag Areas are Four Times the Values Shown).

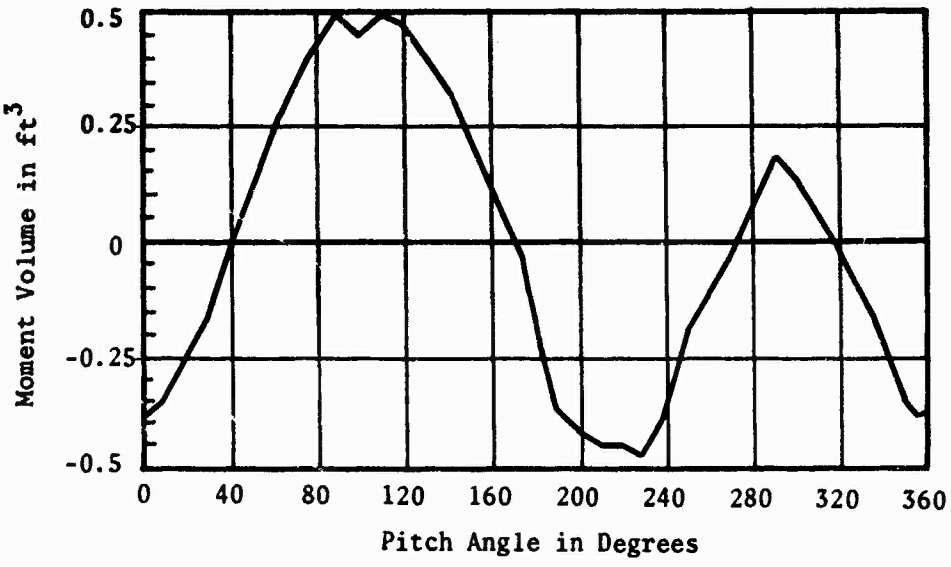


Figure 18. Digitized Fit to the Model Seat Moment Data of Reichenau.[9] M = 0.6 (Half Scale Model; Full Scale Moment Volumes are Eight Times the Values Shown).

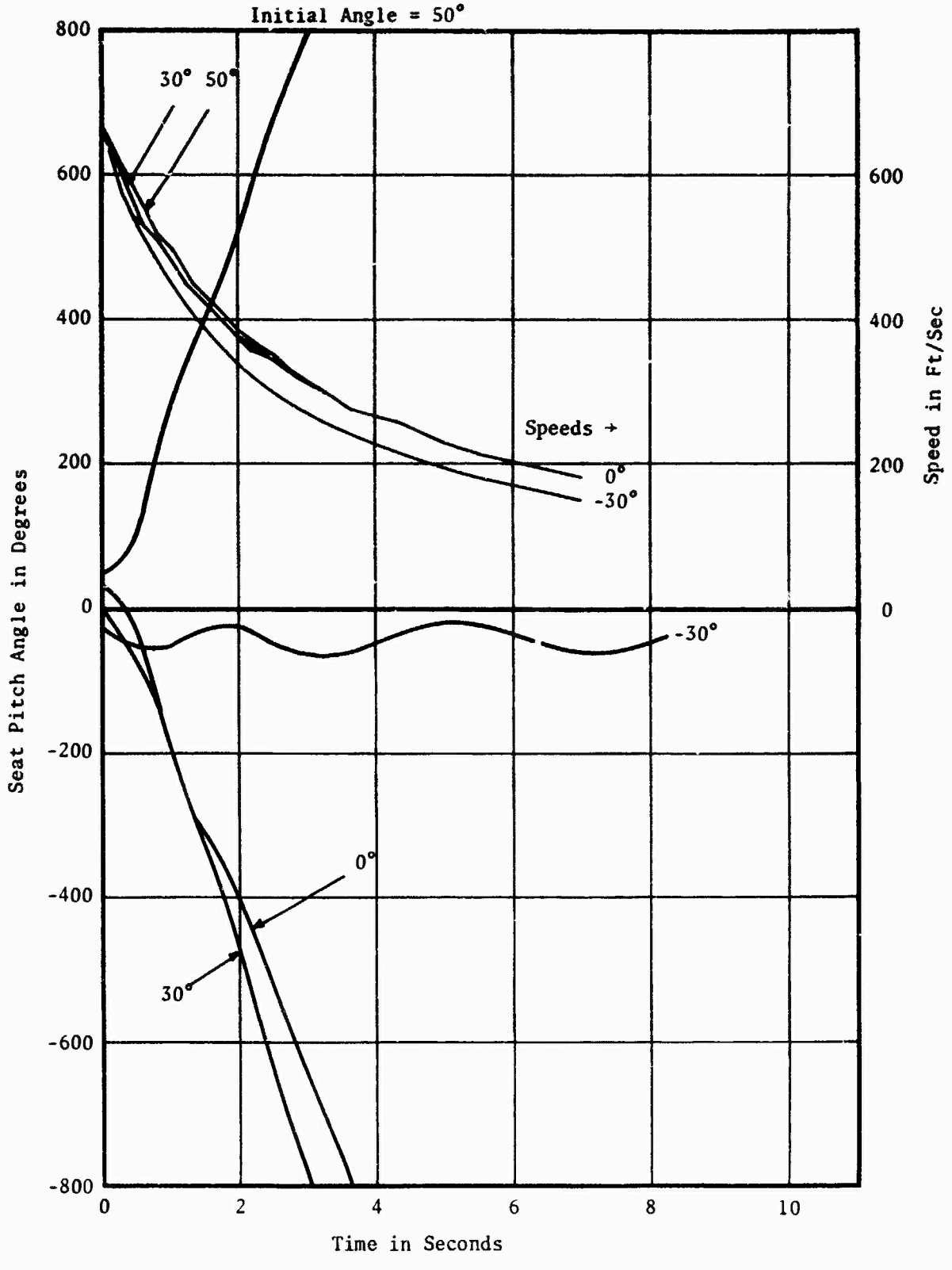


Figure 19. Pitch Motion of an Unstabilized Seat When Ejected at Various Initial Angles, at 670 ft/sec T.A.S., Standard Sea Level. Pitching moment and drag data are taken from Reichenau.[9]

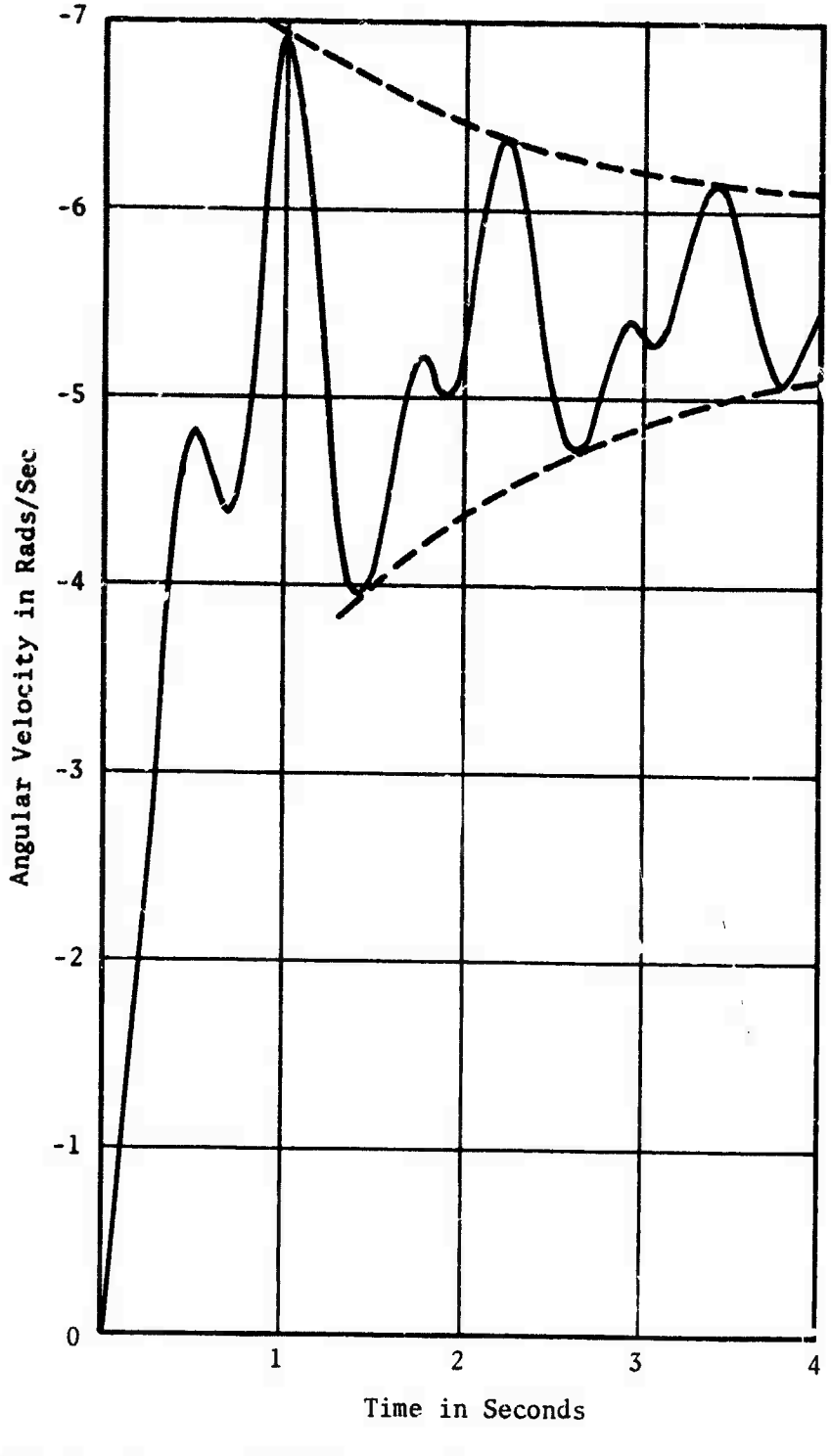


Figure 20. Angular Velocity as a Function of Time for the Case of $\theta_o = +30°$, $r_G = 3.0$ ft at 670 ft/sec T.A.S., Standard Sea Level.

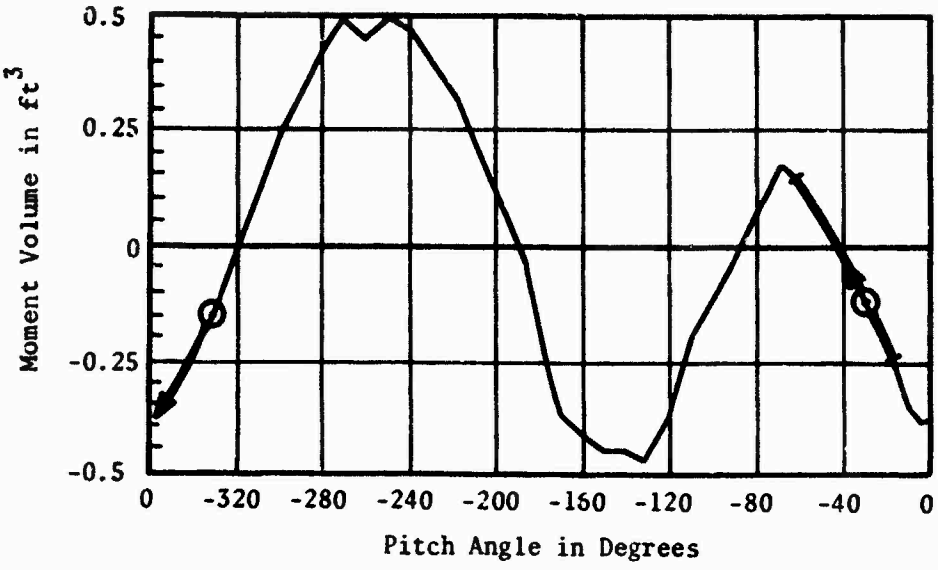


Figure 21. Locus of the +30° and -30° Initial Angle Cases on the Moment Volume Plot. The Arrow Shows the Initial Direction of Rotation from the Initial Condition ⊙.

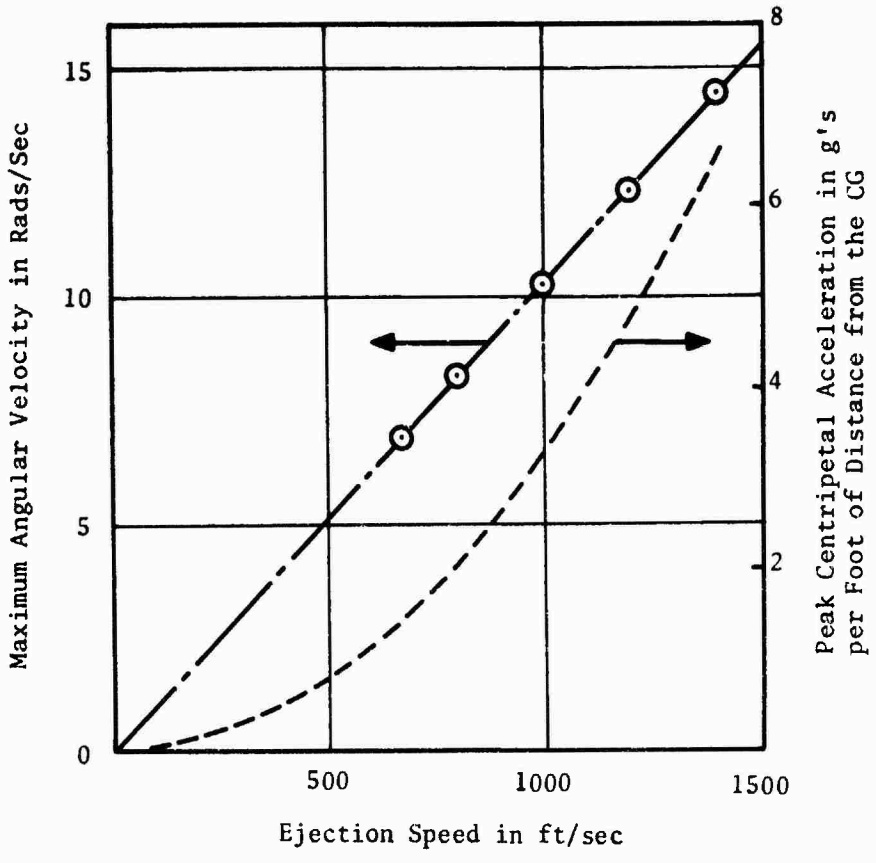


Figure 22. Variation of Maximum Angular Velocity With Initial Airspeed, for the Case of $\theta_o$ = +30°, $r_G$ = 3.0 ft.

fugal acceleration of 4.65 g/foot of distance from the CG; about 14 g at the seat occupant's feet and head, say.

Decreasing the radius of gyration increases the spin rate, as shown by the table below.

Maximum Rotational Rates at 670 ft/sec Initial Velocity

| Initial Angle | 50° | 30° | 0° | -30° | degrees |
|---|---|---|---|---|---|
| Spin Rate for $r_G$ = 3.0 ft | 7.19 | 6.92 | 6.10 | 0.99 | rads/sec |
| Spin Rate for $r_G$ = 2.0 ft | 11.3 | 11.1 | 9.81 | 1.53 | rads/sec |

Roughly, the maximum spin rate seems to vary inversely as the radius of gyration, but no simple correlation is possible. This is to be expected from the form of equation 10.

## Conventional Methods of Applying a Stabilizing Moment

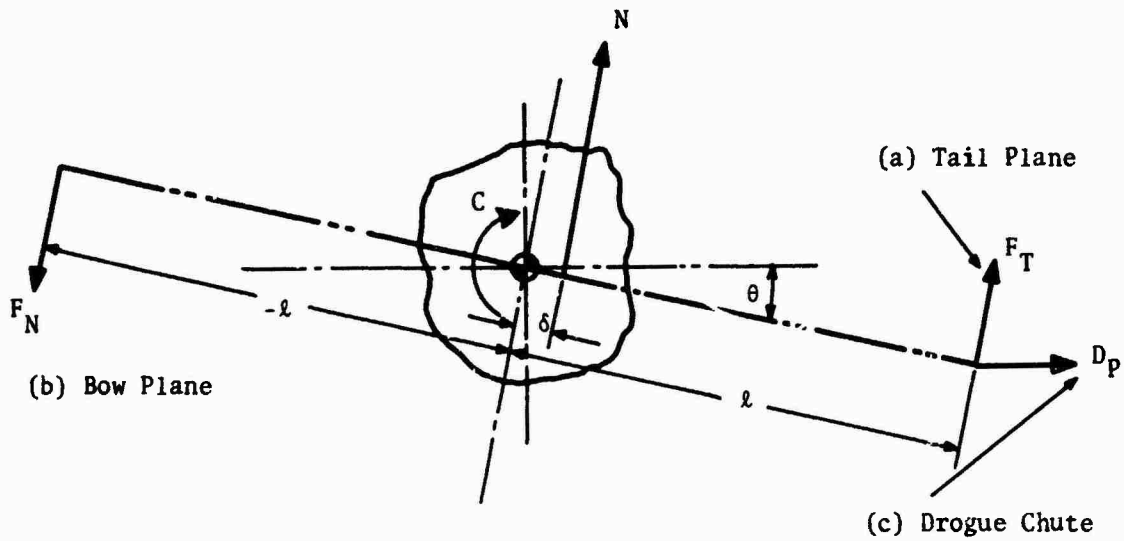


Figure 23. Three Ways of Opposing an Unstable Moment.

The conventional device for stabilizing a body is the tailplane, which is employed in nature by most birds and fish, and seems to have been first proposed for heavier than air flight by Leonardo da Vinci. Its principle attraction for aircraft is its relatively low drag.

If the normal force (N) on the body acts at a distance δ behind the CG, the moment about the CG of a tailplane-equipped body is

$$M = C - N\delta - F_T\ell$$

$$\therefore \quad \frac{\partial M}{\partial \theta} = \frac{\partial C}{\partial \theta} - \left[ \delta \frac{\partial N}{\partial \theta} + \ell \frac{\partial F_T}{\partial \theta} \right]$$

We see that the normal force acts in the same way as a tailplane stabilizing the body if $\delta > 0$ and $\partial N/\partial\theta > 0$.* For most ejection seats $\partial N/\partial\theta > 0$ near $\theta = 0$ but no information as to its aerodynamic center is available,** so that we cannot tell if $\delta$ is positive or negative. Whichever it is, static stability is obtained if

$$\ell \frac{\partial F_T}{\partial \theta} > \left[ \frac{\partial C}{\partial \theta} - \delta \frac{\partial N}{\partial \theta} \right]$$

$\ell \dfrac{\partial F_T}{\partial \theta}$ can be increased by

- increasing the moment arm $\ell$
- increasing $\partial F_T/\partial\theta$ by increasing
  - tailplane area $S_T$
  - tailplane aspect ratio

An ejection seat is almost unique in aeronautics in that it is a compact bluff body with very high drag. Because of the need for compactness, it is almost impossible to have fins fixed on the end of a tailboom prior to ejection; such a stabilizing assembly must be deployed after the seat has cleared the aircraft. This entails the twin disadvantages of mechanical complexity (and weight) and the fact that the stabilizer is not in place when it is first needed. At 500 Kts IAS, a typical seat can have an initial pitch acceleration as high as -150 radians/sec$^2$. Thus, it would require only 70 millisecs to achieve a pitch angle of one quarter of a radian, at which time its pitch rate would be about 10 rads/sec. One can see that a deployable tailplane would have to be in place in much less time than this; a rather formidable engineering problem.

---

* In fact, if $\delta(\partial N/\partial\theta)$ is large enough, the tailplane can be located in front of the CG ($\ell$ negative) to give a canard configuration. In this case, the function of the auxiliary surface is to trim and to provide pitch damping.

** A reasonably detailed review of the literature indicates that no one has ever determined the center of pressure of the normal forces on an ejection seat; or what amounts to the same thing, measured forces and moments about more than one axis center.

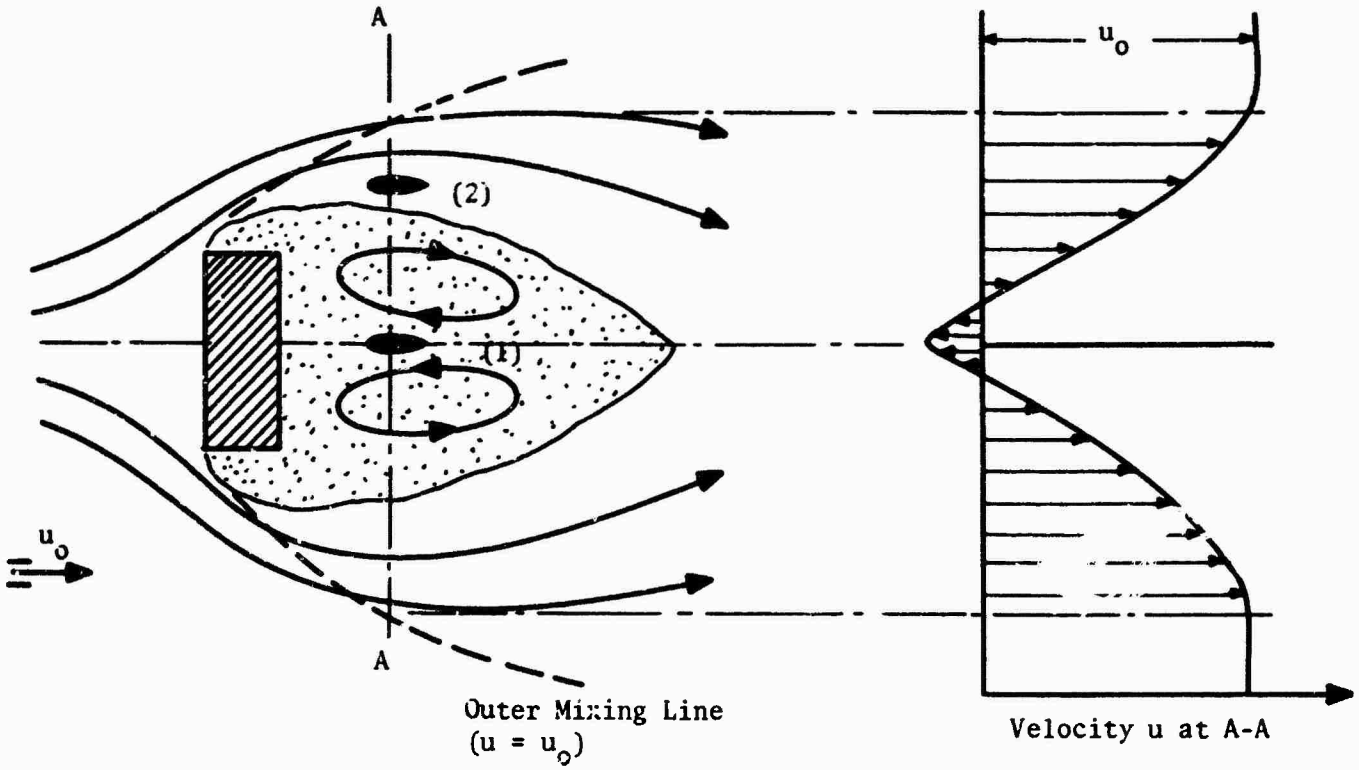


Figure 24. Idealization of an Ejection Seat Wake.

There are also purely aerodynamic problems for a tailplane to contend with when located behind a bluff body. As indicated in figure 24 the wake behind a bluff body is extensive, and it is well recognized that a surface located at position (1) would be quite ineffective. The problems associated with position (2) in figure 24 are not so generally recognized, however. The local streamlines may be moving outwards or inwards, giving rise to corresponding forces on a surface at zero incidence to the undisturbed flow. Additionally, the velocity gradient ("sheared flow") gives rise to an outwards acting force which has been analyzed by a number of investigators. An early treatment by Milne-Thompson[13] for a cylinder of radius (a) gives this force as

$$F = \pi a^2 \rho u_a \frac{du}{dy} \qquad \text{(per unit span)}$$

or

$$C_{F_G} = \frac{F}{2a \frac{1}{2} \rho u_a^2} = \frac{a}{u_a} \frac{du}{dy}$$

where $u_a$ is the velocity at the cylinder's centerline, and du/dy is the velocity gradient normal to the air flow. Notice that the coefficient is independent of velocity and geometric size.

For the wake of a typical ejection seat, $C_{FG}$ on a one-foot diameter cylinder is in the range .05 - 0.2, which corresponds to forces comparable with those induced by circulation for small pitch angles. One can see that if nose down pitch angle (for example) moves a tail surface into a region of greater velocity gradient, the stabilizing negative force due to the circulation change will be offset by an increased positive force due to the velocity gradient.

Finally there is the direct effect of the wake velocity decrement on the tailplane circulation force to consider, an idealized geometry for which is illustrated in figure 25.

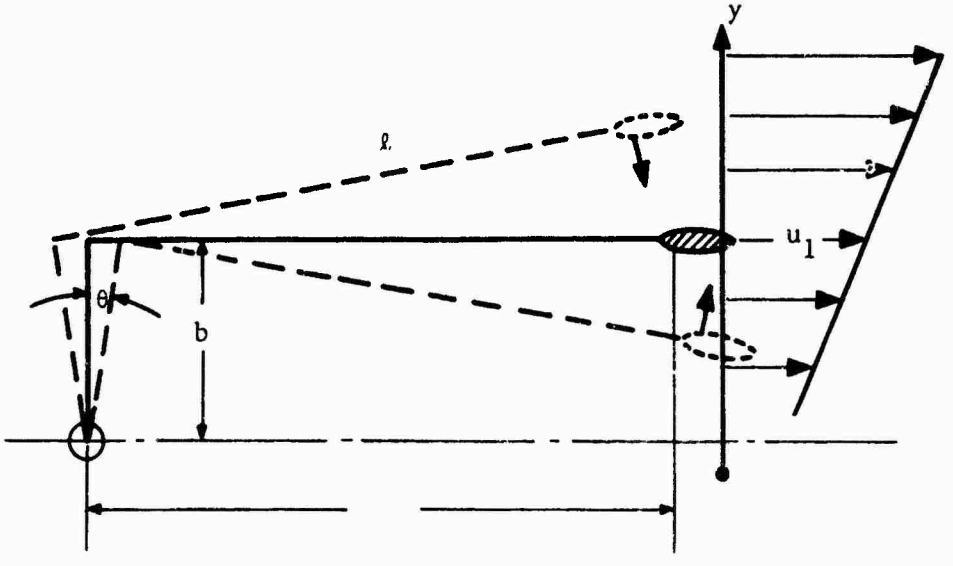


Figure 25. Tailplane in a Linear Wake Gradient.

From figure 25 if the velocity gradient du/dy is assumed to be linear, for simplicity, then the tailplane circulation-induced moment about the CG, due to a pitch angle θ is

$$\Delta M_T = F_T \ell = S_T \ell \frac{1}{2} \rho u^2 \frac{\partial C_N}{\partial \alpha} \sin \theta$$

But

$$u = u_1 \frac{du}{dy} \ell \tan \theta$$

$$\therefore \Delta C_{MT} = \frac{F_T \ell}{\frac{1}{2}\rho u_o^2 S_T \ell} = \frac{\partial C_N}{\partial \alpha} \sin \theta \, (u_1/u_o)^2 \left[ 1 - \frac{du}{dy} \frac{\ell}{u_1} \tan \theta \right]^2$$

The term $(\ell \tan \theta/u_1)(du/dy)$ inside the squared bracket is identical to Milne-Thompson's shear flow force equation just discussed.

Differentiating with respect to 6, we obtain for small angles $\theta$

$$\frac{1}{\left(\frac{u_1}{u_o}\right)^2 \frac{\partial C_N}{\partial \alpha}} \frac{\partial C_{MT}}{\partial \theta} = 1 - 2 \frac{du}{dy} \frac{(\ell \tan \theta)}{u_1}$$

Since $du/dy$ is of order $u_1/\ell \tan \theta$, this can clearly be negative, implying that the aerodynamic surface can degrade rather than improve static stability.

When two surfaces are mounted on either side of the wake (as in the case of twin yaw fins) the combination can still contribute instability, rather than stability, from the combined effects of streamline displacement, shear flow forces and dynamic head loss.

Visconti and Naber[7] found this to be so when they added small fins to a $\frac{1}{8}$ scale seat and found that the yaw instability was actually increased by the fins. They did not explain the phenomenon, other than to observe that "inasmuch as the fins caused the model to become unstable, the adverse fin effectiveness is attributed to large flow angularities which probably exist about a blunt body of this nature."*

Returning now to figure 23 we note that a second conventional method of stabalizing a bluff body - and by far the most usual for ejection seats - is the drogue parachute. In principle, any drag producing device (such as a "balloot" for example) may be used. With the chute deployed, the moment about the CG is

$$M = C - N\delta - D_p \ell \sin \theta$$

$$\therefore \frac{\partial M}{\partial \theta} \simeq \frac{\partial C}{\partial \theta} - \left[\delta \frac{\partial N}{\partial \theta} + \ell D_p\right]$$

Comparing this with the equivalent tailplane equation, we see that

$$\ell D_p \equiv \ell \frac{\partial F_T}{\partial \theta}$$

i.e. $$C_{D_p} S_p \equiv \frac{\partial C_L}{\partial \alpha} S_T$$

---

* They may have been uneasy about their measurements because they did not present yaw moment coefficient $C_M$ data for this configuration, even though all other moments and forces are given.

Since $C_{D_p} \approx 0.6$, and $2 < \frac{\partial C_L}{\partial \alpha} < 5$, the required parachute projected area is almost an order of magnitude larger than the area of an equivalent tailplane having the same moment arm ($\ell$). Also, since a drogue chute is usually centered in the wake, its effectiveness is correspondingly less still. But, in practice, these disadvantages are usually more than offset by the light weight of the drogue system, and the fact that, because the force is rearward acting, a light and easily deployable bridle can be used in place of a boom, to transmit corrective moments to the seat.

Drogue chute deployment still takes a finite time, however, and much ingenuity has gone into minimizing this time. Ideally, the chute should be fully deployed before the seat leaves its rails, and this is often hard to accomplish when the ejection speed is high.

Additionally, as we saw earlier, chute filling time does not vary inversely with time. Relatively speaking, it opens more slowly at the higher speeds. There is also, usually, a fixed delay time associated with firing the deployment mortar. Thus, as ejection speed increases, the unstabilized seat can reach larger and larger perturbation angles, and acquire larger and larger amounts of rotational momentum, and at some critical speed, the drogue chute is unable to stop the seat spinning. The bridle then wraps around the spinning seat and the chute deflates.

Even if these problems could be circumvented, it is generally found that above a certain critical speed, a chute does not open at all. This phenomenon is called "squidding." The writer has related it to parachute elasticity theoretically;[5] Heinrich[8] has demonstrated its dependence on elasticity experimentally.

## SOME NEW APPROACHES TO STATIC STABILITY

Referring again to figure 23, the conventional tailplane stabilizes because the moment arm ($\ell$) and change of lift or normal force with angle ($\partial C_N/\partial\theta$) is positive. If they could both be made negative, the equations would be unchanged, and the system would still be stable. Similarly, there is a negative image of drogue stabilization; namely a negative drag device (a propulsor) in front of the body. If it had a bridle to transmit moments, a tractor rocket could stabilize in this way, provided it was itself stable.

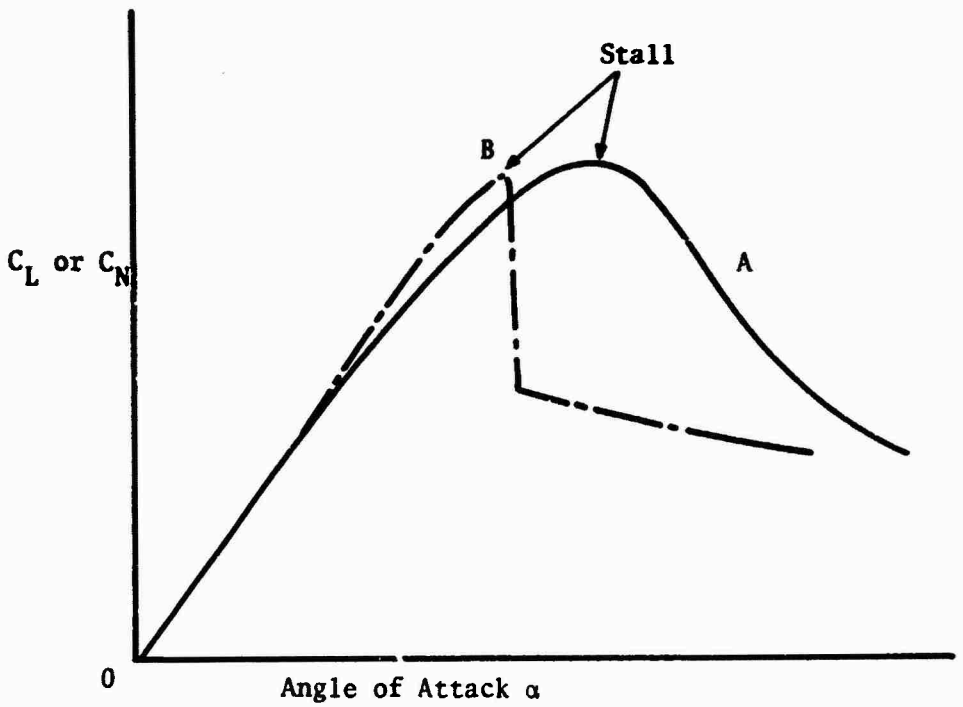


Figure 26. Two Different Lift Curves.

Although airfoil lift curves vary widely, we may roughly characterize them under the two groups sketched in figure 26; gradual stall (curve A) and discontinuous stall (curve B). The latter type of stall may be made piece-wise continuous by the use of wing twist and boundary layer fences.

In the angle of attack range above stall, there is a region where $\partial C_N/\partial\alpha < 0$, so that an ejection seat (or other body) can be stabilized by the opposing stalled surfaces, as indicated in figure 27.

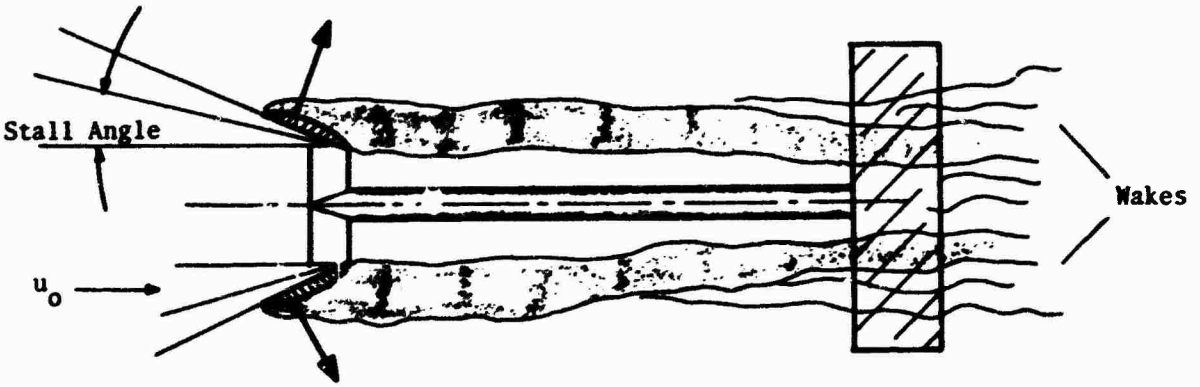


Figure 27. A Stalled Bow Stabilizer.

If the system in figure 27 pitches bow up, the lift on the upper foil is reduced, and that of the lower foil increased, so that there is a restoring force. Unfortunately, a positive pitch rate $d\theta/dt$ reduces the relative air flow angle of the top foil and increases that of the bottom, so that the damping is negative. Unless there are larger sources of positive damping in the system, therefore, a body so stabilized will oscillate with increasing amplitude. This defect does not necessarily rule it out for ejection seat applications, however.

A stalled bow stabilizer will shed two wakes onto the body behind it, and these wakes will have an additional stabilizing effect. With the bow pitched up, the wakes will impinge on the upper half of the ejection seat, reducing its drag, and giving rise to an additional restoring moment. The damping associated with this additional moment will probably be negative, although this aspect could profitable stand more detailed investigation.

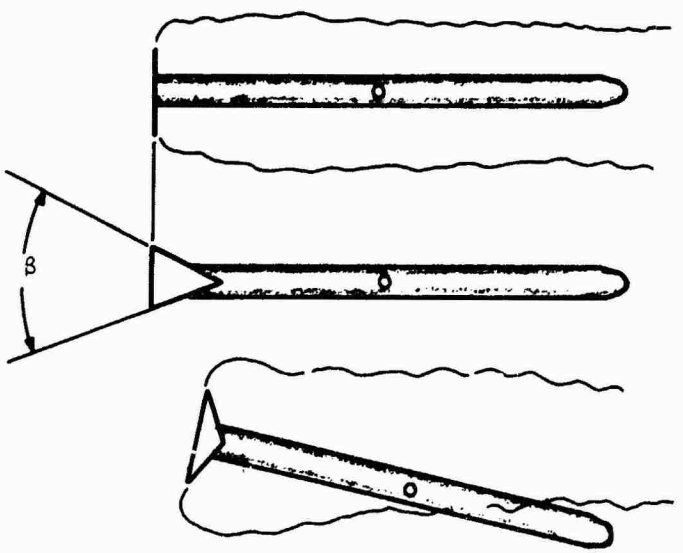


Figure 28. Slender Bodies With Bow Wake Stabilizers.

The wake effect, which is ancillary to the stalled bow stabilizer, can, at least in theory, be employed by itself. The writer knows of no experimental data for the stabilization of bluff bodies by this technique, although the Lockheed F-104, Model B downward ejection seat may have experienced this effect to some extent. Figure 29 shows some rather dramatic results for slender bodies, and in this case at least, the damping was found to be positive. It is probable that for the smaller included cone angles, some of the restoring moment comes from a stabilizing force on the cone, the mechanism being the same as for the stalled bow stabilizer. For the flat plate case, only the wake stabilization effect can be present. The wake effect for $\beta < 180°$ will presumably be greater than for the flat plate, because the cone drag and wake diameter will increase with decreasing $\beta$.

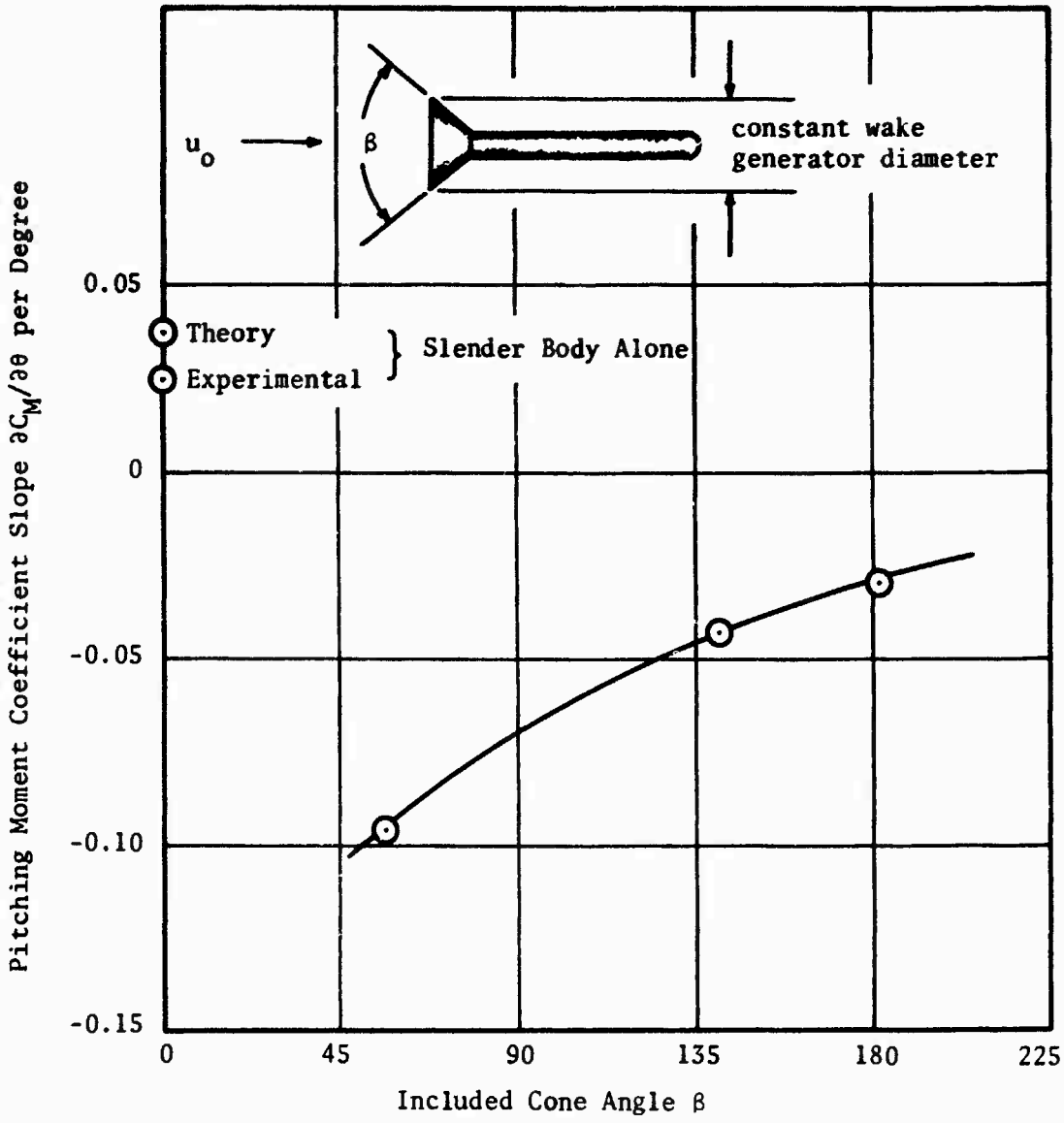


Figure 29. Pitching Moment Derivative for Slender Bodies With and Without Bow Wake Stabilizers. (Reference 10)

Because of the distortion of streamlines around an aircraft, one might expect wake stabilization to be particularly susceptible to aircraft proximity interference. The attitude for trim in the curved flow near the aircraft might be quite different from the trim attitude in free flight. And once such a system is sufficiently perturbed for the wake not to impinge on the seat at all, then all stability is lost. That is to say, a wake stabilization system will only work for small angles of perturbation and flow distortions.

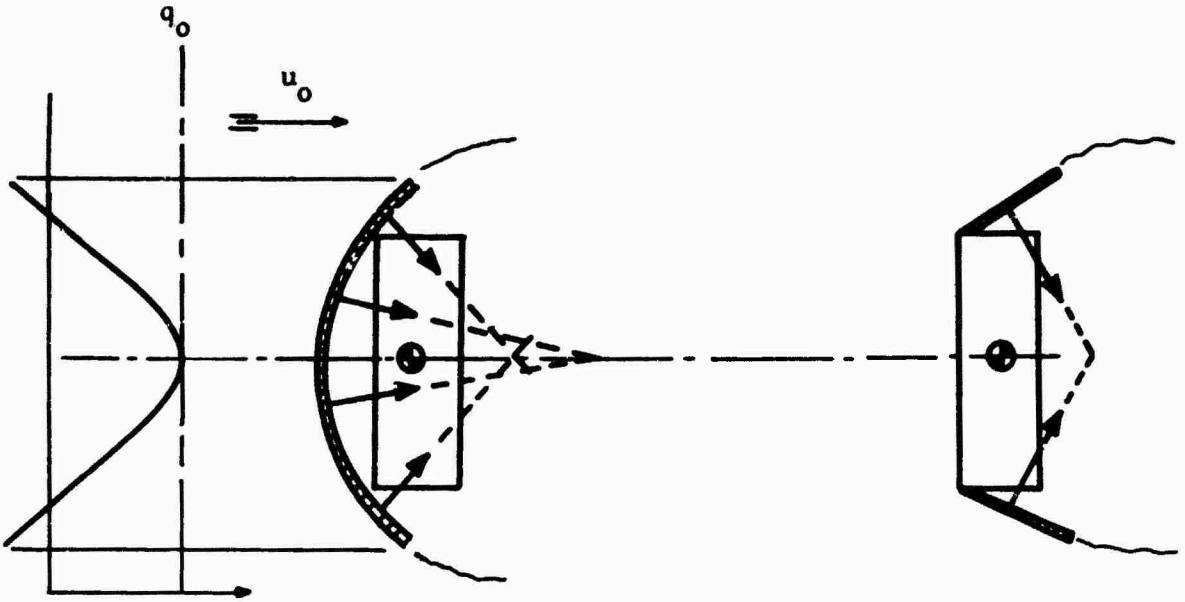


Figure 30. In-Plane Drag Stabilizers.

Figure 30 shows a quite different approach, in which stabilization is obtained by the change in pressure on a continuous surface or discrete surfaces. The roughly hemispherical surface* shown on the left of figure 30 is stable, if the rays normal to its surface pass behind the CG, and the reason is obvious from the pressure distribution. This stabilization technique is analogous to the stabilizing heat shields used in the NASA reentry capsules Mercury, Gemini, and Apollo.

An adaptation of this approach, which is also related to figure 15, is shown on the right of figure 30. As the seat pitches nose up, the normal force on the upper plate is reduced, and that on the lower plate increased, resulting in a stabilizing moment. Damping will be positive. Figure 31 illustrates how such stabilizing plates might be applied to an ejection seat.

As shown in figure 31, drag stabilization plates could be mounted by their leading edges to the seat structure, and actuated mechanically, by ram air, or by gas from a generator.

*Suggested by E.G.U. Band of Payne Inc.

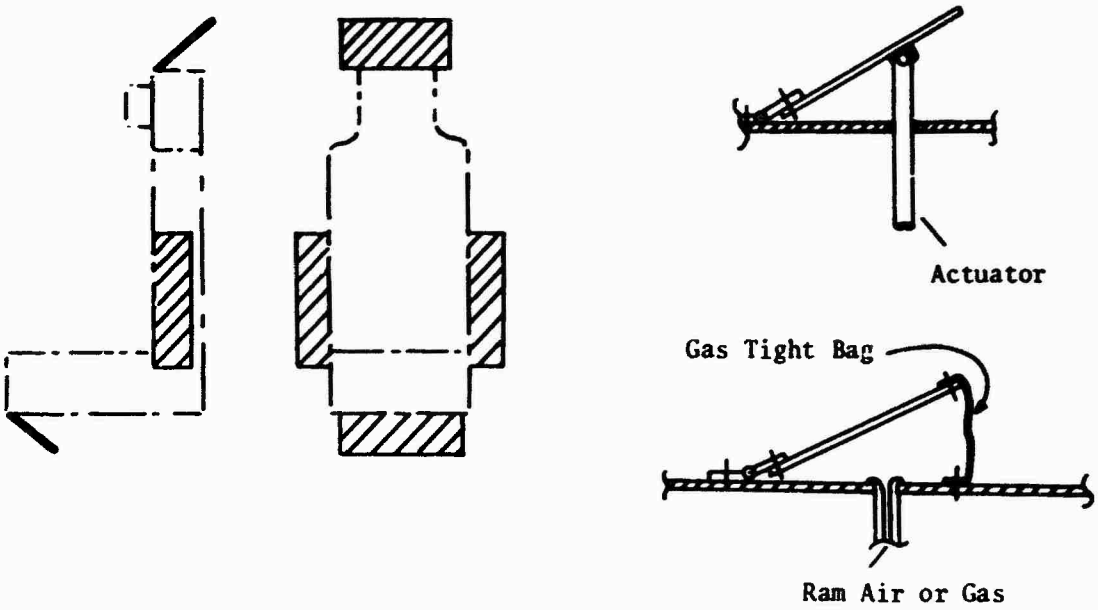


Figure 31. Typical Locations for In-Plane Dtag Stabilizing Plates on an Ejection Seat.

Since it is important for a seat to be stable the moment it leaves the rails, such stabilizing plates would need to be in their deployed condition at that time. There are many, many ways of achieving this, and selection of an optimum configuration for each particular seat design would clearly take some time. A schematic example of a possible configuration is given in figure 32 below.

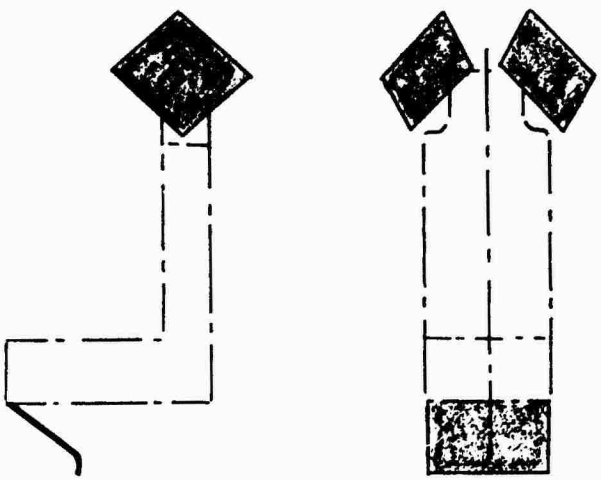

Figure 32. An In-Plane Stabilization Configuration Suitable for Deployment Half-Way Up the Rails.

In such a configuration, the upper plates could start to rotate into position as the seat started to accelerate up the rails. Not only could they be locked in place by the time the seat was half-way up the rails; with proper linkage design, they could also function as helmet loss preventers. The lower plate could also be deployed in the cockpit; in fact, one simple way of deploying it would be to attach its free edge to the cockpit floor structure by a frangible link.

So far, we have discussed in-plane stabilizers as if the seat itself was unstable ($\partial C_m/\partial\theta > 0$), but the absolute value of $C_m$ was negligible in the "flight" attitude. A study of the meager data available shows that while this is true for yaw, it is generally not the case for pitch; put crudely, the drag center is either above or below the CG, and a seat will pitch nose down or up after leaving the rails. This is analogous to the situation shown in figure 33 below.

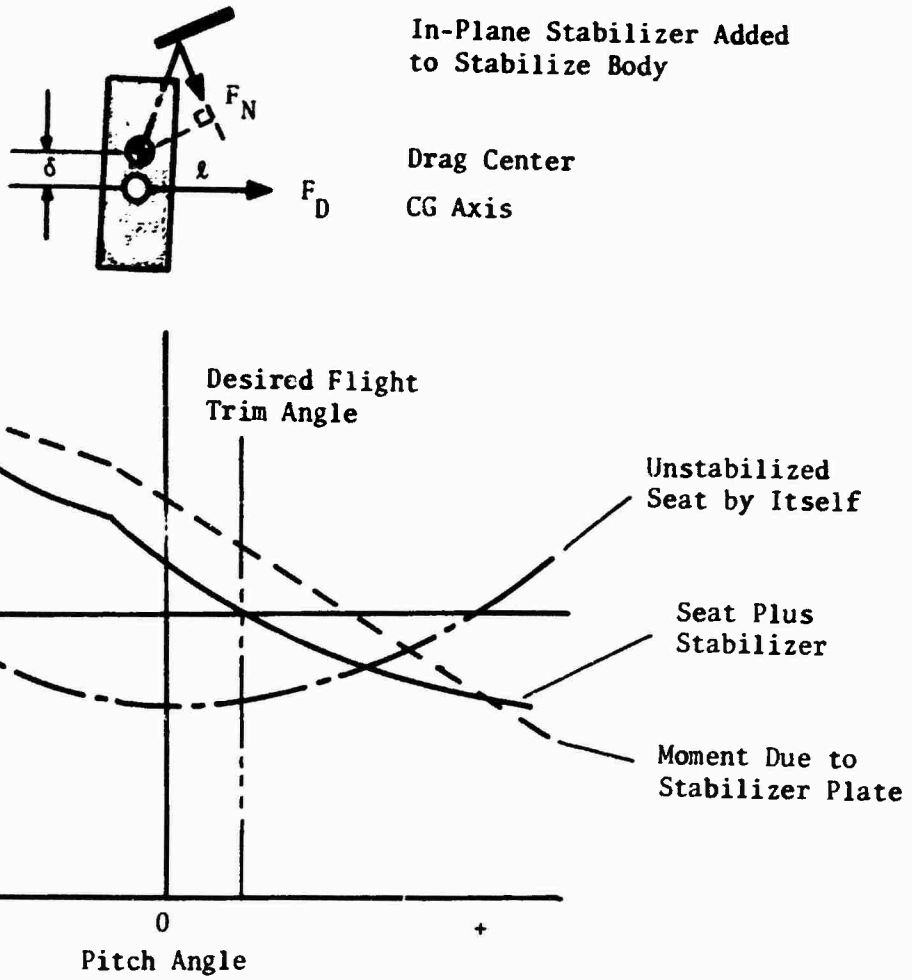


Figure 33. Stabilizing a Seat Which Has a Drag Imbalance.

The condition for trim at the desired angle is, of course,

$$\ell F_N = \delta F_D$$

Since $\ell >> \delta$, it is clear that quite a small stabilizer plate will generally be sufficient, since both $C_D$ and $C_{N\theta}$ will be of the order of unity. Whether the requirement for stability ($\partial C_m/\partial\theta < 0$) will increase the size of the plate depends upon the particular seat, but in general, for the seats we have data on, a plate large enough to trim will also stabilize.

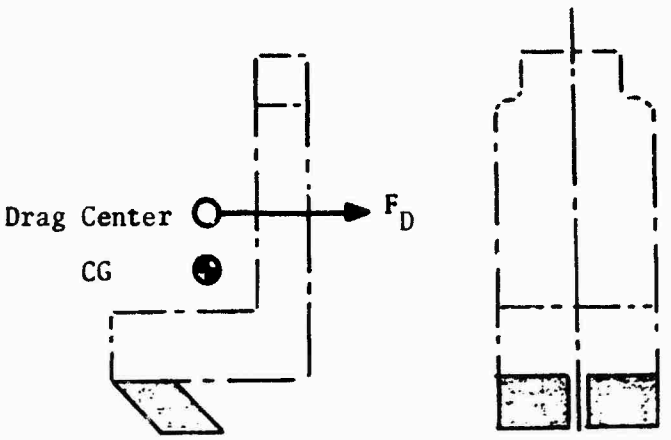


Figure 34. In-Plane Stabilization Plate Configuration Suitable for a Seat Which Has a High Drag Center.

Figure 34 illustrates a practical embodiment of an in-plane stabilizer applied to a seat that has a high drag center, and is unstable in both pitch and yaw. It is somewhat paradoxical that this stabilizer is the simplest of any known solution, not only to design and build for a new seat, but also to retrofit to existing seats.

The stabilizing configurations just described might be suitable for retrofit to existing ejection seats, as well as for new designs. When considering a completely new escape system, particularly if it is for a new aircraft, it might be profitable to consider whether the seat structure itself could be shaped in such a way as to be inherently stable without the need for deployable excrescences; or at least so shaped as to minimize static instability and thus minimize the size of remedial stabilizers.

It is certainly true that the pitching moment curves of the seats tested in References 3, 7, and 9 are completely different. The first has a positive $C_m$ at the ejection angle; the second and third, negative $C_m$. The first has $\partial C_m/\partial\theta \approx 0$ at the ejection angle; the second has an unstable slope; the third has a stable slope at the ejection angle, but will spin into a region of instability because of its negative $C_m$. If such differences can randomly exist, there is latitude for improving the situation with other shapes.

The size of the stabilizing plates so far discussed is somewhat conjectural. Sizing presents difficulties at the moment because of lack of data as to the variation of normal force with angle. Analysis of the closely similar configuration shown in figure 35 below is possible, however, because the plates are assumed to be far enough separated from the seat to act as wings.*

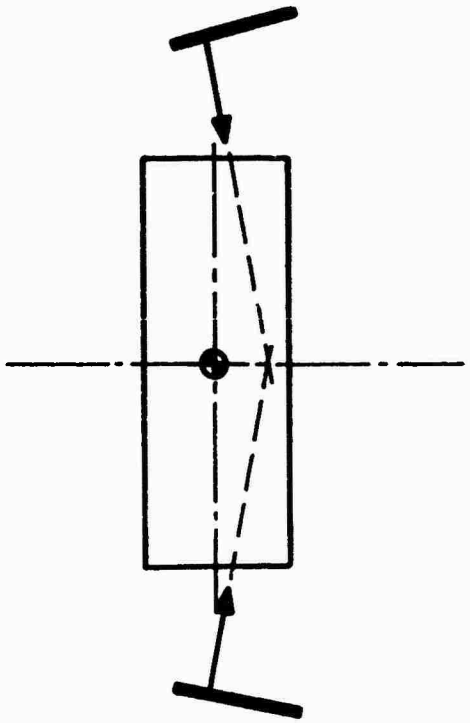

Figure 35. The In-Plane Stabilizer Configuration With Two Unstalled Vanes.

In concluding this section, it is of interest to note that a wing can be trimmed by a form of in-plane stabilizer, as illustrated in figure 36. Taking moments about the CG

$$M = Dh \cos \alpha - La \cos \alpha + M_o$$

which for small angles becomes

$$C_m = \frac{M}{\frac{1}{2} \rho u_o^2 S_W c} = \frac{(C_D S)_B}{S_W} \frac{h}{c} \quad \frac{a}{c} \frac{\partial C_L}{\partial \alpha} \alpha + C_{mo}$$

---

* Note that the plates are assumed to have sharp leading edges so that nose suction cannot reduce the induced drag, which is essentially given by $C_{D_i} = C_n \alpha$. Rounding the nose of the plates would move the center of effort forward and degrade stability!

$$\therefore \quad \frac{\partial C_m}{\partial \alpha} = -\frac{a}{c}\frac{\partial C_L}{\partial \alpha}$$

The wing/stabilizer combination is therefore stable, and it is the natural stability of a wing when the CG is forward of the aerodynamic center. The true function of the stabilizer in this case is to provide a trimming moment so that the wing can fly at a positive angle of attack and develop lift. It also supplies pitch damping of magnitude

$$\frac{\partial C_m}{\partial \dot{\alpha}} = -2\frac{h}{c}\frac{h}{u_o}\frac{S_B}{S_W}C_D$$

A free flying model utilizing these principles, designed and built by Payne Inc.'s Anthony J. Euler, is illustrated in figures 37 and 38.

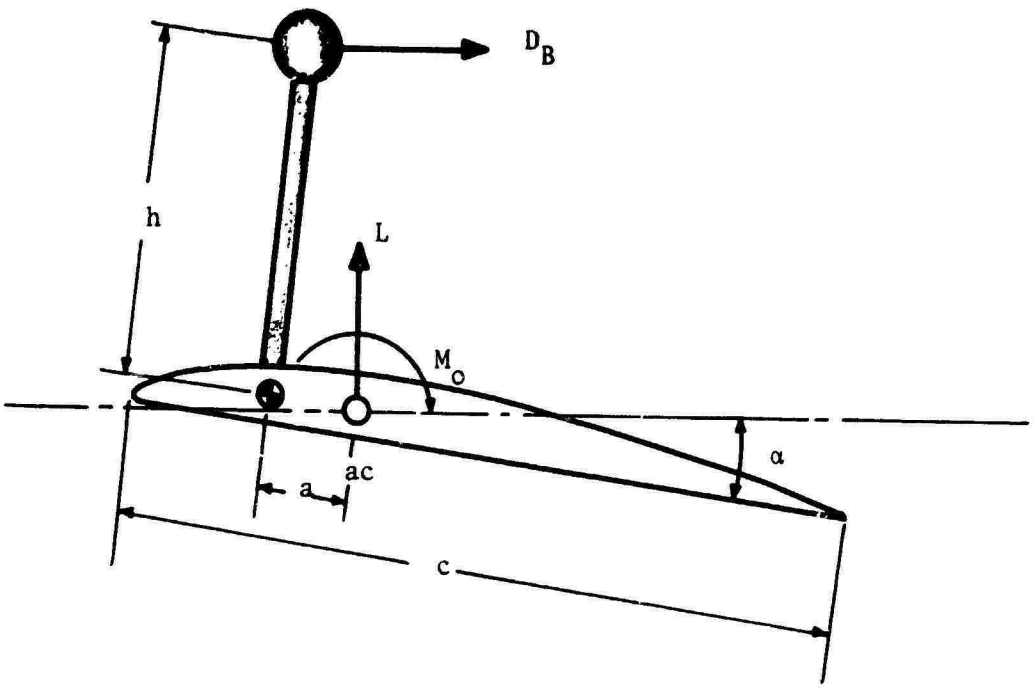


Figure 36. A Drag-Trimmed Wing.

The next section of this report is devoted to analyzing the stability characteristics of the separated plate in-plane stabilizer configuration, on the assumption that interference effects between the seat and the plates can be neglected. A number of analytical procedures naturally suggest themselves. Perhaps the simplest, conceptually, is to regard the plates as "differential drag" devices. With a bow-up movement, the drag of the upper plate is reduced, because it has a smaller angle to the flow, and the drag of the lower plate is increased. The actual analysis of such a model is believed to be somewhat more involved than the normal force method of calculation finally selected.

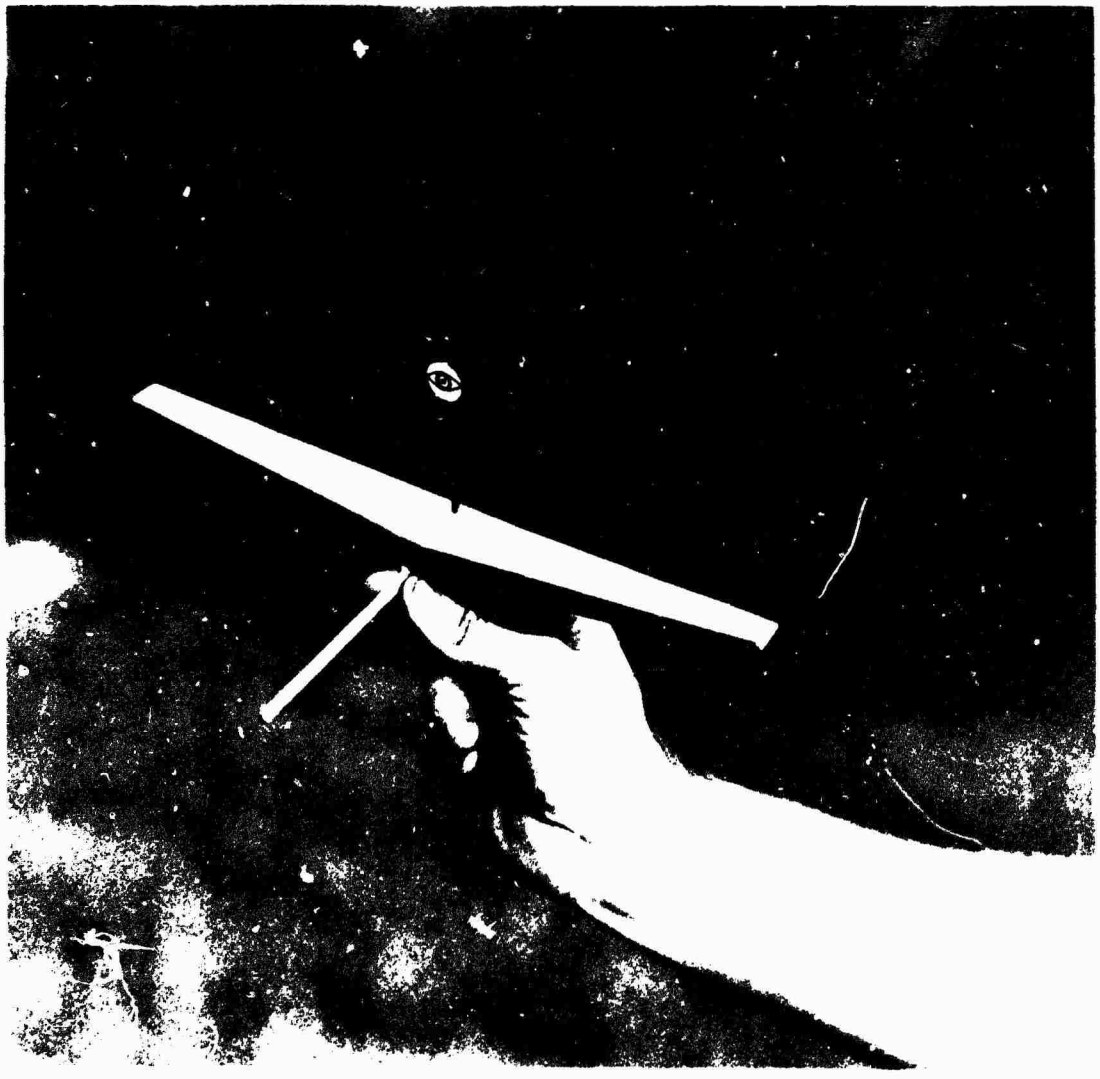

Figure 37. Top View of a Drag Plate Stabilized Flying Model. The Boom Projecting Forward Carries a Small Ballast Weight to Trim the Model.

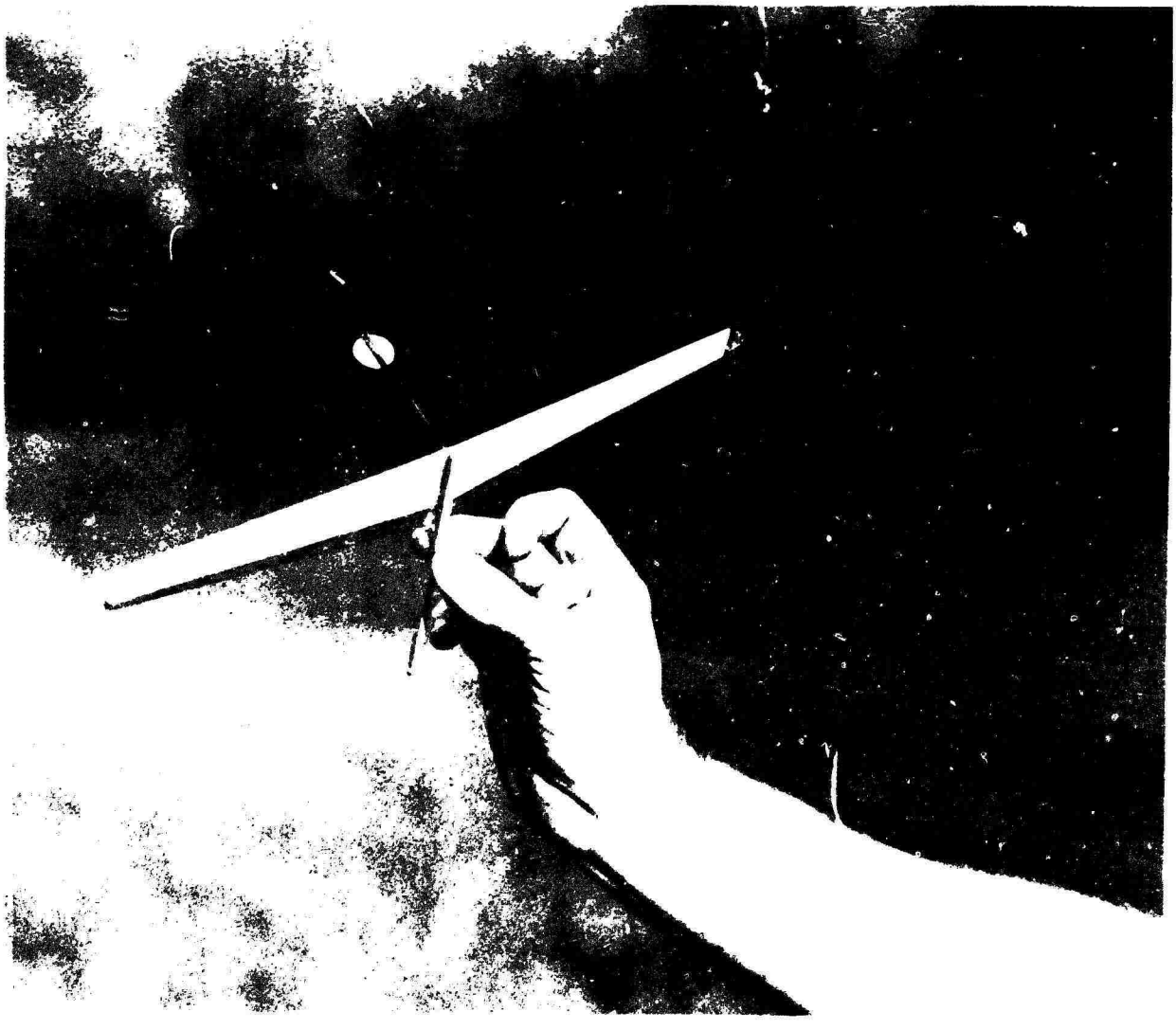

Figure 38. Underneath View of a Drag Plate Stabilized Flying Model.

## ELEMENTARY THEORY OF THE STATIC MOMENT DUE TO AN IN-PLANE STABILIZER PLATE

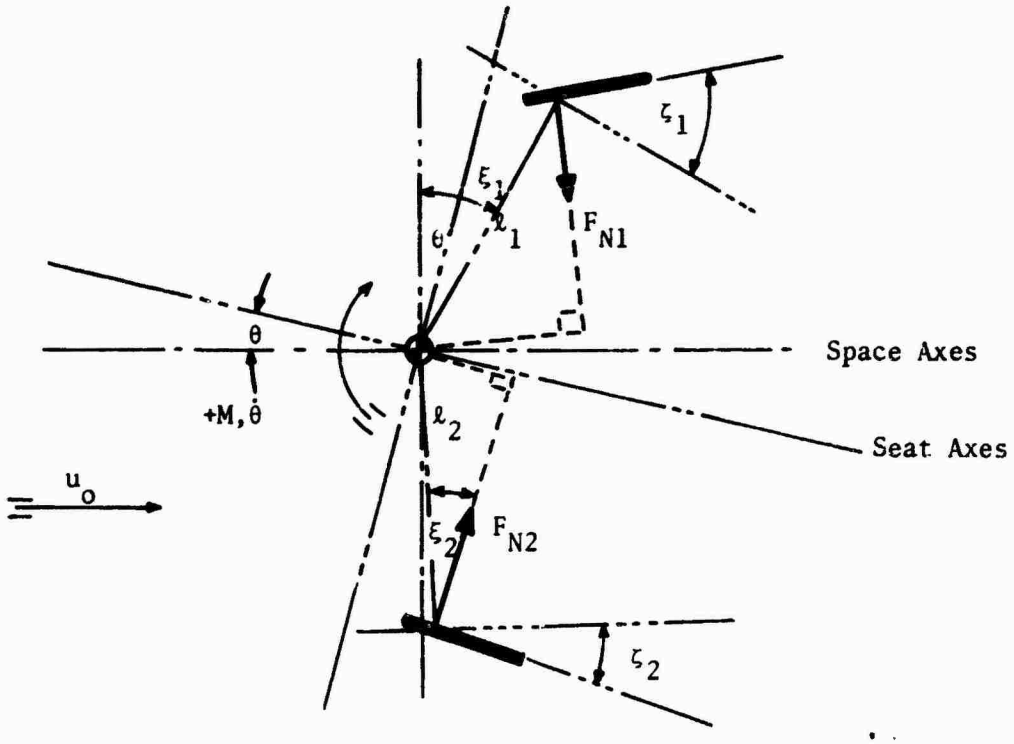


Figure 39. Stabilizer Geometry in the Pitch Plane.

Let $F_N$ = the normal aerodynamic force on the plate

$q_o$ = the dynamic pressure $\frac{1}{2} \rho u_o^2$

$S$ = plate area

$A$ = plate aspect ratio

$C_N$ = normal force coefficient $F_N/q_oS$

$M$ = moment exerted about the CG

$C_m$ = $M/q_o(S_1+S_2)(\ell_1+\ell_2)$

$C_{N\theta}, C_{m\theta}$ = $\partial C_N/\partial\theta$, $\partial C_m/\partial\theta$

## Plate Normal Force Variation

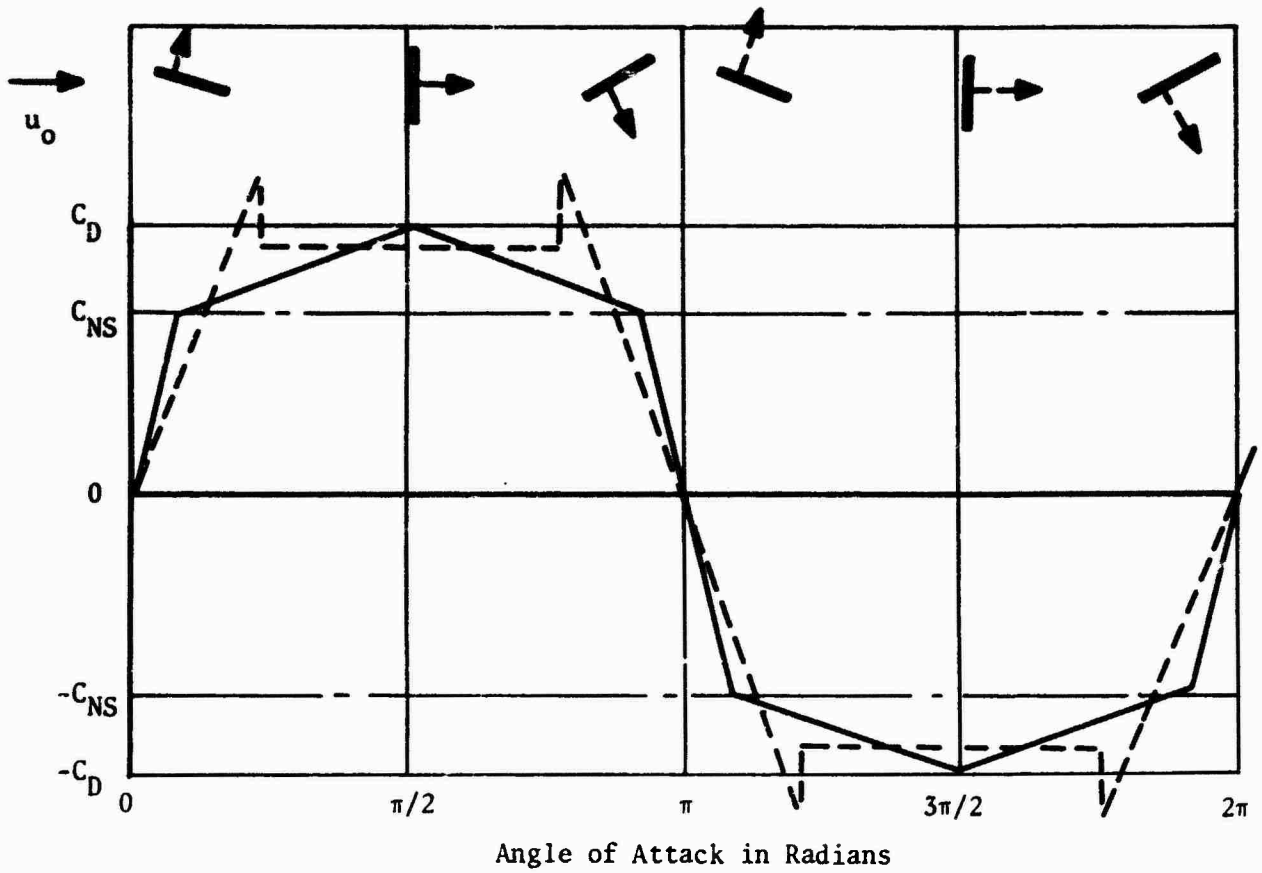


Figure 40. Idealized Variation of the Normal Force Coefficient Variation With Angle of Attack for a Flat Plate. The Full Line is for Aspect Ratio A > 1.74; the Dotted One is for A < 1.74.

There is a surprising paucity of information on the aerodynamic forces acting on flat plates of finite aspect ratio. An approximate picture can be constructed from the data in references 11 and 12, however, and this leads to the following equations, based on the linearization assumptions of figure 40.

The stall coefficient varies with aspect ratio (A) as

$$C_{NS} = 0.7 + e^{(1-A)} \tag{11}$$

At $\alpha = \pi/2$, $C_N = C_{D_{\pi/2}}$, the conventional drag coefficient of a flat plate normal to the flow. Approximately

$$C_{D_{\pi/2}} = 1.16 + .01\ A \quad (1 < A < 50) \tag{12}$$

From simple linearized lifting line theory, the stall angle is

$$\alpha_S = \frac{C_{NS}(2+A)}{2\pi A} \tag{13}$$

For $\alpha < \alpha_S$, $C_N = \frac{2\pi A}{2+A}\alpha$ (14)

(For $\alpha > \alpha_S$ and $A > 1.74$) $$C_N = C_{NS} + (C_{D_{\pi/2}} - C_{NS})\left(\frac{\alpha - \alpha_S}{\frac{\pi}{2} - \alpha_S}\right) \tag{15}$$

(For $\alpha > \alpha_S$ and $1 < A < 1.74$) $$C_N = C_{D_{\pi/2}} \tag{16}$$

The normal force idealizations that result from these equations are illustrated in figure 41.

Moments About the CG

From figure 39, the resultant moment of two plates (1,2) is

$$M = F_1 \ell_1 \sin \zeta_1 - F_2 \ell_2 \sin \zeta_2 \tag{17}$$

Let $L = \ell_1 + \ell_2$, $x_1 = \ell_1/L$, $x_2 = \ell_2/L$, $a_1 = S_1/(S_1+S_2)$,

$a_2 = S_2/(S_1+S_2)$

Then

$$C_m = \frac{M}{q_o L(S_1+S_2)} = C_{N1} a_1 x_1 \sin \zeta_1 - C_{N2} a_2 x_2 \sin \zeta_2 \tag{18}$$

where from figure 39

$$\left.\begin{aligned} \alpha_1 &= \zeta_1 - \xi_1 - \theta \\ \alpha_2 &= \zeta_2 - \xi_2 + \theta \end{aligned}\right\} \tag{19}$$

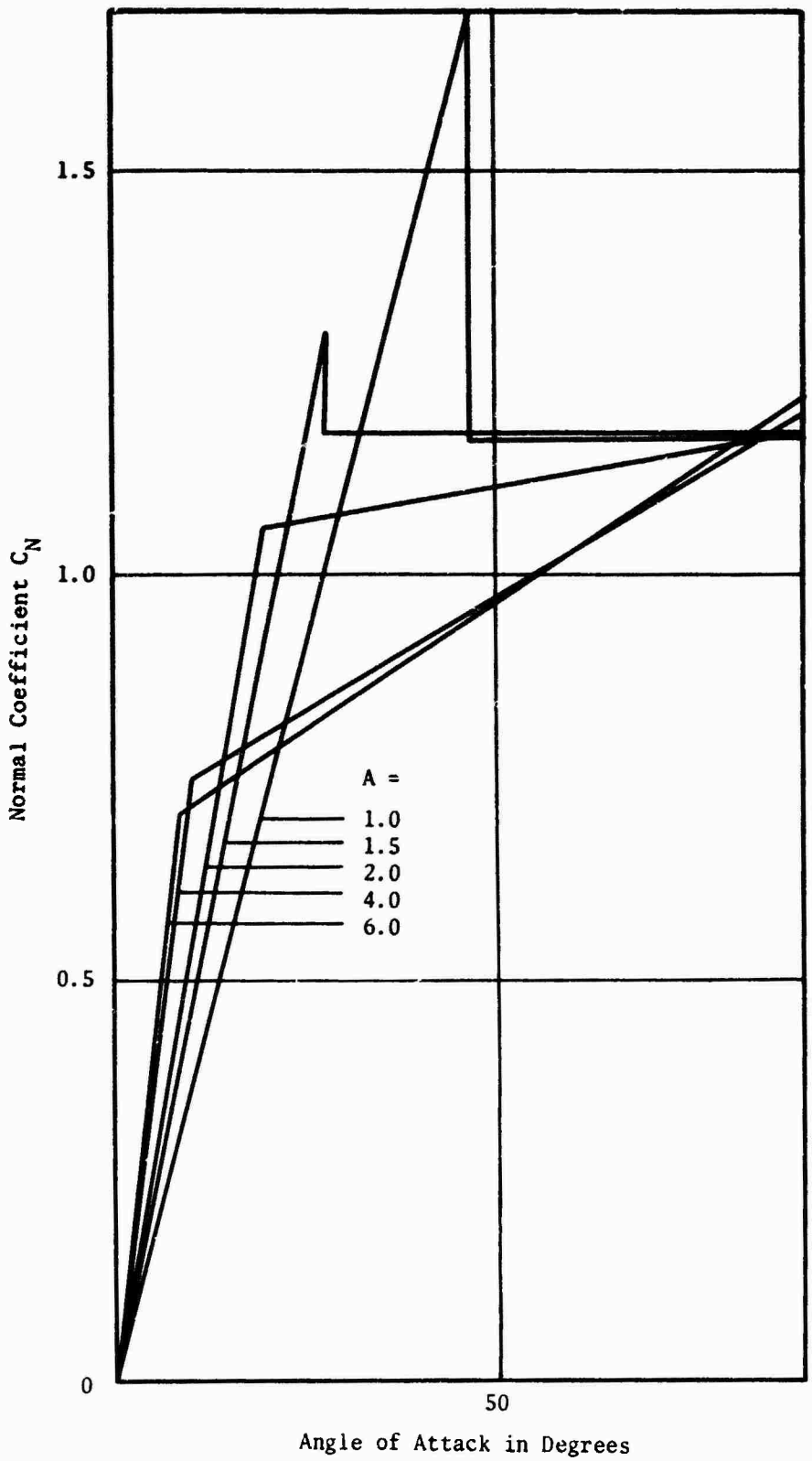


Figure 41. Idealized Normal Force on Rectangular Planform Plates, as a Function of Aspect Ratio (A) and Angle of Attack.

Some results for these equations are given in figures 42 and 43 for the symmetrical case of $a_1 = a_2 = 1/2$, $x_1 = x_2 = 1/2$. The moment curves are piecewise linear, as would be expected from equations 11 through 16, but highly nonlinear through one revolution. The plate combination is only stable at $\theta = 0$, to which it will return from any other angle. Also, static stability at $\theta = 0$ is greatest when the plates are unstalled.

Figure 44 gives the drag component or the normal force for selected aspect ratios, as a function of plate angle.

## Unstalled Static Stability Near $\theta = 0$

For the symmetric case already studied, equation 18 may be written as

$$C_m = \frac{1}{4} \sin \zeta (C_{N1} - C_{N2})$$

If the plates are unstalled, equations 14 and 17 lead to

$$\left.\begin{aligned} C_m &= -\frac{1}{4} \sin \zeta \frac{2\pi A}{(2+A)} \cdot 2\theta \\ \text{and} \\ \frac{\partial C_m}{\partial \theta} &= -\frac{\pi A}{(2+A)} \sin \zeta \end{aligned}\right\} \qquad (20)$$

Stability is clearly a maximum with the plates just at the point of stalling, for $\theta = 0$, even though this is a largely academic result because of the need to stabilize finite perturbations. This maximum is given by

$$\left.\frac{\partial C_m}{\partial \theta}\right|_{max} = -\frac{\pi A}{(2+A)} \sin \left\{ \frac{(2+A)}{2\pi A} \left[0.7 + e^{(1-A)}\right] \right\} \qquad (21)$$

from equations 11 and 13.

When A is large, so that $\sin \alpha_S \simeq \alpha_S$

$$\left.\frac{\partial C_m}{\partial \theta}\right|_{max} \simeq -\frac{1}{2} C_{NS} \qquad (22)$$

That is, about -0.35 to -0.5. The exact variation of equation 21 with aspect ratio is given in figure 45.

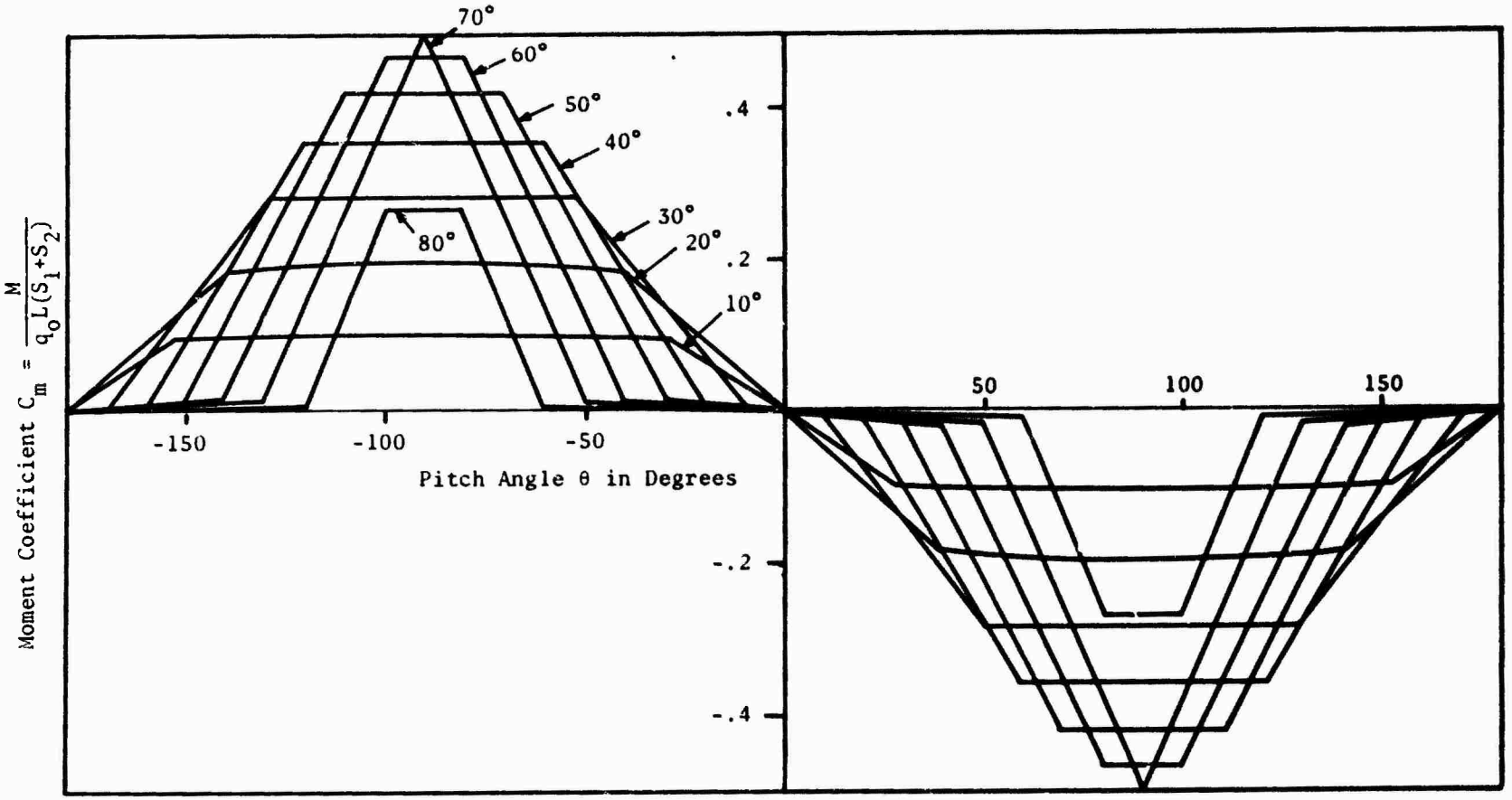


Figure 42. Variation of Moment Coefficient with Plate Angle $\zeta$, for $\xi = 0$, $A = 2.0$.

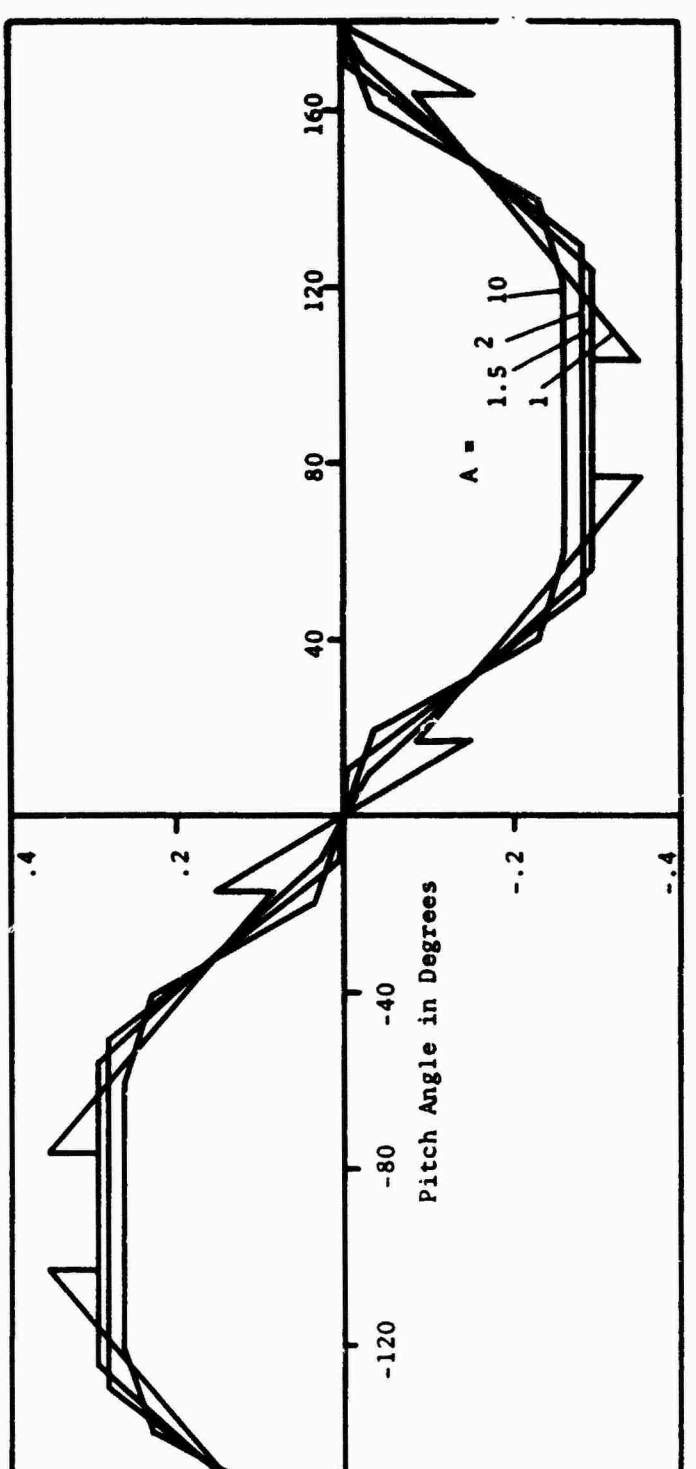


Figure 43. Variation of Moment Coefficient With Pitching Angle and Aspect Ratio (A) for Fixed $\zeta = 30°$, $\xi = 0$.

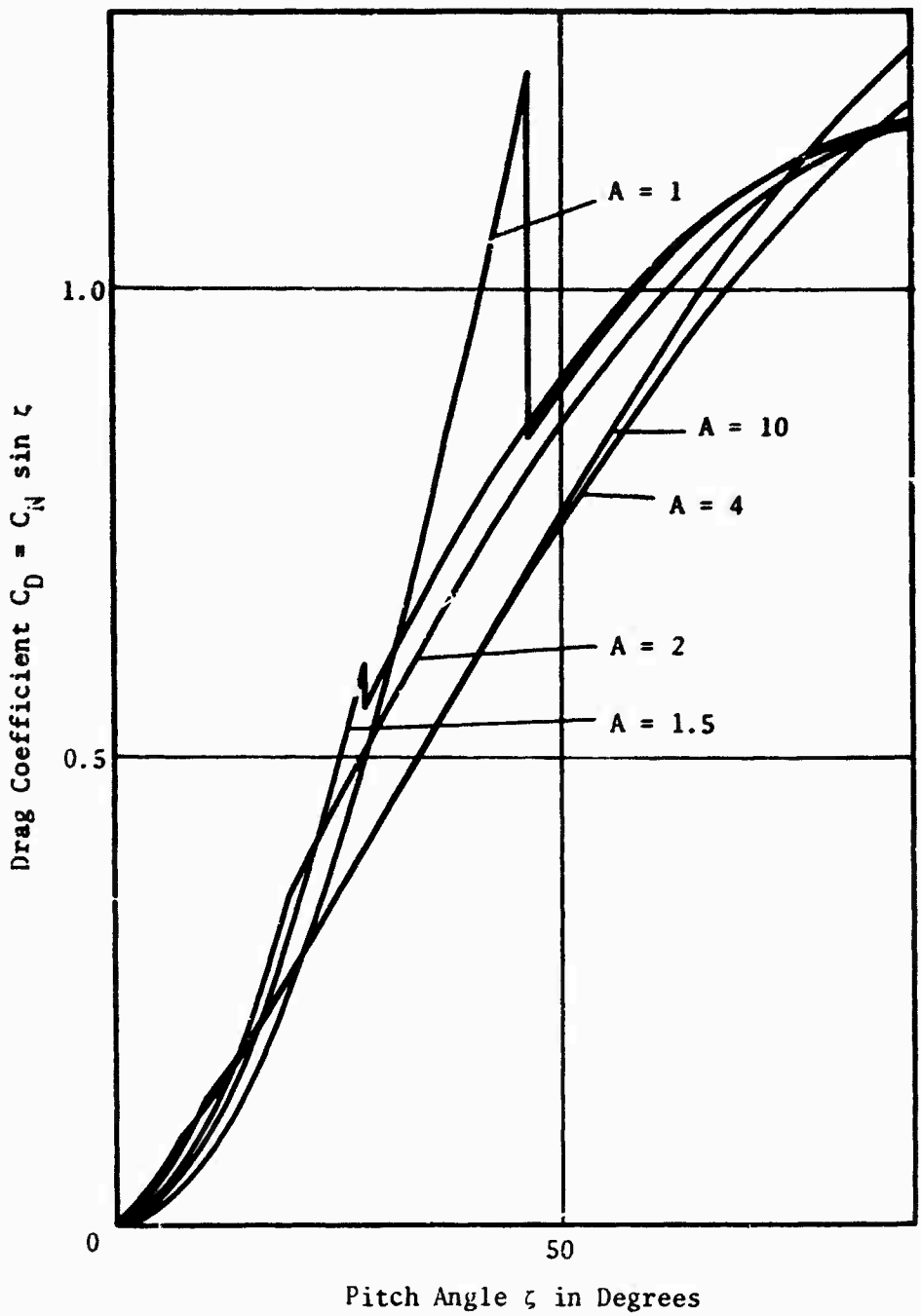


Figure 44. Drag Coefficient of Plates of Various Aspect Ratios (A) as a Function of Angle to the Flow ($\xi = 0$).

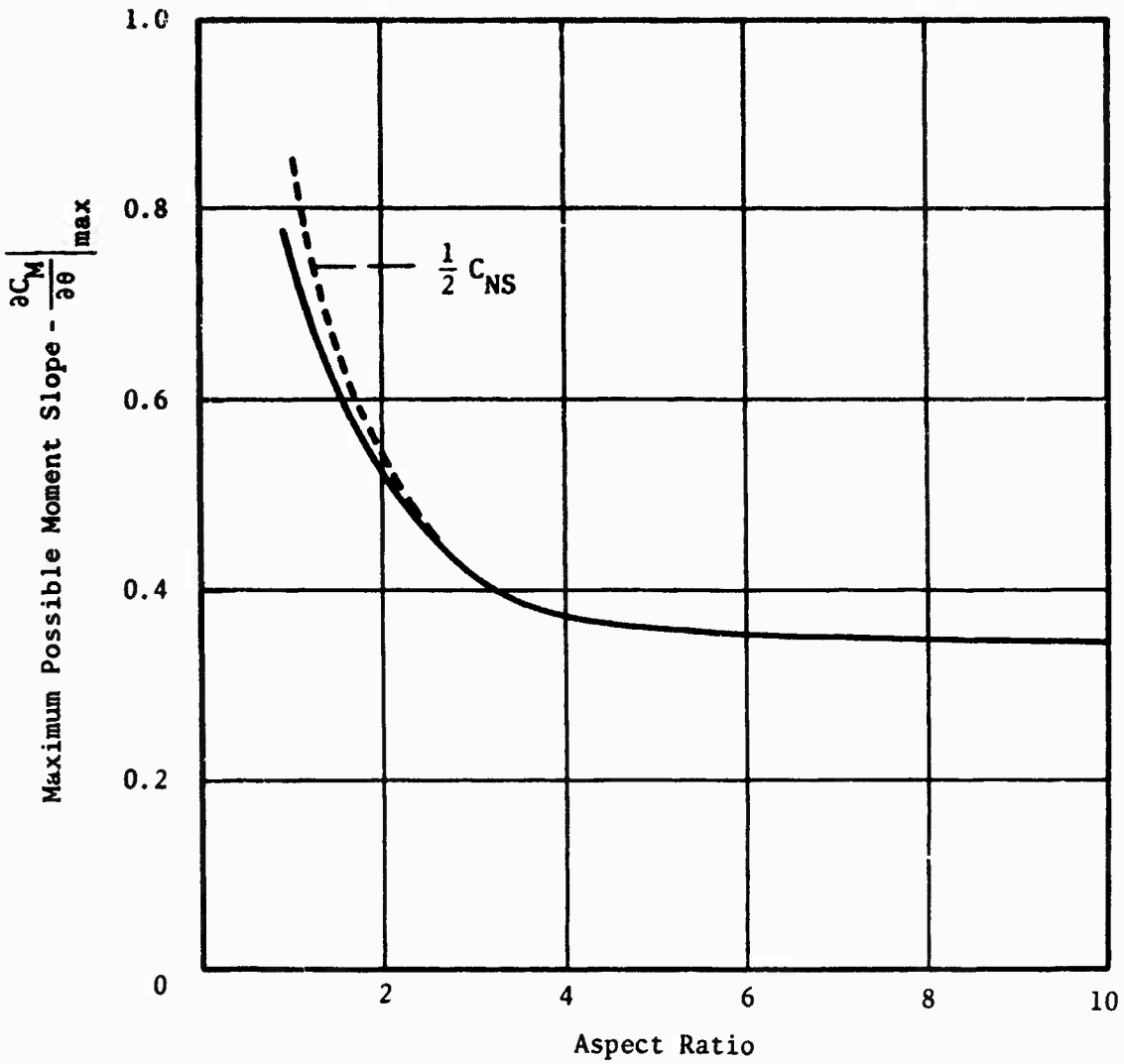


Figure 45. Maximum Possible Moment Slope at $\theta = 0$ for a Flat Plate In-Plane Stabilizer.

## Plate Sizes Needed to Stabilize an Ejection Seat in Pitch

Figure 46 gives the pitching moment for two typical seats.* Seat (A) is not very unstable; its problem is that a positive (nose up) pitching moment acts on it as it comes off the rails which starts it spinning. The single stabilizer plate shown in figure 47(a) will probably be sufficient to both stabilize and trim it, as shown in figure 48(a).

Seat (B) is just the opposite, with a substantial negative (nose down) pitching moment and an unstable slope ($dC_m/d\theta$) when it comes off the seat rails. In this case, a single plate at the top would seem to be appropriate, as shown in figure 47(b). The calculated $C_m$ variation with this addition is shown in figure 48(b).

In neither case have we attempted to optimize the in-plane stabilizer for minimum size or minimum necessary stabilization, nor have we attempted to allow for seat/stabilizer proximity effects. But it seems reasonable to assume that a detailed investigation would enable significant reductions in stabilizer size to be made, along with a more convenient location on the seat.

Additionally, it is found that for the rectangular plates used in this study, the lowest aspect ratio (unity) for which data is available is the most effective. This naturally leads one to wonder whether other planforms - such as deltas - would be even more effective. Also of interest would be a study of the effects of:

- perforated plates
- plate camber
- seat proximity

A further variation on the general theme of an in-plane stabilizer is the use of a fixed normal drag plate which is progressively blanketed from the main flow as the seat rotates, by an existing portion of the seat or occupant. Such a solution has been recently evaluated on the Stencel SIIIS seat as a cure for a negative pitch problem. The plate was located behind the headrest so that its nose-up moment contribution was small at normal trim angles, but increased as the seat pitched forward.

---

* In this section, since the original seat data was presented in a moment coefficient form, we have adhered to the same convention to facilitate comparison.

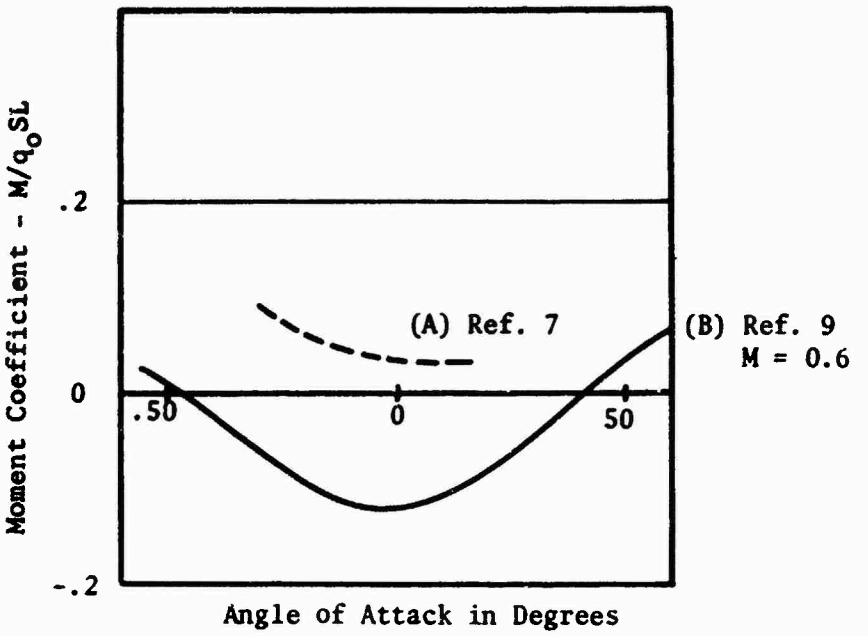


Figure 46. Pitching Moment Coefficient for Two Typical Ejection Seats.

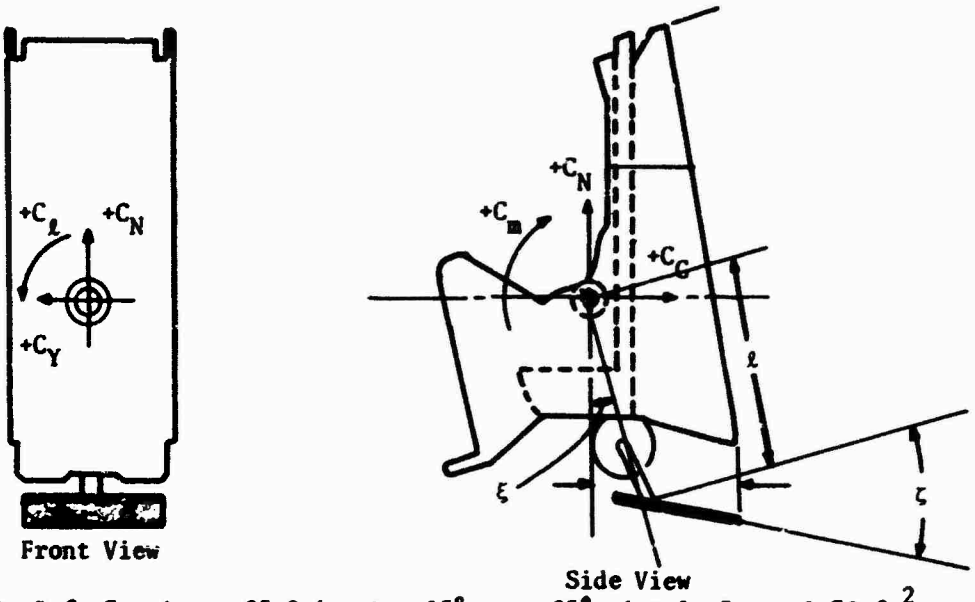


Seat (A), Ref. 7. $\ell_{FS}$ = 23.8 in, $\xi$ = 15°, $\zeta$ = 25°, A = 1, $S_{FS}$ = 1.72 ft$^2$

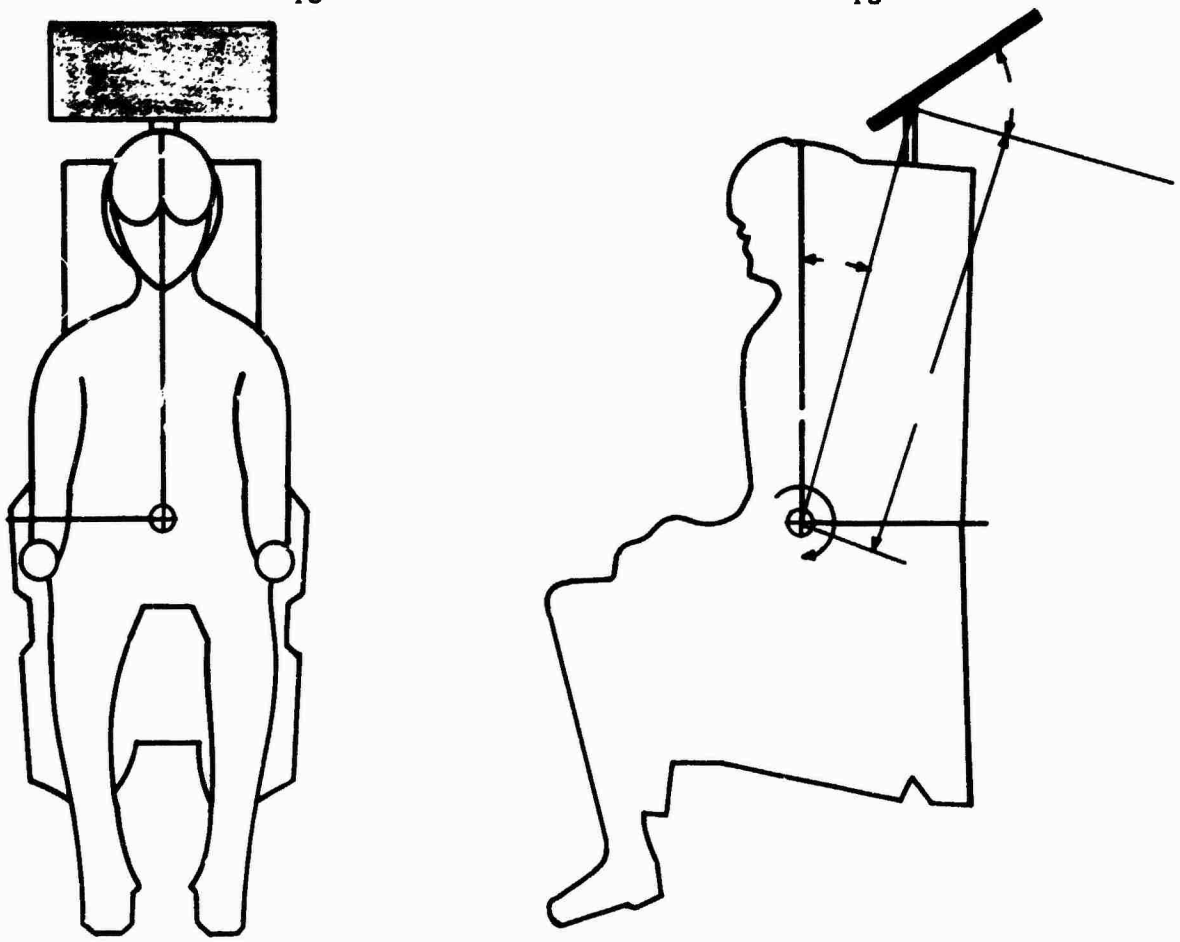

Seat (B), Ref. 9. $\ell_{FS}$ = 33.0 in, $\xi$ = 15°, $\zeta$ = 45°, A = 1, $S_{FS}$ = 2.2 ft$^2$

Figure 47. Remedial In-Plane Stabilizers for the Two Seats of Figure 34.

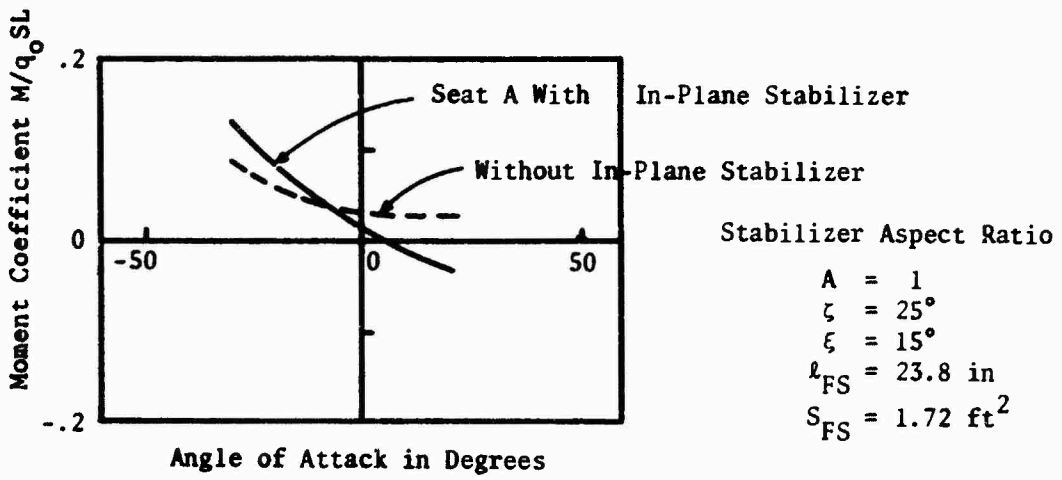


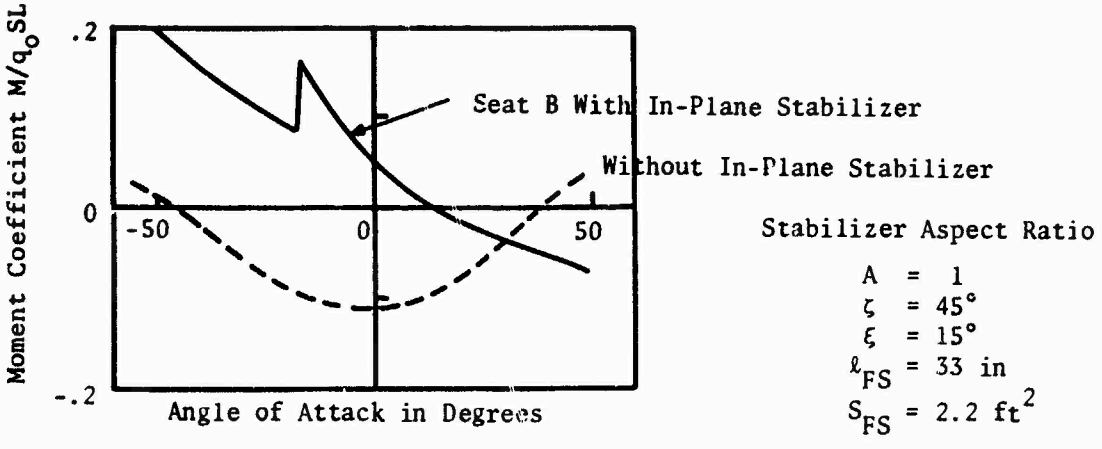


Figure 48. Calculated Pitching Moments for Seats A and B, Using the In-Plane Stabilizers of Figure 35.

## FULL SCALE MEASUREMENTS WITH AN IN-PLANE STABILIZER

Because plate proximity effects could not be calculated accurately, it was decided that an in-plane stabilizer should be evaluated experimentally at the first opportunity, to confirm the validity of the concept. A previously planned wind tunnel test of an F-105 seat, using live human subjects to measure limb dislodgement loads, provided this opportunity. One, two and four plate stabilizer assemblies were built. The sizes were guessed at, because prior to running the experiments, there was no way of knowing the sign of the pitching and yaw moments of the unstabilized seat, let alone their magnitude. In fact, it was hoped that the guessed sizes would be two or three times greater than was really needed; a hope that turned out to be justified.

The stabilizer plates used are illustrated in figures 49 and 50. The experimental procedures are given in reference 6.

Figures 51 and 52 give the average pitching and yawing moments of the unstabilized seat about the CG of an occupied seat. The presence of the seat occupant changes these moments substantially, relative to an empty seat. Figures 53 through 55 show that the stabilizer plates were very effective in stabilizing the seat. The stabilizing volume of the yaw plates was about twice as much as was really needed. As far as pitch is concerned, the single upper plate (figure 49) was about three times larger than needed. An optimized plate might be as small as one-fifth the size actually used.

Representative drag areas for the seat, stabilized and unstabilized, are given in figure 56.

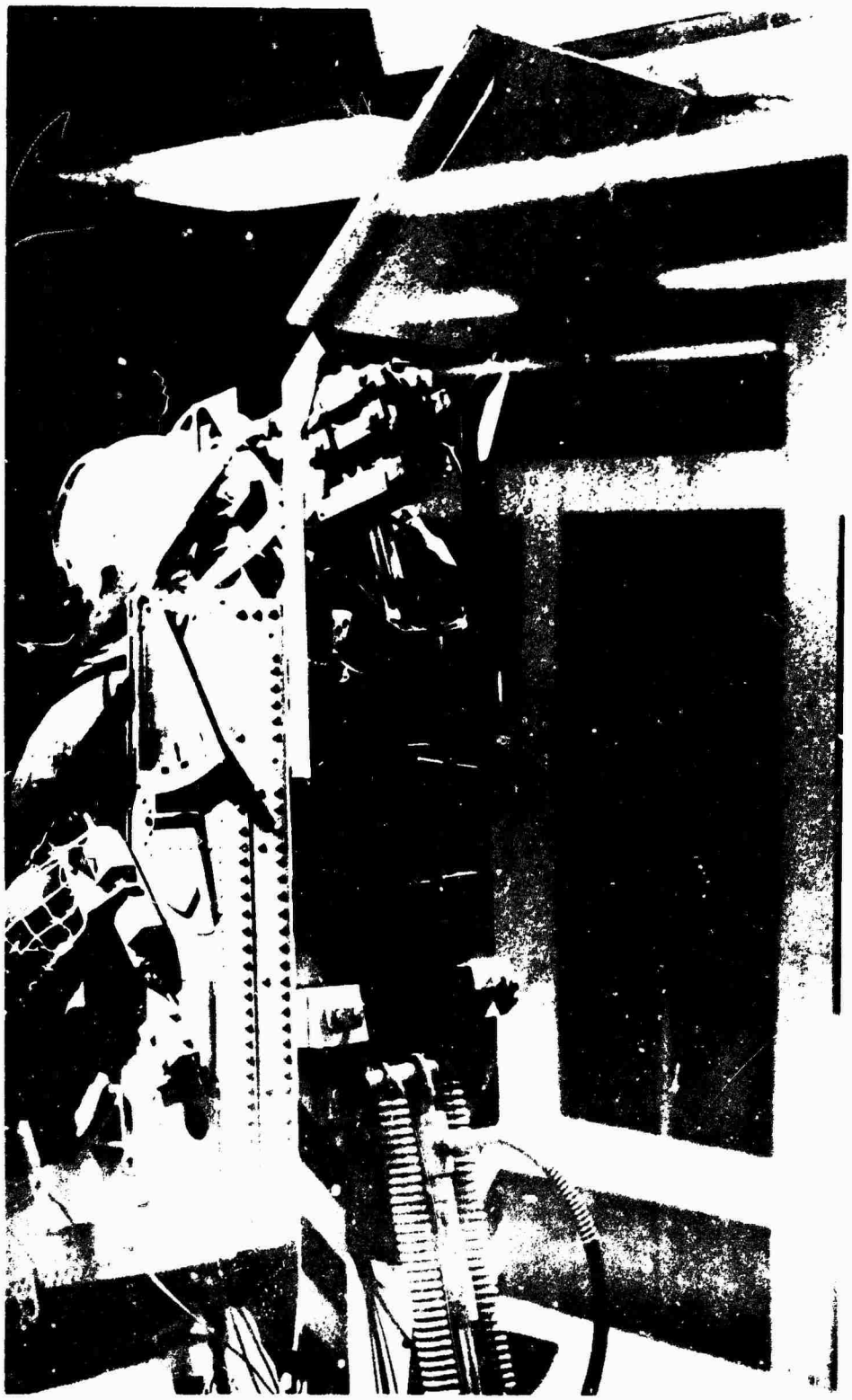

Figure 49. A Single Pitch Stabilizing Plate Mounted on the F-105 Seat.

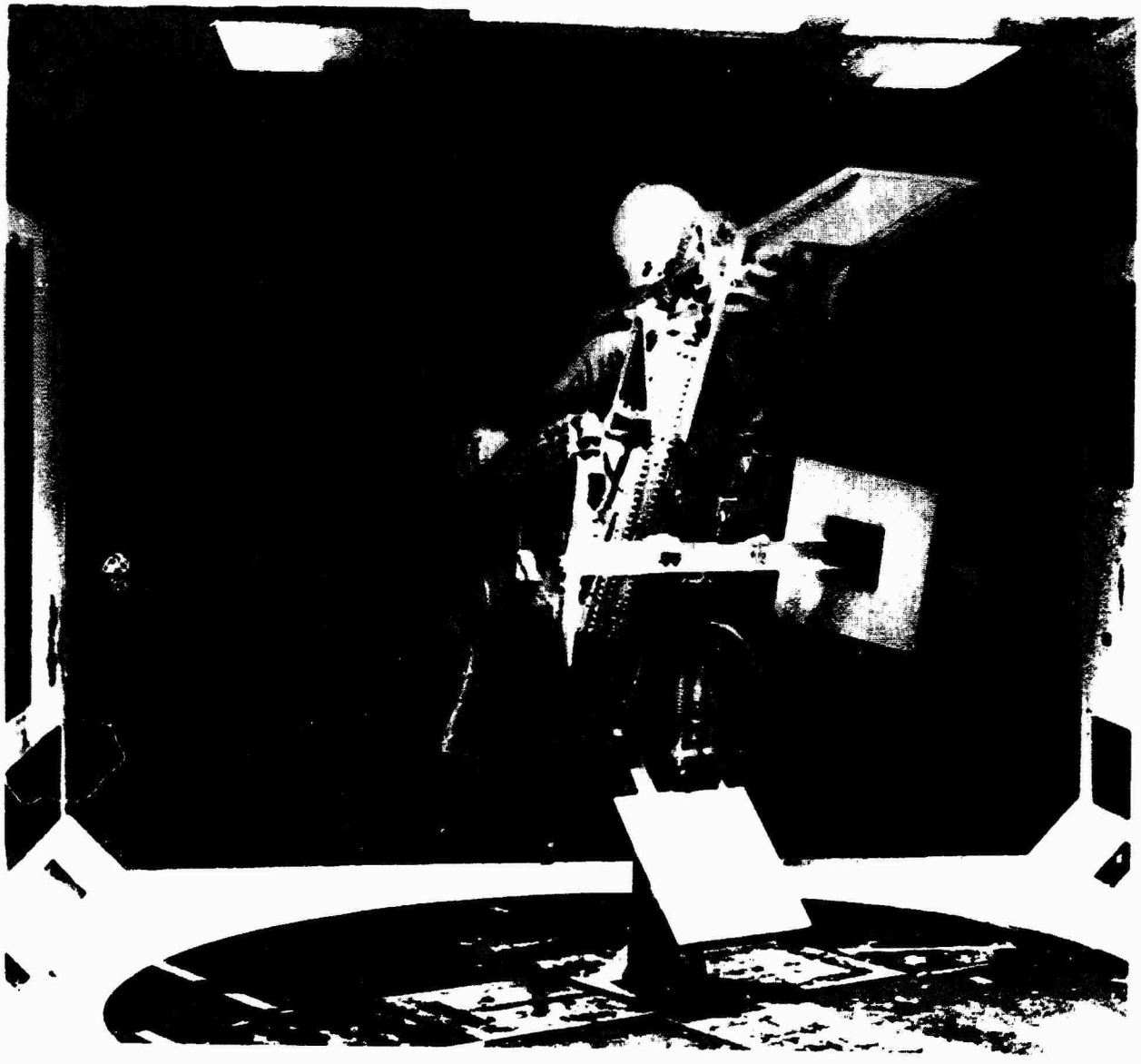

Figure 50. The Full Four-Plate Stabilizer Assembly. As Noted in the Text, the Stabilizing Volume Proved to be Much Larger Than Was Needed.

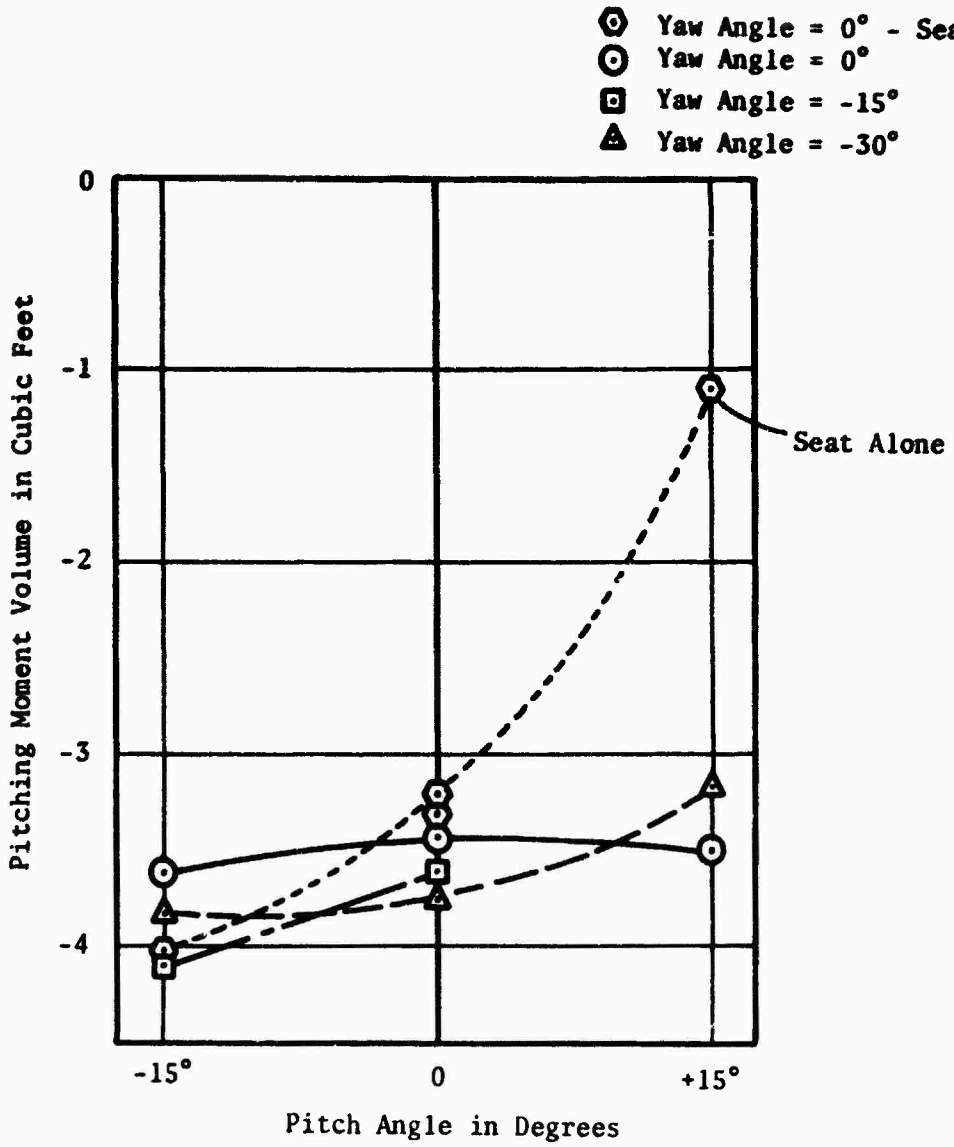


Figure 51. Average Pitching Moment (All Subjects) as a Function of Pitch Angle, for the Standard Side-Arm Configuration.

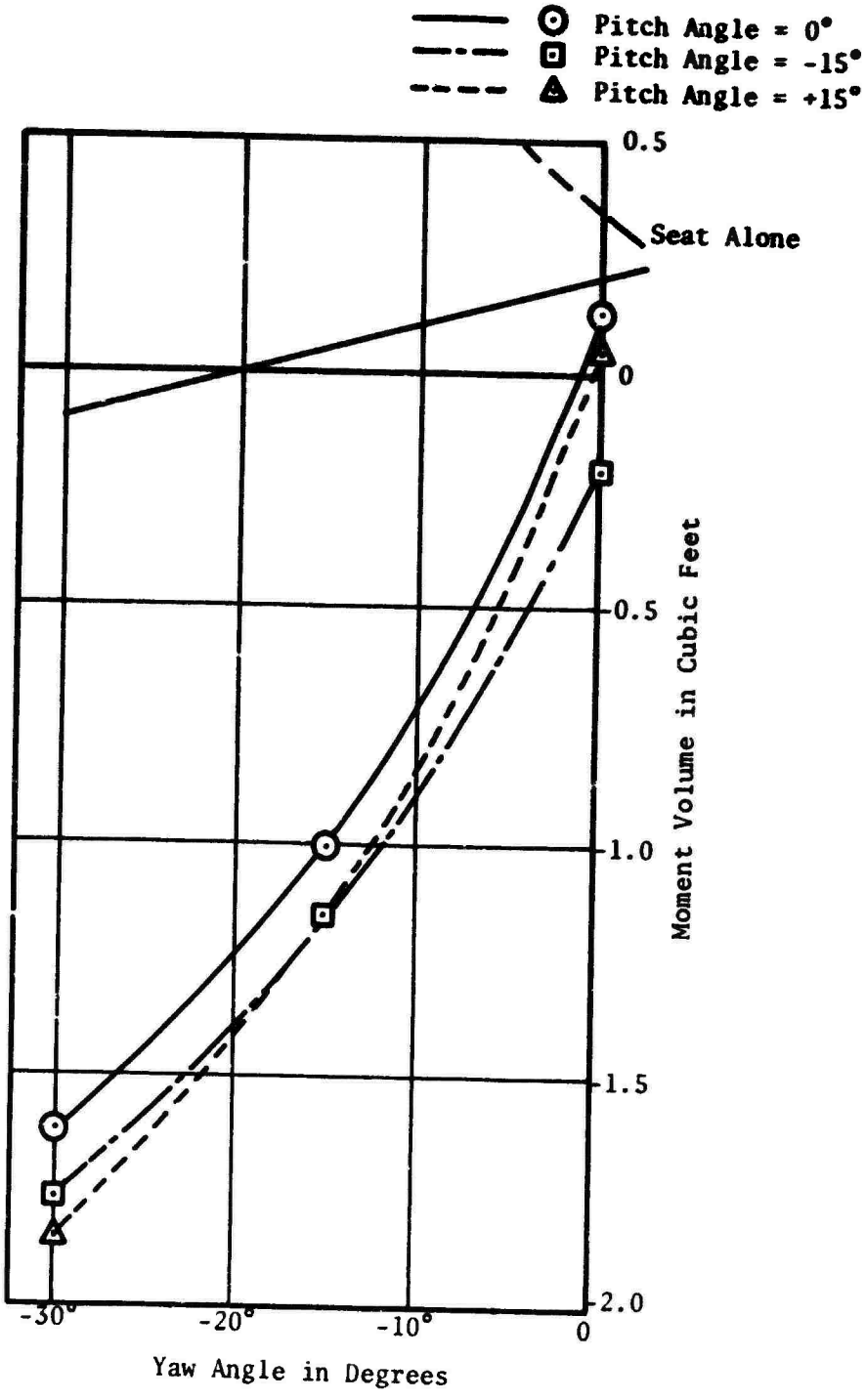


Figure 52. Average Yawing Moment (All Subjects) as a Function of Yaw Angle, for the Standard Side-Arm Configuration.

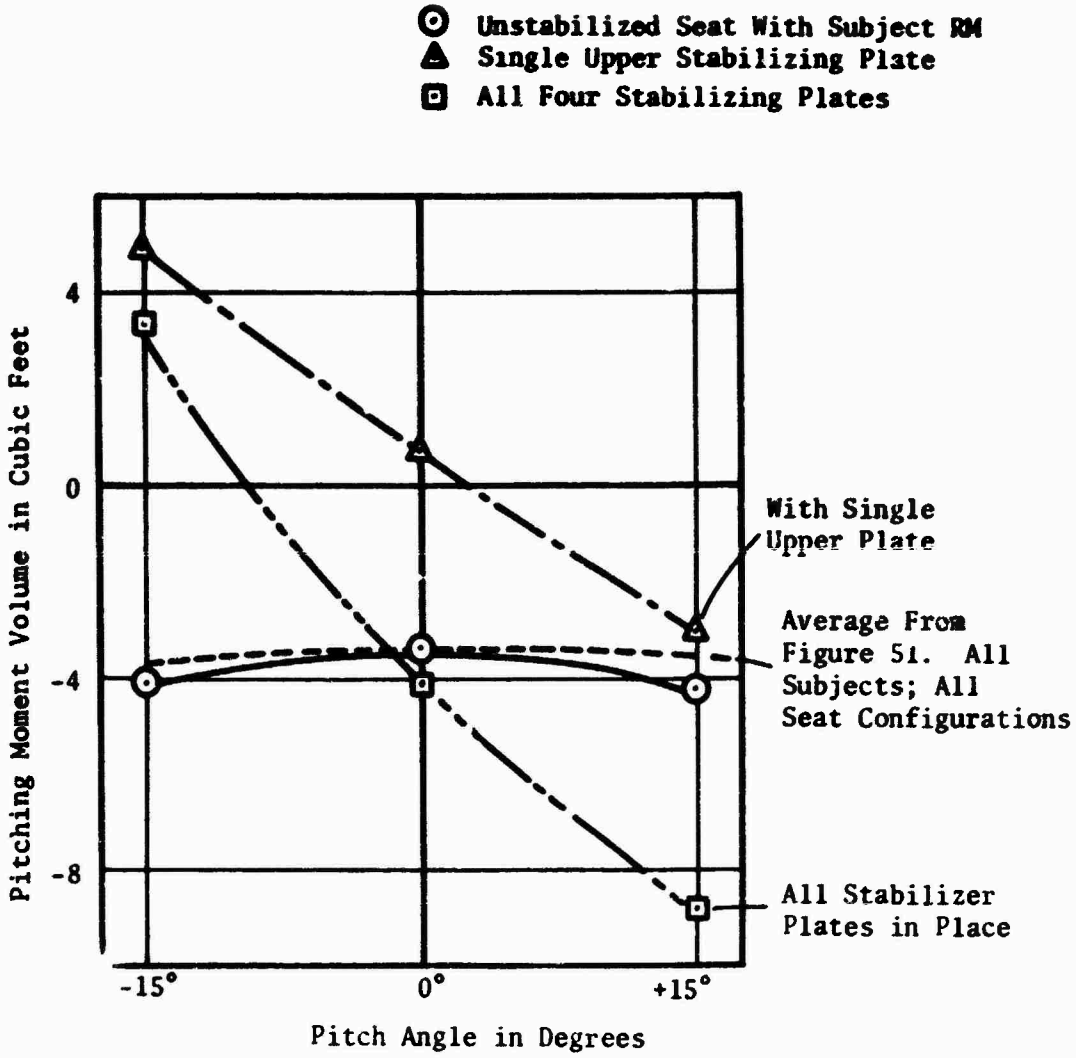


Figure 53. Pitching Moment at Zero Yaw, With and Without In-Plane Stabilizer Plates. Subject RM With Arm and Leg Restraint Nets. Results are not corrected for tunnel wall proximity.

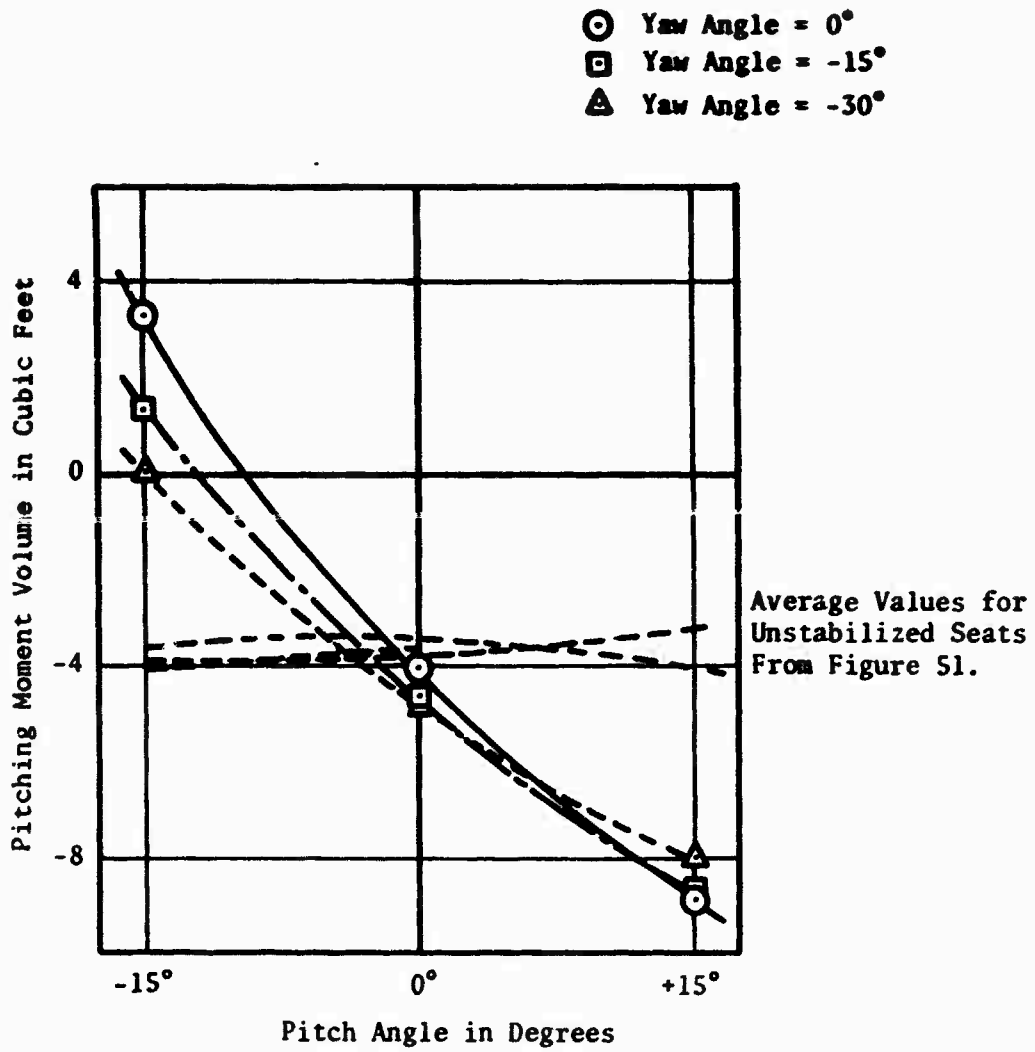


Figure 54. The Effect of Yaw Upon the Seat Pitching Moment When Equipped With All Four Stabilizer Plates. Subject RM With Arm and Leg Restraint Nets. Results are not corrected for tunnel wall proximity.

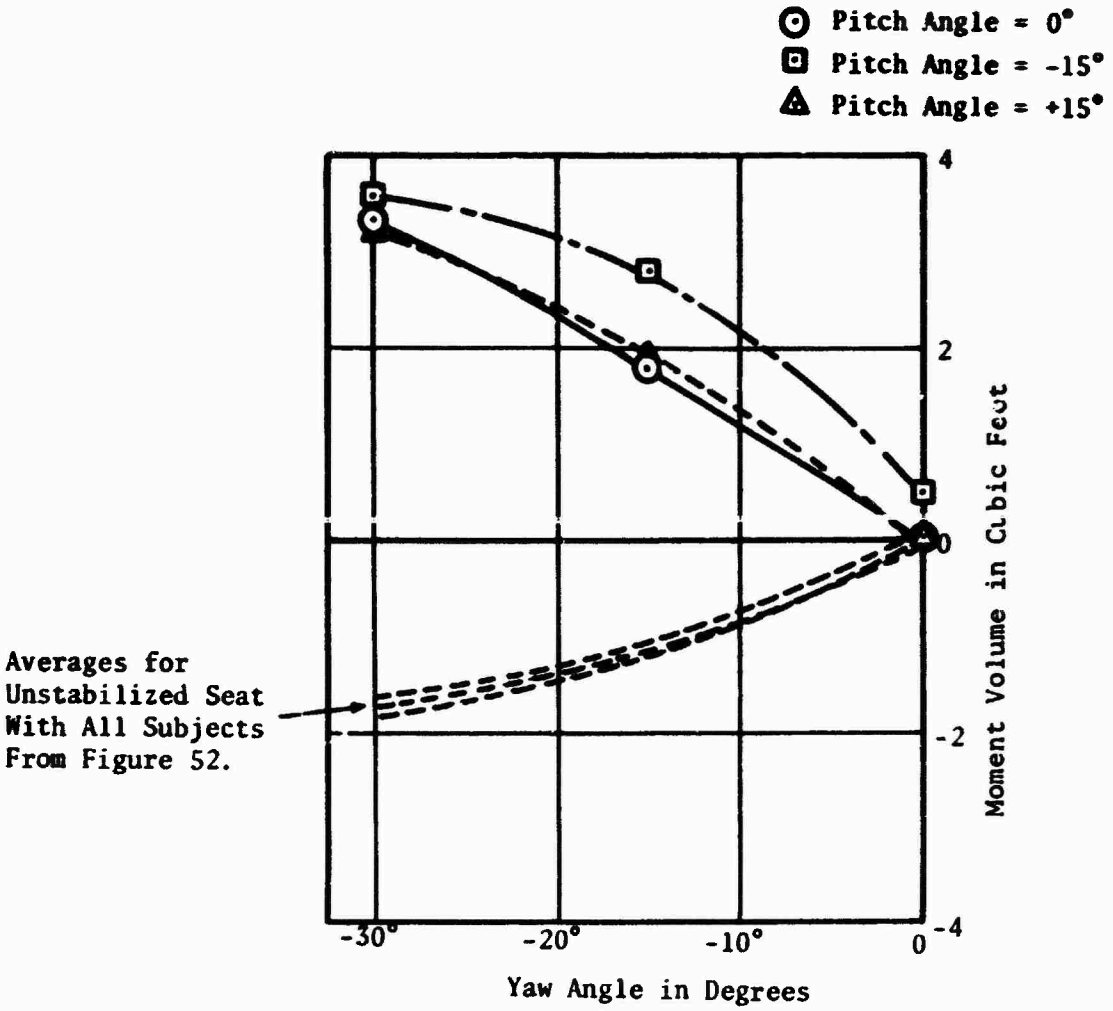


Figure 55. Yaw Volume With Subject RM When the In-Plane Stabilizer Was in Place.

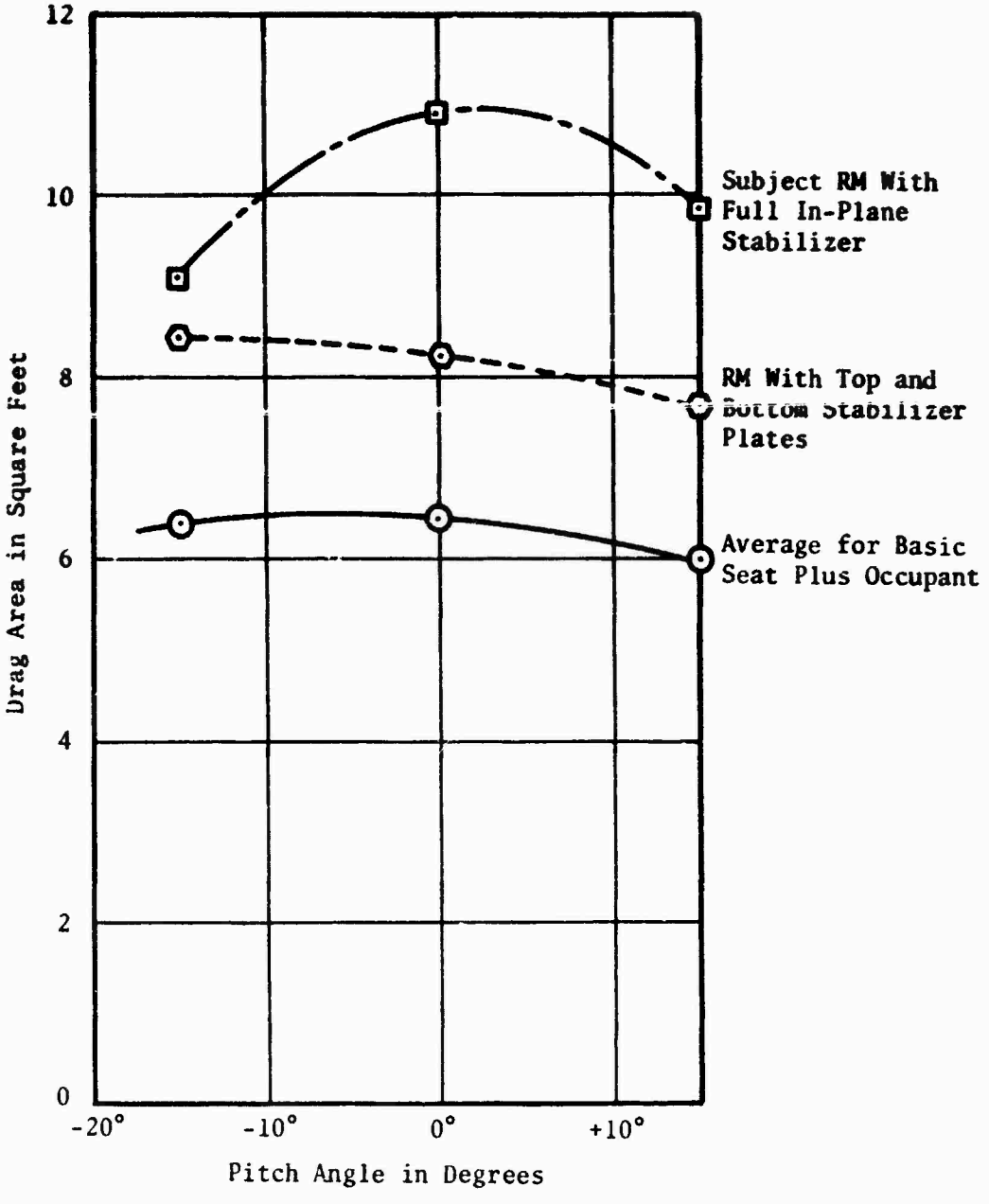


Figure 56. Some Drag Area Measurements for the F-105 Seat, as a Function of Pitch Angle, for Zero Yaw.

## CONCLUSIONS AND RECOMMENDATIONS

We concluded that:

(1) The entrapment nets suggested by Brinkley and similar devices, can largely cure the flail problem in aerodynamically stable seats.

(2) Flail injury at high speeds is unavoidable in an unstable seat.

(3) It is probable that any seat can be stabilized with in-plane stabilizer plates.

(4) A combination of entrapment nets and stabilizer plates can eliminate the flail injury problem, for practical purposes.

We recommended that in-plane stabilizers be developed for new open ejection seats, and as retrofit items for existing seats likely to remain in service. We also recommended that the development of entrapment nets and other devices be continued, with the same objectives in mind.

## REFERENCES


1. Payne, Peter R., and Fred W. Hawker. USAF Experience of Flail Injury for Noncombat Ejections in the Period 1964-1970. Aerospace Medical Research Laboratory, WPAFB, Ohio. AMRL-TR-72-111 (1973).

2. Payne, Peter R. Some Studies Relating to Limb Flailing After an Emergency Escape from an Aircraft. Aerospace Medical Research Laboratory, WPAFB, Ohio. AMRL-TR-73-24 ( 1973).

3. Galigher, L.L. Aerodynamic Characteristics of a Full Scale F-101 Ejection Seat with an Anthropomorphic Dummy at Free Stream Mach Numbers From 0.2 to 0.8. Arnold Engineering Development Center, Arnold AF Station, Tennessee. AEDC-TR-72-38 (February 1972).

4. Payne, Peter R., and E.G.U. Band. "The Pressure Distribution on the Surface of an Ellipsoid in Inviscid Flow." Payne Inc. Working Paper No. 101-15 (July 1972).

5. Payne, Peter R. "A New Look at Parachute Opening Dynamics." Journal of the Royal Aeronautical Society (February 1973).

6. Payne, Peter R., Fred W. Hawker, and Anthony J. Euler. "Stability and Limb Dislodgement Force Measurements With an F-105 Ejection Seat." Payne Inc. Working Paper No. 106-3. (August 1973).

7. Visconti, F. and R.J. Nuber. A Wind Tunnel Investigation of the Static Stability Characteristics of a 1/8-Scale Ejectable Pilot-Seat Combination at a Mach Number of 0.8. Langley Aeronautical Laboratory, Langley Field, Virginia. NACA RM L51H08 (December 1951).

8. Heinrich, H.G. and T.R. Hektner. "Flexibility as Parameter of Model Parachute Performance Characteristics." Paper presented at the AIAA Aerodynamic Deceleration Systems Conference, Dayton, Ohio. AIAA Paper No. 70-1166 (September 1970).

9. Reichenau, D.E.A. Aerodynamic Characteristics of an Ejection Seat Escape System with Cold Flow Rocket Plume Simulation at Mach Numbers from 0.6 Through 1.5. Arnold Engineering Development Center, Arnold AF Station, Tennessee. AEDC-TR-69-218 (October 1969).

10. Shaffer, D.A. "Wind Tunnel Measurements of Slender Body Pitching Moment When an Inverted Cone is Mounted on its Nose." Payne Inc. Working Paper No. 67-2 (January 1966).

11. Hoerner, S.F. Fluid Dynamic Drag. Published by the Author. 148 Busteed Drive, Midland Park, N.J. 07432. (1965).

12. Payne, Peter R. Model Sailplane Design. Percival Marshall & Co., Ltd. London. (1947).

13. Milne-Thomson, L.M. Theoretical Hydrodynamics, Fourth Edition. New York: The MacMillan Company (1960).

# APPENDIX

## AN ALTERNATIVE ANALYSIS OF THE IN-PLANE STABILIZER, INCLUDING QUASI-STATIC TRANSIENT TERMS

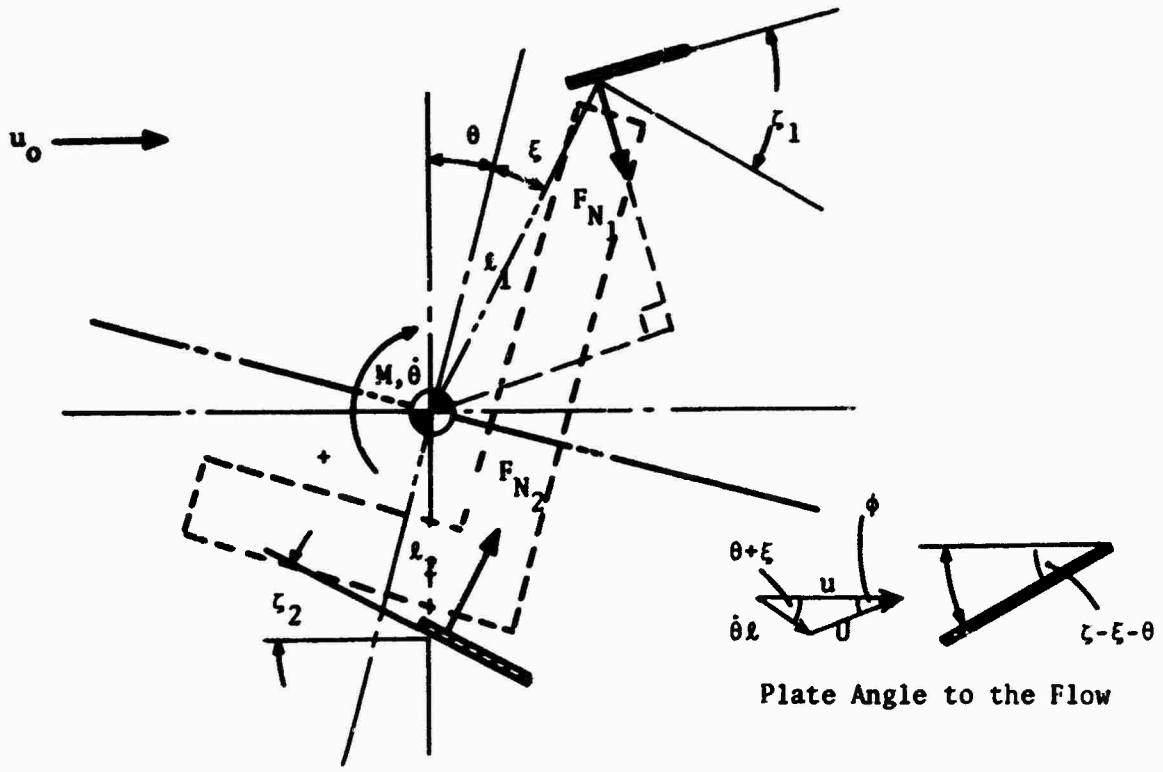


Figure A1. Stabilizer Geometry in the Pitch Plane.

Let $F_N$ = the normal aerodynamic force on a plate

$q_o$ = dynamic pressure $\frac{1}{2}\rho u^2$

$S$ = plate area

$C_N$ = normal force coefficient $F_N/q_oS$

$M$ = moment exerted about the CG by the force $F_N$, positive nose up

$C_M$ = $M/q_oS\ell$

$C_{N_\theta}$, $C_{M_\theta}$ = $\partial C_N/\partial\theta$, $\partial C_M/\partial\theta$

$\lambda$ = $\dot{\theta}\ell/u$, a reduced pitch rate parameter

$C_{N\alpha}$ = $\partial C_N/\partial \sin\alpha$, the normal force coefficient slope with respect to the sine of the angle of attack

Other symbols are as defined in figure A1. Suffixes 1, 2, etc. refer to different plates on the seat.

For plate system (1) in figure A1, and omitting the suffixes for simplicity, the plate moment about the CG is

$$M = F_N \ell \sin\zeta$$

$$= q_o (U/u)^2 S\ell \sin\zeta \, C_{N\alpha} \sin(\zeta-\xi-\theta-\phi)$$

or

$$C_M = (U/u)^2 \sin\zeta \, C_{N\alpha} \sin(\zeta-\xi-\theta-\phi) \qquad (1)$$

From the triangle of velocities

$$U^2 = u^2 + (\dot{\theta}\ell)^2 - 2u\dot{\theta}\ell \cos(\theta+\xi) \qquad (2)$$

Writing $\lambda = \dot{\theta}\ell/u$

$$(U/u)^2 = 1 + \lambda^2 - 2\lambda(\cos\theta\cos\xi - \sin\theta\sin\xi) \qquad (3)$$

From the sine rule

$$\frac{U}{\sin(\theta+\xi)} = \frac{\dot{\theta}\ell}{\sin\phi}$$

$$\therefore \sin\phi = \frac{\lambda \sin(\theta+\xi)}{(U/u)} = \frac{\lambda}{U/u}(\sin\theta\cos\xi + \cos\theta\sin\xi) \qquad (4)$$

Similarly

$$\cos\phi = \frac{1 - \lambda\cos(\theta+\xi)}{U/u}$$

$$= \frac{1 - \lambda(\cos\theta\cos\xi - \sin\theta\sin\xi)}{U/u} \qquad (5)$$

In equation (1)

$$\sin(\zeta-\xi-\theta-\phi) = \sin[(\zeta-\xi) - (\theta+\phi)]$$

$$= \sin(\zeta-\xi)\cos(\theta+\phi) - \cos(\zeta-\xi)\sin(\theta+\phi)$$

$$= \sin(\zeta-\xi)[\cos\theta\cos\phi - \sin\theta\sin\phi] - \cos(\zeta-\xi)[\sin\theta\cos\phi + \cos\theta\sin\phi]$$

Substituting into equation (1), and writing $(\zeta-\xi) = \tau$ for simplicity

$$C_M = C_{N\alpha} \sin\zeta (U/u)^2 \{[\sin\tau\cos\theta - \cos\tau\sin\theta]\cos\phi - [\sin\tau\sin\theta + \cos\tau\cos\theta]\sin\phi\} \quad (6)$$

Substituting equations (4) and (5) for $\sin\phi$, $\cos\phi$ and equation (3) for (U/u)

$$C_M = C_{N\alpha} \sin\zeta \sqrt{1 + \lambda^2 - 2\lambda(\cos\theta\cos\xi - \sin\theta\sin\xi)} \times \{[\sin\tau\cos\theta - \cos\tau\sin\theta][1 - \lambda(\cos\theta\cos\xi - \sin\theta\sin\xi)] - [\sin\tau\sin\theta + \cos\tau\cos\theta]\lambda(\sin\theta\cos\xi + \cos\theta\sin\xi)\}$$

Multiplying out the contents of the curly bracket and cancelling terms leads to

$$C_M = C_{N\alpha} \sin\zeta \sqrt{1 + \lambda^2 - 2\lambda(\cos\theta\cos\xi - \sin\theta\sin\xi)} \times [\sin\tau\cos\theta - \cos\tau\sin\theta - \lambda(\sin\tau\cos\xi + \cos\tau\sin\xi)] \quad (7)$$

$$= C_{N\alpha} \sin\zeta \sqrt{1 + \lambda^2 - 2\lambda\cos(\theta+\xi)}\,[\sin(\tau-\theta) - \lambda\sin(\tau+\xi)]$$

$$= C_{N\alpha} \sin\zeta \sqrt{1 + \lambda^2 - 2\lambda\cos(\theta+\xi)}\,[\sin(\zeta-\xi-\theta) - \lambda\sin\zeta] \quad (7a)$$

For the case of $\lambda = 0$ $(\dot{\theta} = 0)$

$$\left.\begin{aligned} C_{M_{\lambda=0}} &= C_{N\alpha} \sin\zeta[\sin\tau\cos\theta - \cos\tau\sin\theta] \\ &= C_{N\alpha} \sin\zeta \sin(\tau-\theta) \end{aligned}\right\} \quad (8)$$

For small values of $\theta$, $\sin\theta \simeq \theta$, so that

$$C_{M_\theta} \simeq - C_{N\alpha} \sin\zeta\cos\tau = - C_{N\alpha} \sin\zeta\cos(\zeta-\xi) \quad (9)$$

Thus $C_{M_\theta}$ increases with a reduction in $\xi$, if $\zeta$ is fixed. But stalling is limited by $\tau = \zeta - \xi$, the angle the plate makes with the flight path when $\theta = 0$. Thus equation (9) is more meaningfully written as

$$C_{M_\theta} = - C_{N\alpha} \cos \tau \sin(\tau+\xi) \tag{10}$$

Looked at in this way, positive values of the angle $\xi$ are beneficial. Note that in general, there is a coupling between $\theta$ and $\lambda$, and that positive $\lambda$ will generally reduce $C_{M_\theta}$ to some extent.

The damping coefficient $C_{M_\lambda}$ is obtained by differentiating equation (7) with respect to $\lambda$

i.e.

$$\frac{C_{M_\lambda}}{C_{N\alpha}} = \frac{\sin \zeta[\lambda-\cos(\theta+\xi)][\sin(\zeta-\xi-\theta)-\lambda \sin \zeta]}{\sqrt{1 + \lambda^2 - 2\lambda \cos(\theta+\xi)}} - \sin^2\zeta \sqrt{1 + \lambda^2-2\lambda\cos(\theta+\xi)}$$

For values of $\lambda$ much smaller than unity

$$C_{M_\lambda} = - C_{N\alpha}[\sin \zeta \cos(\theta+\xi)\sin(\zeta-\xi-\theta) + \sin^2\zeta] \tag{11}$$

## Comparison Between Conventional and In-Plane Stabilizers

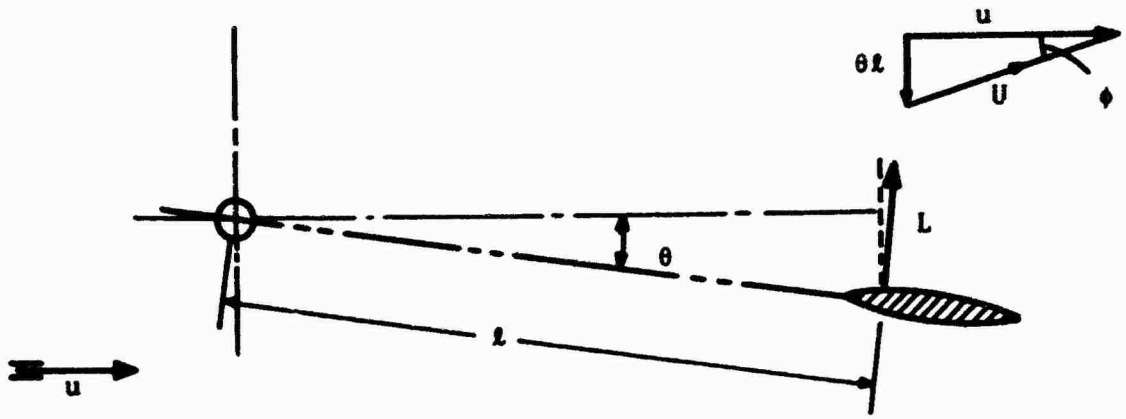


Figure A2. A Conventional Stabilizer.

If $\eta q_o$ is the local dynamic head at a conventional stabilizer the moment exerted about the CG is

$$M = -\eta q_o (U/u)^2 S\ell\, C_{L\alpha} \sin(\theta+\phi)$$

$$C_M = -\eta C_{L\alpha} (1+\lambda^2)(\sin\theta\cos\phi + \cos\theta\sin\phi) \qquad (12)$$

From the velocity diagram, $U = u\sqrt{1+\lambda^2}$

$$\sin\phi = \frac{\dot{\theta}\ell}{U} = \frac{\lambda}{\sqrt{1+\lambda^2}}$$

$$\cos\phi = \frac{u}{U} = \frac{1}{\sqrt{1+\lambda^2}}$$

$$C_M = -\eta C_{L\alpha} [\sqrt{1+\lambda^2}\sin\theta + \lambda\sqrt{1+\lambda^2}\cos\theta] \qquad (13)$$

The derivatives are

$$\frac{C_{M_\theta}}{\eta C_{L\alpha}} = -\sqrt{1+\lambda^2}\cos\theta + \lambda\sqrt{1+\lambda^2}\sin\theta \qquad (14)$$

and

$$\frac{C_{M_\lambda}}{\eta C_{L\alpha}} = -\frac{\lambda}{\sqrt{1+\lambda^2}}\sin\theta - \frac{(1+2\lambda^2)}{\sqrt{1+\lambda^2}}\cos\theta \qquad (15)$$

Note that, as in the in-plane case, $C_{M_\theta}$ is degraded by positive $\lambda$, and that there is a general second order $\theta$ coupling in $\theta$ and $\lambda$. But for practical purposes, with $\theta$ small and $\lambda \ll 1$

$$\left.\begin{aligned}\frac{C_{M_\theta}}{C_{L\alpha}} &= -\eta \\ \frac{C_{M_\lambda}}{C_{L\alpha}} &= -\eta\end{aligned}\right\} \qquad (16)$$

Since $C_{L\alpha} \approx C_{N\alpha}$, very closely, it is now possible to compare the two types of stabilizer.

Angle and rate derivatives are plotted for the in-plane stabilizer in Figures A3 and A4, using equation (9) and (11). For a particular geometry, $\xi = 30°$, say, it is possible to obtain values as high as

$$\frac{C_{M_\theta}}{C_{N\alpha}} = -0.7$$

$$\frac{C_{M_\lambda}}{C_{N\alpha}} = -1.2$$

For a conventional fin in the wake of an ejection seat, values $\eta = 0.2 - 0.3$ are typical, unless very long booms are used. Therefore, in-plane stabilizers are at least as good as, and probably two or three times as effective as conventional fins.

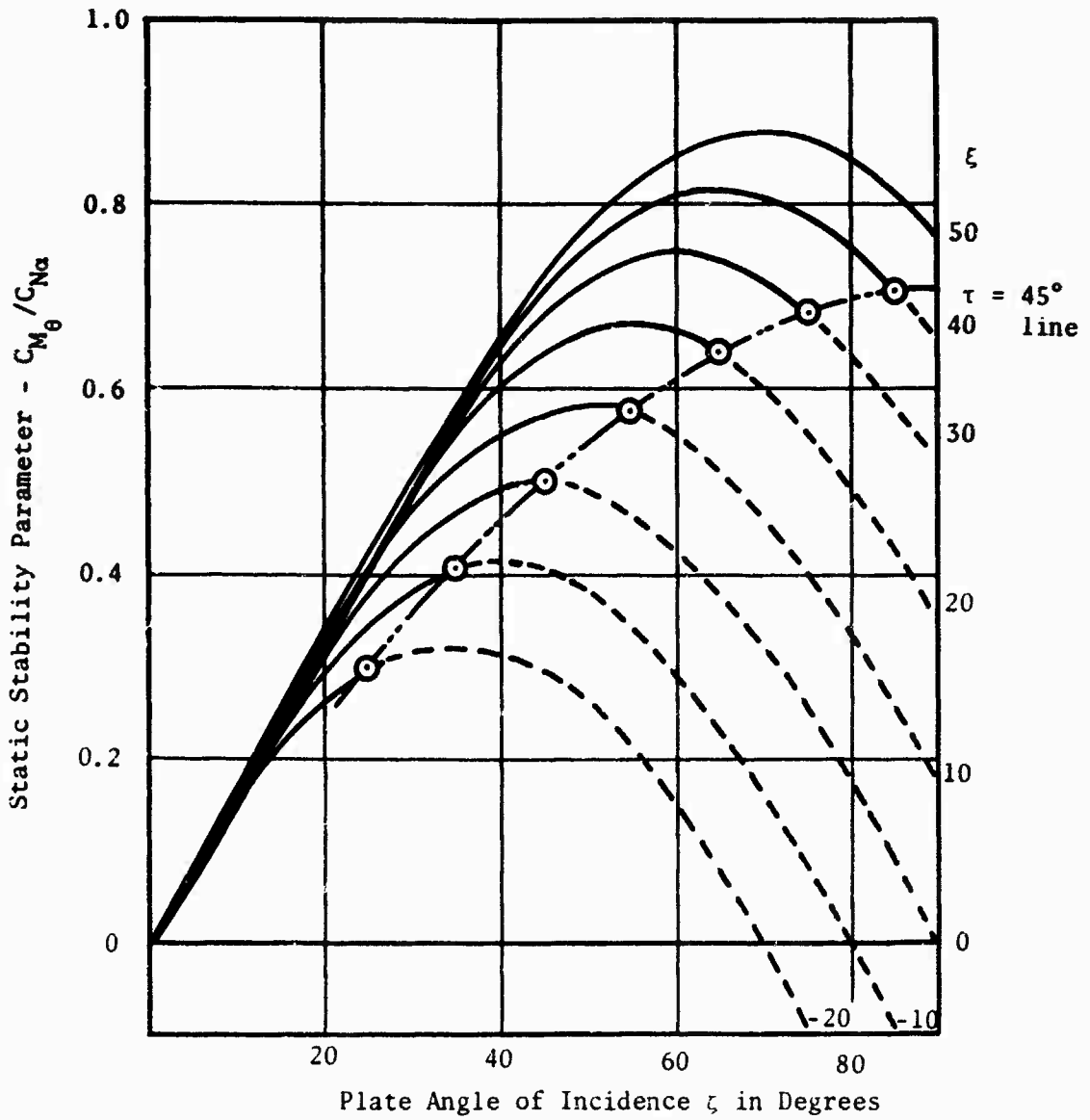


Figure A3. In-Plane Stabilizer Stiffness Derivative as a Function of the Plate Location and Incidence Angles $\xi$ and $\zeta$.

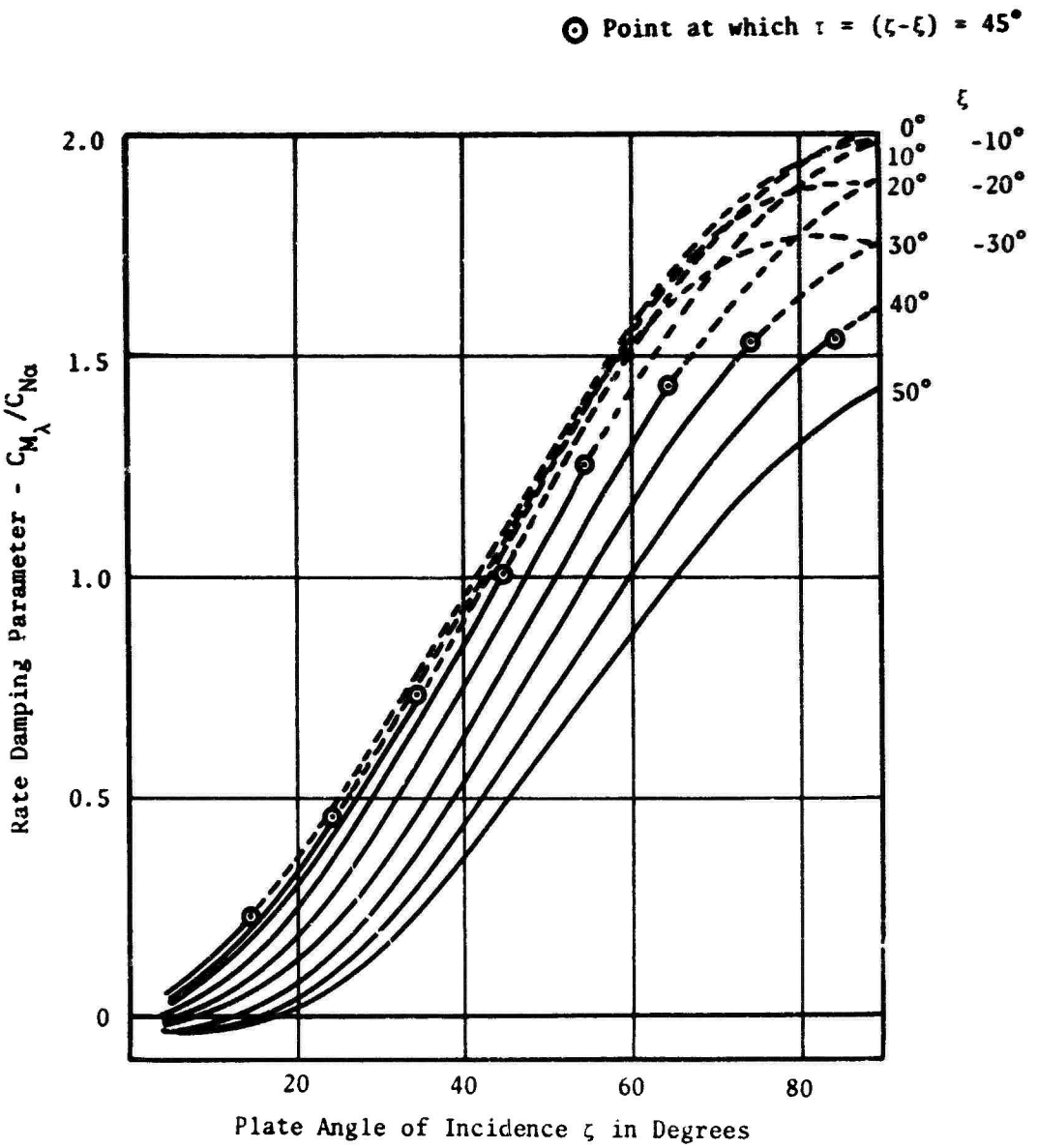


Figure A4. In-Plane Stabilizer Damping Derivative $C_{M_\lambda}$ as a Function of the Plate Location and Incidence Angles $\xi$ and $\zeta$.



☆U.S.Government Printing Office: 1974 — 758-436/689